System Identification via the Proper Orthogonal Decomposition

Timothy Charles Allison

Dissertation submitted to the faculty of the Virginia Polytechnic Institute and State University in partial fulfillment of the requirements for the degree of

Doctor of Philosophy
In
Mechanical Engineering

Daniel J. Inman, Chairman
Christopher A. Beattie
Nakhiah C. Goulbourne
Andrew J. Kurdila
A. Keith Miller

October 26, 2007
Blacksburg, Virginia

Keywords: System Identification, Linear Time-Varying Systems, Nonlinear Dynamics, Proper Orthogonal Decomposition, Deconvolution

System Identification via the Proper Orthogonal Decomposition

Timothy C. Allison

ABSTRACT

Although the finite element method is often applied to analyze the dynamics of structures, its application to large, complex structures can be time-consuming and errors in the modeling process may negatively affect the accuracy of analyses based on the model. System identification techniques attempt to circumvent these problems by using experimental response data to characterize or identify a system. However, identification of structures that are time-varying or nonlinear is problematic because the available methods generally require prior understanding about the equations of motion for the system. Nonlinear system identification techniques are generally only applicable to nonlinearities where the functional form of the nonlinearity is known and a general nonlinear system identification theory is not available as is the case with linear theory. Linear time-varying identification methods have been proposed for application to nonlinear systems, but methods for general time-varying systems where the form of the time variance is unknown have only been available for single-input single-output models. This dissertation presents several general linear time-varying methods for multiple-input multiple-output systems where the form of the time variance is entirely unknown. The methods use the proper orthogonal decomposition of measured response data combined with linear system theory to construct a model for predicting the response of an arbitrary linear or nonlinear system without any knowledge of the equations of motion. Separate methods are derived for predicting responses to initial displacements, initial velocities, and forcing functions. Some methods require only one data set but only promise accurate solutions for linear, time-invariant systems that are lightly damped and have a mass matrix proportional to the identity matrix. Other methods use multiple data sets and are valid for general time-varying systems. The proposed methods are applied to linear time-invariant, time-varying, and nonlinear systems via numerical examples and experiments and the factors affecting the accuracy of the methods are discussed.

Acknowledgements

My first thanks go to my wife, Alexa, for her dedicated support during my doctorate research and coursework. She motivated me to work hard and encouraged me through the whole learning process.

I am extremely grateful to Dan Inman for his support and guidance as my advisor. He allowed me an enormous amount of flexibility in my research, generously sent me to several conferences, and provided advice and support whenever I asked. I firmly believe there is no better place to be a graduate student than at CIMSS. Thanks also to all of my CIMSS colleagues for their everyday help and in studying for qualifying exams, working on homework, setting up experiments, and so on.

I'm also indebted to Keith Miller of Sandia National Laboratories for providing endless enthusiasm for my research and for developing funding to support me on a fellowship. It was a great privilege to work with him both at Sandia and as he served on my committee.

Finally, I'd like to express appreciation to the administrators of the National Physical Science Consortium and the Virginia Space Grant Consortium for their efforts in managing and providing my fellowship funds.

This page intentionally left blank.

Table of Contents

List of Tables

List of Figures

1. Introduction

The Finite Element (FE) method is commonly used to analyze the dynamics of complex structures [1]. Although the method is very powerful and its extensive use in analyses is therefore justified, some of its limitations become apparent when it is applied for analysis of very large, possibly nonlinear structures with millions of degrees of freedom. Months may be required to develop the geometry and form the element mesh for such models. After the model is completed the analysis may require days or weeks of processing time [2]. Finally, there is no guarantee that the analysis will accurately predict behavior of an actual structure. The analysis may be incorrect due to modeling errors (e.g., incorrect assumptions about damping or linearity), parameter errors (e.g., inaccuracy of Young's modulus), or other factors [3]. For this reason, model updating and validation procedures are often employed to ensure that the model accurately produces results that are consistent with experimental measurements.

Many system identification methods have been developed that use experimental response data to improve or create numerical modes for structures. For example, modal analysis is commonly used to compare resonant frequencies and/or mode shapes of linear FE models with experimental results [4]. Model updating is also considered a type of system identification because it applies experimental data to improve the numerical model [5]. Other system identification methods have been developed for linear and nonlinear systems that attempt to develop a numerical model from the data when no finite element model is available. However, current nonlinear identification techniques are only

developed for systems where the functional form of the nonlinearity is known ahead of time.

Linear time-varying systems may be well-suited to model the behavior of nonlinear systems and time-varying system identification has been proposed as an alternative to nonlinear system identification [6], but most linear time-varying identification methods require a prior understanding of the functional form of the time variance. A general method for time-varying system identification was proposed for biological systems in [7], but its application is limited to single-input single-output systems and a large number of data sets are required. Perhaps due to these limitations, linear time-varying methods have not yet been applied for nonlinear system identification.

This dissertation proposes new methods for time-varying system identification of multiple-input multiple-output systems where understanding of the form of the time variance is not required. The methods are based on the Proper Orthogonal Decomposition (POD), a statistical tool for extracting dominant information from experimental data. The POD has been applied in a variety of fields such as fluid mechanics, economics, heat transfer, and, recently, structural dynamics.

The POD is attractive because it can be applied to any linear or nonlinear system to express a measured response as a summation of modes [3]. These modes are generally different from the familiar eigenmodes of a (linear time-invariant) system and can represent the measured response (even for a nonlinear system) to any desired degree of

accuracy by using enough dominant modes. The POD is a linear procedure but it does "not do the physical violence of linearization methods" and has been referred to as a "safe haven in the intimidating world of nonlinearity" [8]. The system identification methods proposed in this dissertation use the POD to cast a measured response into the framework of a modal sum. Ideas from linear system theory and mode summation theory are then applied to develop methods for using the data in the POD to express the response of the system to new excitations.

The research in this dissertation contributes to the existing literature in several ways. First, new methods for identifying time-varying systems from experimental data are defined. These methods do not require any knowledge regarding the form of the time variance in the structure. Next, the methods are applied to nonlinear systems and the strengths and weaknesses of time-varying identification for nonlinear systems are discussed. Finally, new insight into the POD for structural systems is gained as the POD is applied in new ways to system identification.

This dissertation is comprised of six chapters and an appendix. The following chapter is a literature review that discusses the current state-of-the-art in linear time-varying and nonlinear system identification and summarizes many of the limitations of existing theory. The background and calculation of the POD is also summarized and previous applications of the POD to system identification are reviewed. Chapter 3 derives time-varying system identification methods for systems responding to initial displacements, initial velocities, forcing functions, or a combination of all three. Since methods

involving applied loads require the deconvolution of noisy data, a discussion on the difficulties of deconvolution when noise is present is also presented and a solution method is proposed. An overview of various sources of error in the methods is also given. Chapters 4 and 5 apply the methods to numerical models and experimental data for linear and nonlinear systems and present remarks regarding the accuracy of the methods for various types of systems. Finally, conclusions and recommendations for future research are contained in Chapter 6. The appendix at the end contains Matlab codes that were used to implement the proposed identification methods.

2. Literature Review

This section offers a brief review of system identification theory for both nonlinear and linear systems and also discusses the proper orthogonal decomposition and its previous applications to structural dynamics and system identification.

System identification can be most generally described as "the process of developing or improving a mathematical representation of a physical system using experimental data" [9]. Keeping this broad definition in mind, a variety of research topics such as modal testing, system realization, and model updating can all be classified as different approaches to system identification.

In this dissertation, two distinct classes of system identification methods are defined. The first class is composed of methods that must be used in conjunction with an existing numerical model (e.g. a finite element model). As described in Chapter 1, the finite element method is used very extensively in structural dynamics analysis and a wide variety of methods exist for improving these existing models. The second class of methods is those that may be used to develop a model without any prior representation of the system. These methods seek to find input/output models of a given system based solely on experimental measurements. Due to the difficulties that may be associated with finite element modeling, this research is involved with extending this latter class of methods.

2.1 Nonlinear System Identification

The current state of the art in nonlinear system identification techniques is thoroughly reviewed in [3], but a summary of the relevant information is presented here.

Although there are many nonlinear system identification methods, generally all follow the same essential pattern illustrated in Fig. 2.1. First, the experimental data are examined to verify that the system in question is, in fact, responding nonlinearly to the specific input. Next, the location, type, and functional form of the nonlinearity must be determined. Finally, once the nonlinear forms present in the structural equations of motion have been established, the nonlinear parameters (e.g. cubic spring constant, joint parameters, Coulomb friction constant, etc.) can be estimated.

Several methods exist for evaluating the presence of nonlinearity in a signal, but the most popular methods use measured frequency response function (FRF) data from different excitation levels. Nonlinear systems generally do not follow the principle of superposition and their frequency of response typically changes with varying excitation amplitude [3, 10, 11]. Therefore, the FRFs obtained from inputs of varying amplitudes will show amplitude and frequency discrepancies. More recent methods use the Hilbert transform and can detect the presence of nonlinearity from a single FRF [12, 13].

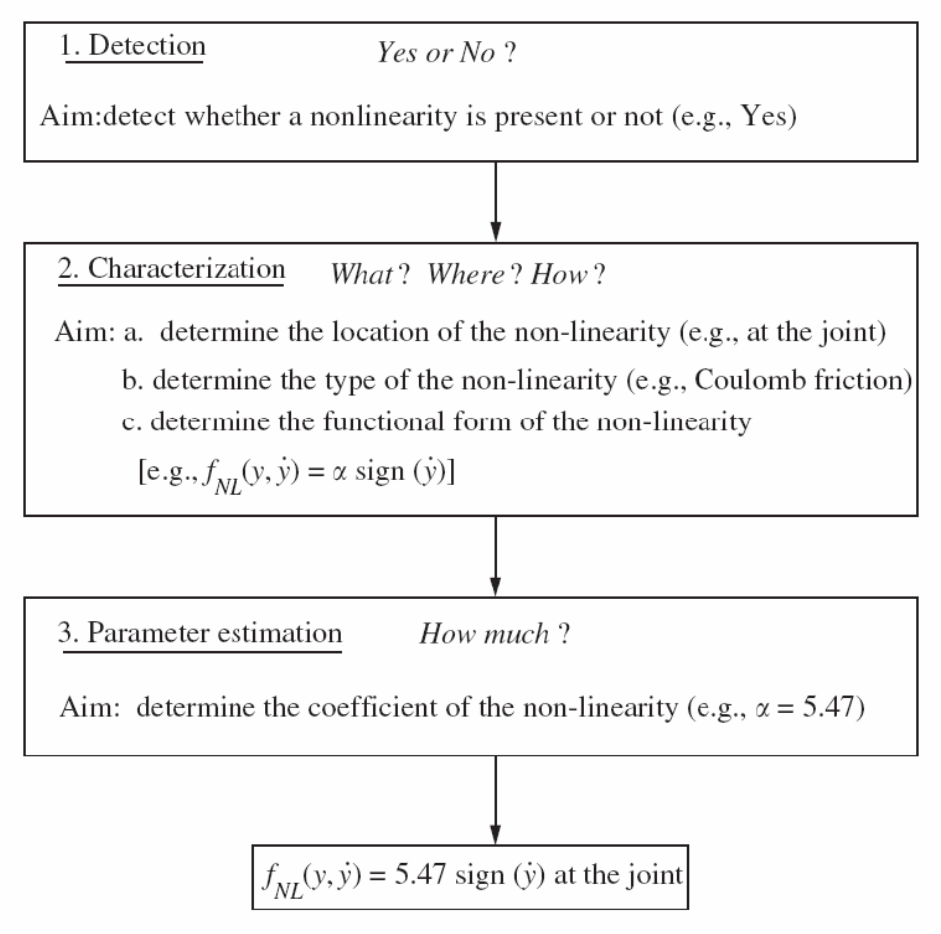

Fig. 2.1 Nonlinear System Identification Process (from [3], used with author's permission)

Once the presence of nonlinearity is established, the next step in the system identification process is characterizing the nonlinearity, i.e. determining its location, mechanism, and functional form. "Characterization is a very challenging step" [3] in the nonlinear system identification process because there exists a wide variety of mechanisms for nonlinearity. The location of a nonlinearity is typically determined by engineering judgment and knowledge about the system (e.g., a joint is a likely source of nonlinearity), which is generally acceptable for simple structures. For complex structures, several methods have been developed to locate nonlinearities [14-16].

Once the nonlinearity has been located, it must be classified, i.e. the mechanism of the nonlinearity must be identified. Questions that must be answered at this stage are "(i) does the nonlinearity come from stiffness or damping (or both)? (ii) does the system have hardening or softening characteristics? (iii) is the restoring force symmetric or asymmetric? (iv) is the nonlinearity weak or strong? (v) is the restoring force smooth or non-smooth?" [3] and (vi) does the system have multiple equilibrium positions? Analysis of the FRFs of the system combined with engineering experience will typically yield insight into the classification process [12, 17].

Next, the functional form of the nonlinearity must be identified, i.e. the nonlinear equation(s) relating the system's dynamics must be defined. If the functional form is not recognizable from the classification of the nonlinearity or from the body of literature, one typically assumes that the functional form of the nonlinearity can be accurately represented by a polynomial series. This assumption may be inaccurate (e.g. for non-smooth nonlinearities [3]) and the method may also suffer from poor numerical conditioning [18].

If all of the nonlinearities in the system have been successfully characterized, then one reaches the final step in the nonlinear system identification procedure, namely, parameter estimation. Several established methods for parameter estimation are reviewed in [3], but the author concludes that although progress is being made, parameter estimation is still

only tractable for simple structures and further research must be completed to estimate a large number of parameters for complex systems.

In some cases, methods may be available for creating a nonlinear model without determining the type or functional form of the nonlinearity. The Volterra kernel method [3, 19] is a popular method for this type of "black box" identification of nonlinear systems. The Volterra method assumes that the functional mapping input to output can be represented as a generalization of the convolution operator, namely the Volterra series. As long as the series converges for a system, identification may be accomplished by identifying the Volterra kernels in each term of the series. The Volterra kernels are typically correlated and can be calculated directly by solving a set of integral-equations. However, this calculation can be difficult and Volterra kernels are often expressed in terms of orthogonalized functions (e.g. a Wiener series) that are much simpler to determine. Unfortunately, systems with discontinuous or non-smooth nonlinearities (e.g. joints or vibroimpacts) do not have a Volterra series representation [3] and the method cannot be used for such systems.

Some key points may now be made about the current state of the art in nonlinear system identification based upon this review. First, although progress is being made, nonlinear system identification is still an active field of research and must continue to progress in order to accommodate complex structures or structures whose nonlinear functional forms are not well understood. Second, due to the wide variety of nonlinearities that may exist, nonlinear system identification "will have to retain its current 'toolbox' philosophy" [3]

for the foreseeable future. Thus, identification of nonlinear structures for which the nonlinearities cannot be adequately characterized remains out of reach.

What may be the key difficulty encountered with nonlinear system identification is explained in [3]:

> "[O]ne is forced to admit that there is no general analysis method that can be applied to all systems in all instances, as it is the case for modal analysis in linear structural dynamics…Two reasons for this failure, namely the inapplicability of various concepts of linear theory and the highly 'individualistic' nature of nonlinear systems. A third reason is that the functional which maps the input to the output is not known beforehand…this represents a major difficulty compared with linear system identification for which the structure of the functional is well defined."

Due to the inherent limitation of nonlinear theory described above, the research described in this dissertation develops several *linear* methods for system identification that, while suffering from limitations of linear theory, can be applied to *any* nonlinear system and are more accurate than other linear system identification techniques in the sense that the methods can reconstruct the original nonlinear response accurately regardless of the type of nonlinearity.

2.2 Linear Time-Varying System Identification

As explained in Section 2.1, the limitations and complexities of nonlinear theory motivate the application of linear system identification methods to nonlinear systems. Linear theory, of course, is unable to capture many of the behaviors exhibited by nonlinear systems, but linearization is nevertheless performed quite often because powerful tools and intuition have been developed for linear systems. Linearization is often justified

because many nonlinear systems are locally linear, i.e. their behavior is approximately linear over a limited range of motion.

Almost all linear system identification techniques that are presently used (e.g. the Eigensystem Realization Algorithm) assume that, in addition to being linear, the system is time-invariant [9]. Although this restriction simplifies the mathematics considerably, linear time-varying systems are better suited to model the dynamic behavior of nonlinear systems and linear time-varying system identification has been proposed (but never actually applied) as an attractive alternative to nonlinear system identification [6]. Unfortunately, as is the case with nonlinear system identification methods, most linear time-varying system identification methods require an a priori knowledge of the nature of the time variation. If there is even a slight error in the assumed form of the time variation, these methods have been shown to completely fail [20].

A general method for modeling arbitrary linear time-varying systems was proposed for biological applications in [7]. Unfortunately, the method requires a very large number of data sets (equal to the number of time samples required to capture the system's impulse response function, i.e. until the impulse response dies out) and is only developed for single-input single-output systems. However, this method is, to this author's knowledge, the only method available for arbitrary linear time-varying system identification.

The methods proposed in this research extend the capabilities of current linear time-varying system identification methods. The new methods require fewer data sets than the

method presented in [7] and may be applied to multiple-input multiple-output systems. In addition, the new methods are derived and based on the familiar concepts of mode summation theory in structural dynamics. Finally, the methods are also applied to nonlinear systems as proposed in [6] and their performance is evaluated.

2.3 The Proper Orthogonal Decomposition (POD)

The POD is a statistical method for extracting significant shapes and their corresponding amplitude modulations that are present in a displacement field time history. The POD is an attractive tool because it is a linear procedure and its governing mathematics is therefore relatively straightforward. However, it is often applied to both linear and nonlinear problems to extract dominant information from a response. In fact, the POD has been referred to as a "safe haven in the intimidating world of nonlinearity" because it is a linear procedure but does "not do the physical violence of linearization methods" [8].

The POD, also known as the Karhunen-Loève decomposition or principle component analysis, has been applied in many fields, including fluid mechanics, statistics, oceanography, meteorology, psychology, and economics. The method has been used in fluid mechanics to extract coherent structures from a turbulent flow [8] or to generate a basis for model reduction of unsteady viscous flows [21]. The POD has also recently been applied in structural dynamics for model order reduction [22-27], vibration control [28, 29], structural health monitoring [30-32], modal analysis [33, 34], sensor validation [35, 36], nonlinear vibration analysis [37, 38], and system identification [39-42]. A more

detailed overview of the applications of the POD in structural dynamics may be found in [43].

The POD can be computed by several methods [43]. This section explains how the POD is computed with the singular value decomposition of a snapshot matrix. First, a system response is generated by exciting the system by applying a load or imposing an initial condition, or both simultaneously. Next, the displacement at m degrees of freedom is sampled n times and the data are arranged in a "snapshot" matrix W :

$$W = \begin{bmatrix} w_1(t_1) & w_1(t_2) & \cdots & w_1(t_n) \\ w_2(t_1) & w_2(t_2) & & \\ \vdots & & \ddots & \\ w_m(t_1) & & & w_m(t_n) \end{bmatrix} \tag{2.1}$$

Next, the singular value decomposition of W is computed:

$$W = U\Sigma V^T \tag{2.2}$$

In Eq. (2.2), the columns $\mathbf{u}_i$ of U are the Proper Orthogonal Modes (POMs), the columns $\mathbf{v}_i$ of V are the proper orthogonal coordinate (POC) histories that correspond to each POM, and Σ is a diagonal matrix whose diagonal elements σ_i are the proper orthogonal values (POVs) corresponding to each POM. The POC histories describe the amplitude modulation of each POM and the POVs describe the relative significance of each POM in the response W [43, 44]. If the system is a linear and lightly damped with a mass matrix proportional to the identity matrix then the POMs will be equal to the linear normal modes [44]. For nonlinear systems if a single nonlinear normal mode is excited

then the first POM is a linear approximation to the excited nonlinear normal mode [44, 45]. The percentage of signal energy captured by a single POM $\mathbf{u}_i$ is given by

$$\varepsilon_i = \frac{\sigma_i}{\sum_{j=1}^{m} \sigma_j}. \tag{2.3}$$

Typically, only POMs that constitute a certain percentage of signal energy (e.g. 99% or 99.9%) are considered [8, 33, 43]. If k dominant POMs are considered then we may approximate W as a summation of POMs and corresponding POC histories, shown below (noting that Σ is diagonal):

$$W \approx \sum_{i=1}^{k} \sigma_i \mathbf{u}_i \mathbf{v}_i^T \tag{2.4}$$

We note that even signals generated by nonlinear systems may be represented by a summation of POMs. The POMs are "appealing for nonlinear system identification", in part because they "obey a 'sort of principle of superposition' due to the fact that the original signal is retrieved when all of the modal contributions are added up" [3]. In addition, the POMs are the optimal basis for reconstructing the original displacement efficiently. In other words, W may be approximated using fewer POMs than any other modes while maintaining the same level of accuracy. Finally, it should be noted that the POMs and POC histories are orthonormal:

$$U^T U = V^T V = I \tag{2.5}$$

Although this section has focused on calculation of the POMs, POVs, and POC histories by performing a singular value decomposition, these quantities may also be determined when calculating the POD by other methods [43]. The singular value decomposition is used in this instance for its simplicity and convenient expression as a summation of modes.

Most applications of the POD use only the POMs, meaning that only the spatial information about the system is obtained. The only documented use for the POC histories is to examine their frequency content to determine which linear normal modes are represented in each POM [33, 43]. This research describes a new application for the POC histories by using them with the other components of the POD to predict the response of the system to new excitations.

Finally, there are features of the POD that affect its usefulness for modeling applications. First, the POMs are excitation dependent, i.e. although a few dominant POMs may accurately describe the original response, there is no guarantee of their accuracy when they are used to predict the response to a new excitation. Although research is being performed to develop an a priori estimate of this error [45], a satisfactory estimate is still beyond reach. Another limitation presents itself when the POD is applied for model reduction of a large system. In order to construct an original data set and determine dominant POMs, one must first simulate a response using the full-order model. Therefore, the POD is most useful for model reduction applications where multiple

responses must be simulated. Despite these limitations, the POD is considered a useful tool for structural dynamics analyses, particularly for nonlinear systems.

2.4 Use of the POD in Structural Dynamics System Identification

The POD has been used for structural dynamics system identification purposes in several recent publications. This section reviews the literature and discusses how the research presented in this dissertation differs from existing methods.

First, two publications describe research that combines the POD with other established system identification methods. References [39] and [40] use a limited number of dominant POMs to significantly reduce the number of coordinates in a measured data set. Then, the Eigensystem Realization Algorithm (ERA) is applied to the reduced coordinate data to construct a reduced-order state space model for the system. The research described in this dissertation formulates a new linear time-varying system identification method and can be applied to nonlinear systems without requiring characterization of the nonlinearities.

Another strategy for system identification is model updating, where experimental data are compared with simulation data from a finite element model and adjustments are made to the finite element model so that its prediction matches the experiment. The POD has been applied in a model updating strategy in [41]. Specifically, the POMs are compared for both experimental and simulated data and an optimization procedure is employed to estimate nonlinear parameters. Unfortunately, a model updating approach requires that a

finite element model be constructed and a simulation be generated for comparison with the experimental data. The methods presented in Chapter 3 construct a predictive model from experimental data *without* requiring prior construction of a finite element model.

Finally, a method was presented in [42] for detecting nonlinearity in a system. As the degree of nonlinearity was increased a transfer of energy from low to high order POMs was observed as measured by the corresponding POV. Although this method is useful for the first step of the nonlinear system identification process, it does not yield a model and the remaining steps of the process must be completed before a model is obtained. The method proposed in this research differs in that it yields a predictive model for a system.

To summarize, the methods proposed in this research improve upon previous applications of the POD to system identification in two ways. First, the proposed methods construct a predictive model for time-varying or nonlinear systems. Second, the proposed methods are able to construct the model without requiring any prior knowledge regarding the equations of motion for the structure.

3. Development of POD-based System Identification Methods

In this section, new POD-based system identification methods are presented for three classes of system responses. The first methods apply to systems that are excited only by initial conditions and whose response is accordingly labeled a free response. Next, methods are developed for systems that are subjected to an applied forcing function and start at rest. Because the responses of these types of systems are entirely due to the applied forces, their response is termed a forced response. Systems responding to both initial conditions and applied forces are considered in the "mixed response" section. Since both the forced- and mixed-response methods involve deconvolution operations, a section on the challenges of deconvolution is also included with a description of a proposed solution method. Finally, a section is included that discusses the various sources of error that are present in the predicted responses for various methods.

3.1 Proper Orthogonal Coordinate Histories

Because all of the methods involve modifying the proper orthogonal coordinate (POC) histories in order to predict responses to new excitations, an analytical expression for the POC histories is developed in this section. The displacement $w(x,t)$ of a vibratory system is governed by the (generally time-varying) equation

$$\mathbf{M}\{\ddot{w},t\}+\mathbf{D}\{\dot{w},t\}+\mathbf{L}\{w,t\}=f(x,t) \tag{3.1}$$

Where $\mathbf{M}$, $\mathbf{D}$, and $\mathbf{L}$ are mass, damping, and stiffness operators, respectively, and $f(x,t)$ is a distributed forcing function. At this point we do not make any assumptions

about the form of $\mathbf{M}$, $\mathbf{D}$, and $\mathbf{L}$ other than that they are linear. The solution to Eq. (3.1) may be computed by approximating the displacement variable with a modal sum:

$$w(x,t) \approx \sum_{i=1}^{k} u_i(x) T_i(t) \tag{3.2}$$

In this paper we assume that the POMs are used as the modes $u_i(x)$. If this is the case then the modal coordinates $T_i(t)$ are equivalent to the POCs scaled by the POVs. In other words, the scaled POC histories $\hat{\mathbf{v}}_i = \sigma_i \mathbf{v}_i$ are time-sampled forms of the modal coordinates. We may then combine Eqs. (3.1) and (3.2) to obtain a matrix ordinary differential equation for the POCs:

$$M(t)\ddot{\mathbf{T}}(t) + D(t)\dot{\mathbf{T}}(t) + K(t)\mathbf{T}(t) = \mathbf{q}(t) \tag{3.3}$$

In Eq. (3.3), the quantities $M(t)$, $D(t)$, and $K(t)$ are the mass, damping, and stiffness matrices formed by taking inner products of the POMs with the respective operators [47]. The quantity $\mathbf{q}(t)$ is a vector of modal forces obtained by forming the inner product of the POMs with the applied load $f(x,t)$. In general, the matrices in Eq. (3.3) are full and an expression for the POCs is found by converting Eq. (3.3) to state form:

$$\begin{Bmatrix} \dot{\mathbf{T}}(t) \\ \ddot{\mathbf{T}}(t) \end{Bmatrix} = A(t) \begin{Bmatrix} \mathbf{T}(t) \\ \dot{\mathbf{T}}(t) \end{Bmatrix} + B(t)\mathbf{q}(t) \tag{3.4}$$

In Eq. (3.4), $A(t)$ and $B(t)$ are state matrices formed from $M(t)$, $D(t)$, and $K(t)$:

$$A(t)=\begin{bmatrix} 0 & I \\ -M(t)^{-1}K(t) & -M(t)^{-1}D(t) \end{bmatrix} \tag{3.5}$$

$$B(t)=\begin{bmatrix} 0 \\ M(t)^{-1} \end{bmatrix} \tag{3.6}$$

The solution to Eq. (3.4) is given by [47]:

$$\begin{Bmatrix} \mathbf{T}(t) \\ \dot{\mathbf{T}}(t) \end{Bmatrix} = \Phi(t)\begin{Bmatrix} \mathbf{T}(0) \\ \dot{\mathbf{T}}(0) \end{Bmatrix} + \int_0^t \Phi(t-\tau)B(t-\tau)\mathbf{q}(\tau)d\tau \tag{3.7}$$

where $\Phi(t)$ is the state transition matrix, which for time-varying systems can be computed from the Peano-Baker series [48]:

$$\Phi(t) = I + \int_0^t A(\sigma_1)d\sigma_1 + \int_0^t A(\sigma_1)\int_0^{\sigma_1} A(\sigma_2)d\sigma_2 d\sigma_1 + \ldots \tag{3.8}$$

The scaled POC histories are obtained from the upper-half partition of Eq. (3.7), i.e.

$$\mathbf{T}(t) = \begin{bmatrix} \Phi_{11}(t) & \Phi_{12}(t) \end{bmatrix}\begin{Bmatrix} \mathbf{T}(0) \\ \dot{\mathbf{T}}(0) \end{Bmatrix} + \int_0^t \Phi_{12}(t-\tau)M^{-1}(t-\tau)\mathbf{q}(\tau)d\tau \tag{3.9}$$

where $\Phi(t)$ is partitioned into four equal submatrices:

$$\Phi(t)=\begin{bmatrix} \Phi_{11}(t) & \Phi_{12}(t) \\ \Phi_{21}(t) & \Phi_{22}(t) \end{bmatrix} \tag{3.10}$$

If a system is linear, lightly damped, has a mass matrix proportional to the identity matrix, and is responding to initial conditions only, then the POMs are equivalent to the eigenmodes of the system [44, 45] and the mass and stiffness matrices in Eq. (3.3) are

diagonal. If proportional damping exists, then the damping matrix is also diagonal and the state matrix $A(t)$ is a block matrix composed of four equally sized submatrices that are diagonal. If $A(t)$ is composed of diagonal submatrices, then so are all of the integrals of $A(t)$ and matrix products of $A(t)$ with its integrals in Eq. (3.8). Because every term in Eq. (3.8) is composed of diagonal submatrices, then the submatrices of $\Phi(t)$ in Eq. (3.10) are all diagonal.

An example is now presented of a system that meets the requirements for the POMs to be equal to the eigenmodes. Consider the nondimensional mass-spring system shown in Fig. 3.1.

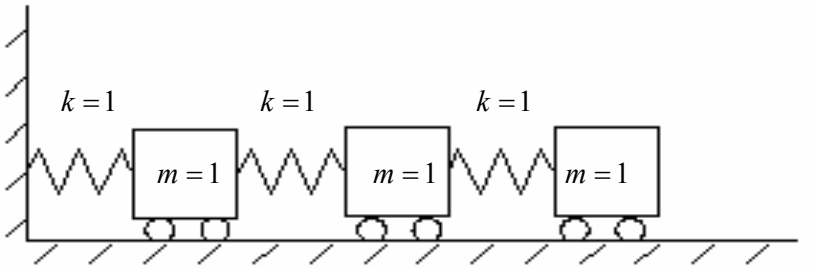

Fig. 3.1 Example Mass-Spring System with Equal Masses

The mass matrix for the system is

$$M = \begin{bmatrix} 1 & 0 & 0 \\ 0 & 1 & 0 \\ 0 & 0 & 1 \end{bmatrix}$$

and the stiffness matrix is

$$K = \begin{bmatrix} 2 & -1 & 0 \\ -1 & 2 & -1 \\ 0 & -1 & 1 \end{bmatrix}.$$

This system is undamped and the mass matrix is proportional to (in fact, it is equal to) the identity matrix. The eigenmodes (scaled so that they are orthonormal) for the system are:

$$\begin{bmatrix} \psi_1 & \psi_2 & \psi_3 \end{bmatrix} = \begin{bmatrix} 0.328 & 0.737 & -0.591 \\ 0.591 & 0.328 & 0.737 \\ 0.737 & -0.591 & -0.328 \end{bmatrix}$$

The system is given an initial displacement of $\mathbf{w}_0 = \begin{bmatrix} 0 & 0 & 1 \end{bmatrix}^T$ and the response is sampled every 0.1 s for 120 seconds. The proper orthogonal modes for the system may be computed from the measured response and are equal to:

$$\begin{bmatrix} \mathbf{u}_3 & \mathbf{u}_1 & \mathbf{u}_2 \end{bmatrix} = \begin{bmatrix} 0.3246 & 0.7398 & -0.5893 \\ 0.5836 & 0.3337 & 0.7403 \\ 0.7443 & -0.5843 & -0.3235 \end{bmatrix}$$

We note that the order of the POMs is not the same as that of the eigenmodes. This is because the third eigenmode is most active in the measured response and is therefore approximated by the POM that corresponds to the highest POV, i.e. the first POM. The POMs and eigenmodes, although very similar, are not exactly equal. However, the study in [45] demonstrated empirically that the difference in POMs and eigenmodes disappears as number of samples and the total measurement time increase. In this case, we will show that the POMs and eigenmodes are similar enough that the assumption of diagonal

submatrices of $\Phi(t)$ holds. The PO-modal mass and stiffness matrices are calculated to be:

$$M' = \begin{bmatrix} 1 & 0 & 0 \\ 0 & 1 & 0 \\ 0 & 0 & 1 \end{bmatrix}$$

$$K' = \begin{bmatrix} 1.5546 & 0.0004 & 0.0126 \\ 0.0004 & 3.2469 & 0.0178 \\ 0.0126 & 0.0178 & 0.1983 \end{bmatrix}$$

We note that although the modal stiffness matrix is not diagonal, it is diagonally dominant. The modal matrices may now be used to form the state matrix A:

$$A = \begin{bmatrix} 0_{3\times3} & I_{3\times3} \\ -K' & 0_{3\times3} \end{bmatrix}$$

Finally, the state transition matrix $\Phi(t)$ may be formed at every time step from the series in Eq. (3.8). Although it is impractical here to show all of the data at multiple time steps, we can illustrate the diagonal dominance of the various submatrices of $\Phi(t)$ by examining the 2-norm of each matrix element over a time range. The values of each element of $\Phi(t)$ were calculated at every 0.1 s for 10 seconds and a vector was formed containing the time-series data for each element, i.e.:

$$\underline{\Phi}_{ij} = \begin{bmatrix} \Phi_{ij}(t_1) \\ \Phi_{ij}(t_2) \\ \vdots \\ \Phi_{ij}(t_{100}) \end{bmatrix}$$

The 2-norm of each vector $\underline{\Phi}_{ij}$ was then calculated. The 2-norms for each element of $\Phi(t)$ are shown below:

$$\begin{bmatrix} \|\underline{\Phi}_{11}\|_2 & \|\underline{\Phi}_{12}\|_2 & \cdots & \|\underline{\Phi}_{16}\|_2 \\ \|\underline{\Phi}_{21}\|_2 & \|\underline{\Phi}_{22}\|_2 & & \\ \vdots & & \ddots & \\ \|\underline{\Phi}_{61}\|_2 & & & \|\underline{\Phi}_{66}\|_2 \end{bmatrix} = \begin{bmatrix} 50.60 & 0.00 & 0.01 & 32.40 & 0.00 & 0.02 \\ 0.00 & 49.36 & 0.00 & 0.00 & 15.90 & 0.01 \\ 0.01 & 0.00 & 53.33 & 0.02 & 0.01 & 240.57 \\ 78.34 & 0.00 & 0.01 & 50.60 & 0.00 & 0.01 \\ 0.00 & 167.66 & 0.01 & 0.00 & 49.36 & 0.00 \\ 0.01 & 0.01 & 9.44 & 0.01 & 0.00 & 53.33 \end{bmatrix}$$

Clearly, the diagonal terms in each of the four submatrices of $\Phi(t)$ contain much larger values than the off-diagonal terms. Thus, we will describe methods for systems that are lightly damped with a mass matrix proportional to the identity matrix where these terms are neglected. Even in cases where the POMs are not exactly equal to the eigenmodes, the modal matrices may be diagonally dominant and the approximation may still be accurate, as was demonstrated by this example.

3.2 Free Response

This section provides several methods for using the POMs and POC histories obtained from a system's response to an original set of initial conditions to predict the system's response to other initial conditions. Specifically, if an initial displacement is used to generate the original response, a method is presented for predicting the response to a new initial displacement, and likewise for velocities. An original method termed 'POV Recalculation' is described first that was developed without using the state-space concepts described in Section 3.1 (see [49] and [50]). The method of POV recalculation is then explored in the state-space framework to show that it is equivalent to assuming

that the modal matrices are diagonal. Finally, a new method is proposed using multiple data sets for systems that may have full modal matrices.

3.2.1 Method of POV Recalculation

This section describes the original proposed method for performing free response predictions. As shown in Eq. (2.2), the matrices U, V and Σ describe completely a system's response to an excitation without requiring information about the system's governing equations of motion. Suppose that an initial displacement profile $\mathbf{w}_0$ or velocity profile $\dot{\mathbf{w}}_0$ was imposed to form W. We now wish to modify the matrices to describe the system's response to a different initial displacement profile $\tilde{\mathbf{w}}_0$. Since the matrices U, V and Σ represent a given response (linear or nonlinear) as a modal sum, we draw upon ideas from mode summation theory to develop a method for modifying them to predict a response to a new set of initial conditions.

When solving vibration problems (e.g., the wave equation) analytically using separation of variables, a typical approach is to express the response as a summation of spatial eigenfunctions, temporal functions, and coefficients that indicate the relative significance of each mode in the response. While the eigenfunctions and temporal functions do not depend on the initial conditions, the significance coefficients do depend on them and are calculated using inner products of the eigenfunctions with the initial displacement or velocity profile [51].

Our original approach mimics this pattern and assumes that U and V do not change for a given system, but that the participation of each POM, measured by σ_i, changes to represent the response to new initial conditions. If these assumptions are made then the response $\widetilde{W}$ to $\widetilde{\mathbf{w}}_0$ may be written as

$$\widetilde{W} \approx \sum_{i=1}^{k} \widetilde{\sigma}_i \mathbf{u}_i \mathbf{v}_i^T \tag{3.11}$$

where the tilde notation indicates that the values in the diagonal matrix Σ have changed, although $\widetilde{\Sigma}$ is still diagonal. Methods for calculating the new POVs are now presented separately for responses to initial displacements and initial velocities.

We now explain how to calculate the new POVs for a system excited by initial displacements. We begin by writing the first column of Eq. (3.11), which corresponds to the initial time $t = t_0$:

$$\widetilde{\mathbf{w}}_0 \approx \sum_{i=1}^{k} \widetilde{\sigma}_i \mathbf{u}_i v_{i,0} \tag{3.12}$$

In Eq. (3.12), the scalar $v_{i,0}$ is the first element in each POC history $\mathbf{v}_i$. The new POVs $\widetilde{\sigma}_i$ are the only unknowns in Eq. (3.12). We recall that the POMs are orthonormal and multiply both sides of Eq. (3.12) on the left by $\mathbf{u}_j^T$ to eliminate all but the j^{th} term in the summation. The resulting equation may be solved for $\widetilde{\sigma}_j$:

$$\widetilde{\sigma}_j = \frac{\mathbf{u}_j^T \widetilde{\mathbf{w}}_0}{v_{j,0}}, \; j = 1,2,\ldots,k. \tag{3.13}$$

We note that Eq. (3.13) is valid for any POV-initial displacement pair. Inserting the original POVs and original initial displacement profile into Eq. (3.13) yields:

$$\sigma_j = \frac{\mathbf{u}_j^T \mathbf{w}_0}{v_{j,0}}, j = 1,2,\ldots,k. \tag{3.14}$$

Because the original POVs are finite we may conclude that the initial value of each POC history $v_{j,0}$ is nonzero and that new POVs calculated from Eq. (3.13) will always be finite. After the new POVs $\tilde{\sigma}_j$ have been calculated, the response to $\tilde{\mathbf{w}}_0$ may be approximated using Eq. (3.11), replacing the dummy index variable *j* with *i*.

If an initial velocity profile $\dot{\mathbf{w}}_0$ is applied to form W, the response to a different velocity profile $\dot{\tilde{\mathbf{w}}}_0$ may be calculated using the same reasoning given for initial displacements. However, we first take the time derivative of Eq. (3.11) in order to deal with velocities instead of displacements:

$$\dot{\tilde{W}} \approx \sum_{i=1}^{k} \tilde{\sigma}_i \mathbf{u}_i \dot{\mathbf{v}}_i^T \tag{3.15}$$

We consider the first column of Eq. (3.15), corresponding to $t = t_0$:

$$\dot{\mathbf{w}}_0 \approx \sum_{i=1}^{k} \sigma_i \mathbf{u}_i \dot{v}_{i,0} \tag{3.16}$$

Again, we may use the orthogonality of the POMs to solve for the POVs. For initial velocities, the new POVs are calculated from

$$\widetilde{\sigma}_j = \frac{\mathbf{u}_j^T \dot{\widetilde{\mathbf{w}}}_0}{\dot{v}_{j,0}}, j = 1,2,\ldots,k. \tag{3.17}$$

In Eq. (3.17), the time derivative of the POC histories at $t = t_0$ may be calculated from the original velocity profile $\dot{\mathbf{w}}_0$ if it is known. Eq. (3.17) is valid for any set of initial velocity and corresponding POVs, so we may replace $\widetilde{\sigma}_j$ and $\dot{\widetilde{\mathbf{w}}}_0$ with the original values and solve for $\dot{v}_{j,0}$

$$\dot{v}_{j,0} = \frac{\mathbf{u}_j^T \dot{\mathbf{w}}_0}{\sigma_j}, j = 1,2,\ldots,k. \tag{3.18}$$

By using the new POVs calculated from Eqs. (3.13) (for initial displacements) or (3.17) (for initial velocities) in Eq. (3.11), we are able to predict the free response of a system to a variety of initial conditions using only data obtained from the original POD. A flowchart describing the POVR method for initial displacements is shown in Fig. 3.2 below. The method for initial velocities is very similar and a separate flowchart is not provided.

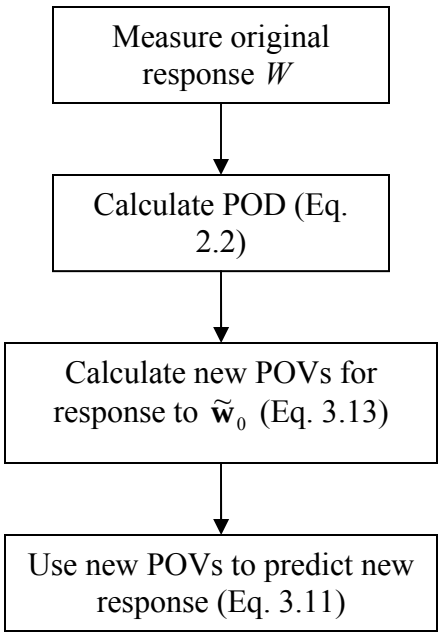

Fig. 3.2 Flowchart for POVR Method

3.2.2 POV Recalculation from a State-Space Perspective

This section interprets the method given in 3.2.1 from the perspective introduced in Section 3.1 and exposes a hidden assumption in the first method. If we assume that the original response was formed by imposing an initial displacement on the structure then the expression for the scaled POC histories is quite simple:

$$\mathbf{T}(t) = \Phi_{11}(t)\mathbf{T}(0) \tag{3.19}$$

If we assume that $\Phi_{11}(t)$ is diagonal (a true assumption if the conditions outlined in Section 3.1 are met) then the expression is simplified even more and a single scaled POC history can be written as

$$T_j(t) = \Phi_{11,j}(t)T_j(0) \tag{3.20}$$

or in time-sampled form at all time steps as

$$\hat{\mathbf{v}}_j = \sigma_j \mathbf{v}_j = \underline{\phi}_{11,j} \hat{v}_{j,0} \tag{3.21}$$

where $\underline{\phi}_{11,j}$ is a vector containing the values of the j^{th} diagonal element of $\Phi_{11}(t)$ at every time step. The POC history may be modified to represent the response to a new initial condition:

$$\tilde{\hat{\mathbf{v}}}_j = \underline{\phi}_{11,j} \tilde{\hat{v}}_{j,0} = \frac{\sigma_j \mathbf{v}_j \tilde{\hat{v}}_{j,0}}{\hat{v}_{j,0}} \tag{3.22}$$

The initial values for the scaled POC histories are related to the initial displacement profiles through a POM:

$$\begin{bmatrix} \hat{v}_{j,0} & \tilde{\hat{v}}_{j,0} \end{bmatrix} = \mathbf{u}_j^T \begin{bmatrix} \mathbf{w}_0 & \tilde{\mathbf{w}}_0 \end{bmatrix} \tag{3.23}$$

Finally, we may insert Eq. (3.23) into Eq. (3.22) to rewrite the modified POC history as

$$\tilde{\hat{\mathbf{v}}}_j = \sigma_j \mathbf{v}_j \frac{\mathbf{u}_j^T \tilde{\mathbf{w}}_0}{\mathbf{u}_j^T \mathbf{w}_0} = \sigma_j \mathbf{v}_j \frac{\tilde{\sigma}_j}{\sigma_j} = \tilde{\sigma}_j \mathbf{v}_j \tag{3.24}$$

where $\tilde{\sigma}_j$ is the new POV obtained from Eq. (3.13). Eqs. (3.20) – (3.24) show that the method of POV recalculation explained in Section 3.2.1 assumes that the modal matrices in Eq. (3.3) are diagonal, although this assumption was not obvious from the formulation of the method. It is trivial to show that the same assumption is made for initial velocity profiles. The method of POV recalculation is therefore invalid for structures with arbitrary damping or with a mass matrix not proportional to the identity matrix.

3.2.3 Multiple Data Set Method

The previous section demonstrated that the method of POV recalculation is only valid for structures with light or no damping and mass matrices proportional to the identity matrix. This section proposes a method for using multiple data sets to identify relevant matrices $\Phi_{11}(t)$ (for initial displacements) and $\Phi_{12}(t)$ (for initial velocities) without assuming anything about their form. Examination of Eq. (3.19) suggests that data sets resulting from *k* linearly independent initial velocity profiles may be used to solve for $\Phi_{11}(t)$. First the data sets must all be approximated in terms of the original POMs because the state-space formulation in Section 3.1 used only one set of POMs (see Eq. (3.2)). This approximation is peformed as:

$$ {}^{j}W \approx UU^{T}\left({}^{j}W\right) = U\left({}^{j}\hat{V}^{T}\right), j = 1,2,\ldots,k \tag{3.25} $$

In Eq. (3.25), the columns of ${}^{j}\hat{V}$ now describe the time modulations of the original POMs in the new response. The new POC histories for all *k* data sets at a particular time step t_i can now be written in terms of $\Phi_{11}(t_i)$:

$$ \begin{bmatrix} \hat{v}_1(t_i) & {}^{2}\hat{v}_1(t_i) & \cdots & {}^{k}\hat{v}_1(t_i) \\ \hat{v}_2(t_i) & {}^{2}\hat{v}_2(t_i) & \cdots & {}^{k}\hat{v}_2(t_i) \\ \vdots & \vdots & \ddots & \vdots \\ \hat{v}_k(t_i) & {}^{2}\hat{v}_2(t_i) & \cdots & {}^{k}\hat{v}_k(t_i) \end{bmatrix} = \Phi_{11}(t_i)\left[\hat{\mathbf{v}}_0 \quad {}^{2}\hat{\mathbf{v}}_0 \quad \cdots \quad {}^{k}\hat{\mathbf{v}}_0\right] = \Phi_{11}(t_i)\hat{V}_0 \tag{3.26} $$

If the initial displacement profiles are linearly independent then we may solve for $\Phi_{11}(t_i)$:

$$\Phi_{11}(t)=\begin{bmatrix} \hat{v}_1(t_i) & {}^2\hat{v}_1(t_i) & \cdots & {}^k\hat{v}_1(t_i) \\ \hat{v}_2(t_i) & {}^2\hat{v}_2(t_i) & \cdots & {}^k\hat{v}_2(t_i) \\ \vdots & \vdots & \ddots & \vdots \\ \hat{v}_k(t_i) & {}^2\hat{v}_2(t_i) & \cdots & {}^k\hat{v}_k(t_i) \end{bmatrix}\hat{V}_0^{-1} \tag{3.27}$$

After $\Phi_{11}(t_i)$ has been obtained from Eq. (3.27) at every time step, the POC histories representing a response to a new initial displacement profile may be calculated at each time step from

$$\begin{bmatrix} \tilde{\hat{v}}_1(t_i) \\ \tilde{\hat{v}}_2(t_i) \\ \vdots \\ \tilde{\hat{v}}_k(t_i) \end{bmatrix} = \Phi_{11}(t_i)\tilde{\hat{\mathbf{v}}}_0 \tag{3.28}$$

and the new response in physical coordinates may be calculated:

$$\tilde{W} \approx \sum_{j=1}^{k} \mathbf{u}_j \tilde{\hat{\mathbf{v}}}_j^T \tag{3.29}$$

The procedure is very similar for initial velocity profiles. The POC histories for k data sets may be expressed as

$$\begin{bmatrix} \hat{v}_1(t_i) & {}^2\hat{v}_1(t_i) & \cdots & {}^k\hat{v}_1(t_i) \\ \hat{v}_2(t_i) & {}^2\hat{v}_2(t_i) & \cdots & {}^k\hat{v}_2(t_i) \\ \vdots & \vdots & \ddots & \vdots \\ \hat{v}_k(t_i) & {}^2\hat{v}_2(t_i) & \cdots & {}^k\hat{v}_k(t_i) \end{bmatrix} = \Phi_{12}(t_i)\left[\dot{\hat{\mathbf{v}}}_0 \quad {}^2\dot{\hat{\mathbf{v}}}_0 \quad \cdots \quad {}^k\dot{\hat{\mathbf{v}}}_0\right] = \Phi_{11}(t_i)\dot{\hat{V}}_0 \tag{3.30}$$

where the initial time derivatives of the POC histories may be calculated using the original initial velocity profiles and the original POMs, i.e.

$$\left[\dot{\hat{\mathbf{v}}}_0 \quad {}^2\dot{\hat{\mathbf{v}}}_0 \quad \cdots \quad {}^k\dot{\hat{\mathbf{v}}}_0\right] = U^T\left[\dot{\mathbf{w}}_0 \quad {}^2\dot{\mathbf{w}}_0 \quad \cdots \quad {}^k\dot{\mathbf{w}}_0\right] \tag{3.31}$$

If the initial velocity profiles are chosen so that they are linearly independent then we may solve for $\Phi_{12}(t_i)$:

$$\Phi_{12}(t_i) = \begin{bmatrix} \hat{v}_1(t_i) & {}^2\hat{v}_1(t_i) & \cdots & {}^k\hat{v}_1(t_i) \\ \hat{v}_2(t_i) & {}^2\hat{v}_2(t_i) & \cdots & {}^k\hat{v}_2(t_i) \\ \vdots & \vdots & \ddots & \vdots \\ \hat{v}_k(t_i) & {}^2\hat{v}_2(t_i) & \cdots & {}^k\hat{v}_k(t_i) \end{bmatrix} \dot{\hat{V}}_0^{-1} \tag{3.32}$$

Finally, the POC histories corresponding to a new initial velocity profile are calculated from

$$\begin{bmatrix} \tilde{\hat{v}}_1(t_i) \\ \tilde{\hat{v}}_2(t_i) \\ \vdots \\ \tilde{\hat{v}}_k(t_i) \end{bmatrix} = \Phi_{12}(t_i)\tilde{\dot{\hat{\mathbf{v}}}}_0 \tag{3.33}$$

and the new response in physical coordinates may be obtained from Eq. (3.29).

Both of the free response methods obtained in this section are very similar to the method proposed in [52] for solving for the full state transition matrix $\Phi(t)$. The method proposed here requires far fewer data sets, however, because (1) only the submatrices of $\Phi(t)$ that are necessary for predicting the response of the displacement states are calculated and (2) the size of $\Phi(t)$ is reduced considerably because the optimality of the POD allows the original response to be approximated by only using a few dominant POMs.

A flowchart describing the MDS method for initial displacements is given in Fig. 3.3. The method for initial velocities is trivially similar and a separate flowchart is unnecessary.

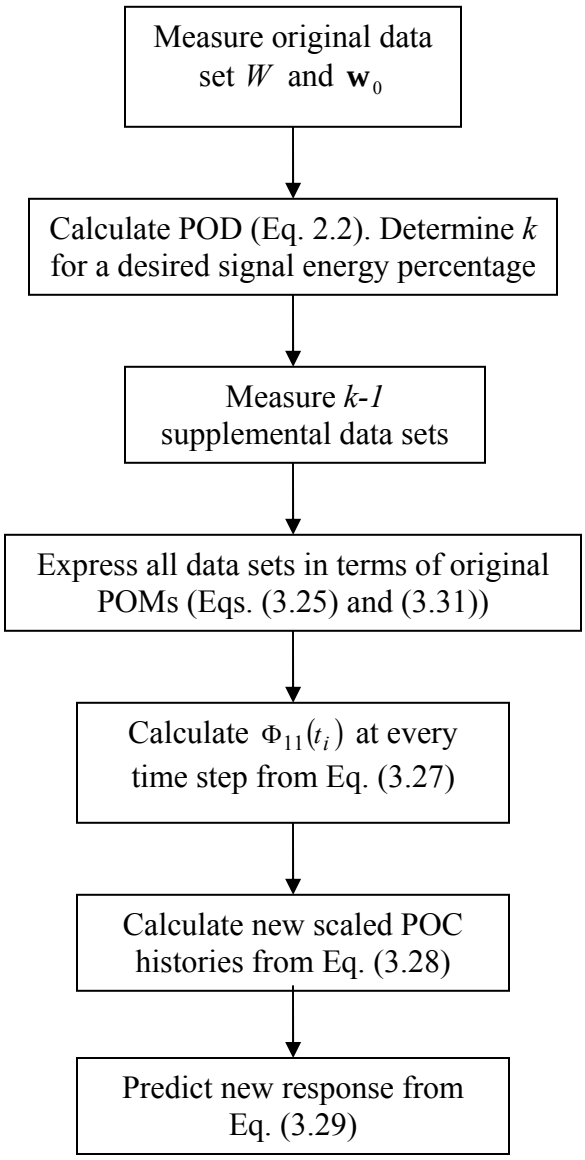

Fig. 3.3 Flowchart for MDS Method

3.3 Forced Response

This section builds upon this concepts introduced in Section 3.1 to develop two methods (see [53]) for modifying the POC histories obtained from a system's forced response to create a system model for predicting system responses to new loads. If the system starts at rest, the POCs are found from the upper half of the second term in Eq. (3.7):

$$\mathbf{T}(t) = \int_0^t C(t-\tau)\mathbf{q}(\tau)d\tau = C(t) * \mathbf{q}(t) \tag{3.34}$$

In Eq. (3.34), the square matrix $C(t)$ is of dimension *k* and is defined as the upper-half partition of the matrix product $\Phi(t)B(t)$, i.e.

$$C(t) = \begin{bmatrix} \Phi_{11}(t) & \Phi_{12}(t) \end{bmatrix} \begin{bmatrix} 0 \\ M^{-1} \end{bmatrix} = \Phi_{12}(t)M^{-1} \tag{3.35}$$

Eq. (3.34) shows that the POC histories are the result of a matrix-vector convolution. Our strategy for system identification, then, is to calculate the matrix $C(t)$ through deconvolution methods. Once $C(t)$ has been calculated, the response of the system to new loads may be predicted by convolving $C(t)$ with a new modal force vector.

We will now set up the deconvolution problem that must be solved to compute the matrix $C(t)$ at each time from the POC histories. First, we write the i^{th} row of Eq. (3.34) in time-sampled form to express a scaled POC history as a sum of convolutions

$$\hat{\mathbf{v}}_i = \mathbf{c}_{i1} * \mathbf{q}_1 + \mathbf{c}_{i2} * \mathbf{q}_2 + \cdots + \mathbf{c}_{ik} * \mathbf{q}_k \tag{3.36}$$

where the *n*-vectors $\mathbf{c}_{ij}$ and $\mathbf{q}_j$ are the time-sampled forms of $C_{ij}(t)$ and $q_j(t)$, respectively. Next, we sample the applied load $f(x,t)$ at the same locations and time steps used to form W in Eq. (3.1) and store the data in a force matrix F:

$$F = \begin{bmatrix} f_1(t_1) & f_1(t_2) & \cdots & f_1(t_n) \\ f_2(t_1) & f_2(t_2) & & \\ \vdots & & \ddots & \\ f_m(t_1) & & & f_m(t_n) \end{bmatrix} \tag{3.37}$$

The modal forces are computed by taking the inner product of the POMs with the force matrix:

$$\mathbf{q}_i = \mathbf{u}_i^T(F), i = 1, 2, \ldots, k \tag{3.38}$$

The convolution of $\mathbf{c}_{ij}$ and $\mathbf{q}_j$ in the time domain may be written as a summation [58]:

$$(\mathbf{c}_{ij} * \mathbf{q}_j)[t_s] = \Delta t \sum_{p=1}^{s} \mathbf{c}_{ij}[t_p]\mathbf{q}_j[t_{s-p+1}], s = 1, 2, \ldots, n \tag{3.39}$$

When the summation in Eq. (3.39) is performed for all times $s = 1, 2, \ldots, n$, the convolution may be written as a matrix-vector product:

$$\mathbf{c}_{ij} * \mathbf{q}_j = \Delta t \begin{bmatrix} \mathbf{q}_j[t_1] & 0 & \cdots & 0 \\ \mathbf{q}_j[t_2] & \mathbf{q}_j[t_1] & \ddots & \vdots \\ \vdots & \vdots & \ddots & 0 \\ \mathbf{q}_j[t_n] & \mathbf{q}_j[t_{n-1}] & \cdots & \mathbf{q}_j[t_1] \end{bmatrix} \begin{bmatrix} \mathbf{c}_{ij}[t_1] \\ \mathbf{c}_{ij}[t_2] \\ \vdots \\ \mathbf{c}_{ij}[t_n] \end{bmatrix} = \breve{Q}_j \mathbf{c}_{ij} \tag{3.40}$$

We will refer to the Toeplitz matrix $\breve{Q}_j$ in Eq. (3.40) as a convolution matrix for $\mathbf{q}_j$. We now use convolution matrices to write each convolution in Eq. (3.36) as a matrix-vector product:

$$\hat{\mathbf{v}}_i = \breve{Q}_1\mathbf{c}_{i1} + \breve{Q}_2\mathbf{c}_{i2} + \cdots + \breve{Q}_k\mathbf{c}_{ik} \tag{3.41}$$

Now we may write the convolution for all *k* POC histories in matrix form:

$$\hat{V} = \begin{bmatrix}\breve{Q}_1 & \breve{Q}_2 & \cdots & \breve{Q}_k\end{bmatrix}\begin{bmatrix}\mathbf{c}_{11} & \mathbf{c}_{21} & \cdots & \mathbf{c}_{k1} \\ \mathbf{c}_{12} & \mathbf{c}_{22} & \cdots & \mathbf{c}_{k2} \\ \vdots & \vdots & \ddots & \vdots \\ \mathbf{c}_{1k} & \mathbf{c}_{2k} & \cdots & \mathbf{c}_{kk}\end{bmatrix} = \begin{bmatrix}\breve{Q}_1 & \breve{Q}_2 & \cdots & \breve{Q}_k\end{bmatrix}\overline{C} \tag{3.42}$$

In Eq. (3.42), the matrix $\overline{C}$ contains the information in $C(t)$ at all *n* time steps. The dimensions of $\overline{C}$ are $nk \times k$. We are unable to solve for $\overline{C}$ by solving Eq. (3.42) because it is a system of only nk equations and $\overline{C}$ is composed of nk^2 unknown terms. The next two sections present two methods for computing $\overline{C}$. First, as explained in Section 3.1, systems that meet special conditions will have a diagonal $C(t)$ matrix, and the deconvolution may be performed separately for each POM using only a single load-response data set (see [54]). If the system does not meet the necessary conditions then we propose a second method that incorporates load and response data from multiple load cases in order to add rows to Eq. (3.42) and solve for the full $\overline{C}$ matrix (see [55]).

3.3.1 The Single-Load Method

If a system is lightly damped and has a mass matrix proportional to the identity matrix, then the POMs are equivalent to the eigenmodes of the system and we can conclude that

the matrix $C(t)$ in Eq. (3.35) is diagonal because $\Phi_{12}(t)$ and $M(t)$ are both diagonal. In this case, the terms in Eq. (3.42) due to off-diagonal elements of $C(t)$ vanish and the diagonal elements of $C(t)$ can be calculated by solving the linear system

$$\hat{\mathbf{v}}_i = \breve{Q}_i \mathbf{c}_{ii}, \; i = 1, 2, \ldots, k \tag{3.43}$$

Once the diagonal elements of $C(t)$ have been calculated, we can use them to form modified POC histories to represent the response to a new load $\widetilde{f}(x,t)$. First, $\widetilde{f}(x,t)$ is written in matrix form as $\widetilde{F}$ and new modal forces $\tilde{\mathbf{q}}_i$ are formed as in Eq. (3.38). Next, the modal forces are convolved with the diagonal elements of $C(t)$ to form new POC histories:

$$\widetilde{\hat{\mathbf{v}}}_i = \widetilde{\breve{Q}}_i \mathbf{c}_{ii}, \; i = 1, 2, \ldots, k \tag{3.44}$$

In Eq. (3.44), the matrices $\widetilde{\breve{Q}}_i$ are convolution matrices formed from the new modal forces. Finally, the new POC histories are used with the original POMs to predict the response of the system to $\widetilde{F}$:

$$\widetilde{W} = \sum_{i=1}^{k} \mathbf{u}_i \widetilde{\hat{\mathbf{v}}}_i^T \tag{3.45}$$

A flowchart describing the SL method is shown in Fig. 3.4.

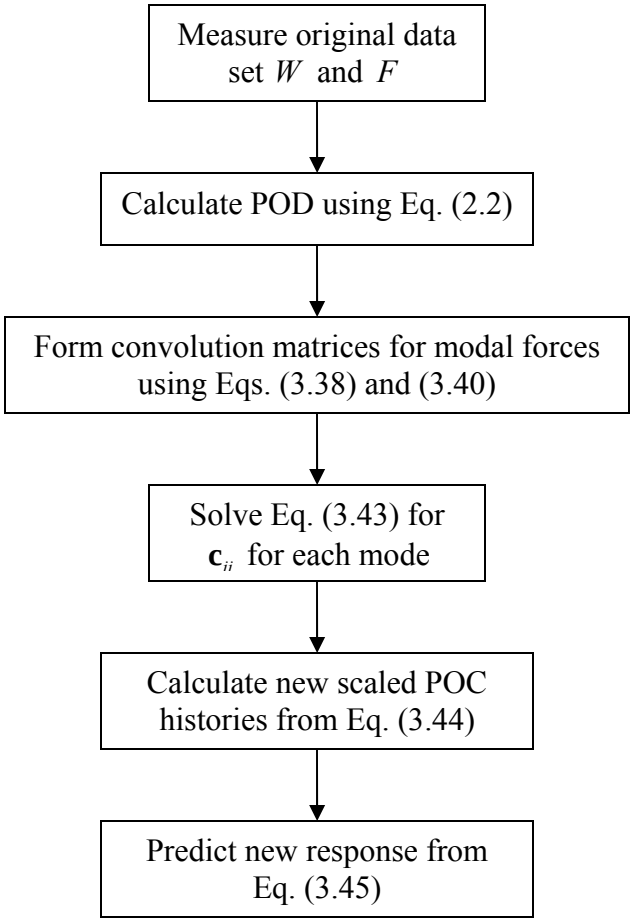

Fig. 3.4 Flowchart for SL Method

3.3.2 The Multiple-Load Method

If the structure does not meet the conditions required for the single-load method, it is possible to use multiple sets of load-response data to solve for $\overline{C}$. When we measure response data from a second applied load, the response may be approximated using the *original* POMs as

$$ {}^2W \approx UU^T\left({}^2W\right) = U\left({}^2\hat{V}^T\right) \tag{3.46}$$

where the columns of ${}^2\hat{V}$ are the time modulations of the original POMs in the second measured response. We use the original POMs because the expression for $C(t)$ was

developed using only one set of POMs in Eq. (3.2). The modal forces may also be computed for the second load case using the original POMs:

$$ {}^{2}\mathbf{q}_i = \mathbf{u}_i^T \left({}^{2}F \right) \tag{3.47} $$

In Eq. (3.47), ${}^{2}F$ is a matrix similar to F in Eq. (3.37), but it contains force data for the second load case. We may repeat this procedure for k sets of load and response data and add a sufficient number of rows to Eq. (3.42) to solve for $\overline{C}$:

$$ \begin{bmatrix} \hat{V} \\ {}^{2}\hat{V} \\ \vdots \\ {}^{k}\hat{V} \end{bmatrix} = \begin{bmatrix} \breve{Q}_1 & \breve{Q}_2 & \cdots & \breve{Q}_k \\ {}^{2}\breve{Q}_1 & {}^{2}\breve{Q}_2 & \cdots & {}^{2}\breve{Q}_k \\ \vdots & \vdots & \ddots & \vdots \\ {}^{k}\breve{Q}_1 & {}^{k}\breve{Q}_2 & \cdots & {}^{k}\breve{Q}_k \end{bmatrix} \overline{C} \tag{3.48} $$

In Eq. (3.48), ${}^{j}\breve{Q}_i$ is defined as the convolution matrix for the i^{th} modal force and the j^{th} load case. Once $\overline{C}$ has been identified by solving Eq. (3.48), we may compute POC histories for the response to a new force $\widetilde{F}$. New modal forces are calculated as in Eq. (3.38) and formed into convolution matrices as shown in Eq. (3.40). The new POC histories are then calculated by convolving the new modal forces with $\overline{C}$:

$$ \widetilde{\hat{V}} = \begin{bmatrix} \widetilde{\breve{Q}}_1 & \widetilde{\breve{Q}}_2 & \cdots & \widetilde{\breve{Q}}_k \end{bmatrix} \overline{C} \tag{3.49} $$

Once the new POC histories have been calculated, Eq. (3.45) may be used to calculate the predicted response of the system to the new load. A flowchart for the ML method is provided in Fig. 3.5.

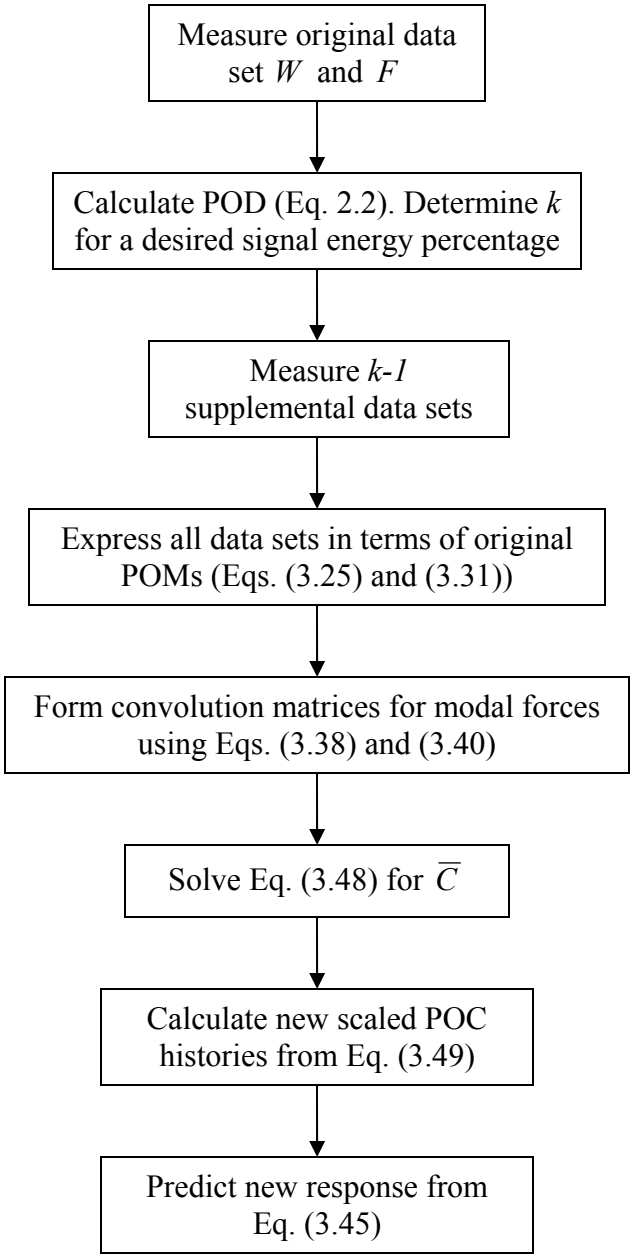

Fig. 3.5 Flowchart for ML Method

3.4 Mixed Response

The previous sections introduced methods for using strictly free or forced responses of a system to predict new free or forced responses, respectively, but the methods could not be combined, i.e. a measured free response could not be used to predict a forced response or

vice versa. This section describes a method from [56] and [57] for using measured mixed responses of a system to form a predictive model for both free and forced responses. The method assumes that the structure is lightly damped and that the mass matrix is proportional to the identity matrix and that the POMs are therefore equal to the eigenmodes.

We begin by measuring three distinct sets of response data that all result from separate combinations of both applied loads and initial conditions. The data are arranged in snapshot matrices ${}^{a}W$, ${}^{b}W$ and ${}^{c}W$. We now calculate the POD of the first snapshot matrix:

$$ {}^{a}W \approx \left({}^{a}U\right)\left({}^{a}\Sigma\right)\left({}^{a}V^{T}\right) = \left({}^{a}U\right)\left({}^{a}\hat{V}^{T}\right) \tag{3.50} $$

In Equation (3.50) we have combined the POVs with the POC histories. Equation (3.50) is an approximation because we have kept only the k dominant POMs. We may approximate the snapshot matrix ${}^{b}W$ using the first set of POMs as

$$ {}^{b}W \approx \left({}^{a}U\right)\left({}^{a}U^{T}\right)\left({}^{b}W\right) \tag{3.51} $$

where the approximation is now transformed into the subspace spanned by the POMs ${}^{a}U$. We may rewrite Equation (3.51) as

$$ {}^{b}W \approx \left({}^{a}U\right)\left({}^{b}\hat{V}^{T}\right) \tag{3.52} $$

where ${}^{b}\hat{V}^{T}$ contains the time modulations of the POMs ${}^{a}U$ in the response ${}^{b}W$. Similarly, ${}^{c}W$ can be approximated by

$$ {}^{c}W \approx \left({}^{a}U\right)\left({}^{c}\hat{V}^{T}\right) \tag{3.53} $$

where

$$ {}^{c}\hat{V}^{T} = \left({}^{a}U^{T}\right)\left({}^{c}W\right) \tag{3.54} $$

Using the POV recalculation and single-load identification methods outlined in the previous sections, we now write each POC history as a superposition of free and forced responses:

$$ {}^{a}\hat{\mathbf{v}}_{i} = {}^{a}\sigma_{i,disp}\mathbf{v}_{i,disp} + {}^{a}\sigma_{i,vel}\mathbf{v}_{i,vel} + {}^{a}\tilde{\tilde{Q}}_{i}\mathbf{c}_{ii} \tag{3.55} $$

$$ {}^{b}\hat{\mathbf{v}}_{i} = {}^{b}\sigma_{i,disp}\mathbf{v}_{i,disp} + {}^{b}\sigma_{i,vel}\mathbf{v}_{i,vel} + {}^{b}\tilde{\tilde{Q}}_{i}\mathbf{c}_{ii} \tag{3.56} $$

$$ {}^{c}\hat{\mathbf{v}}_{i} = {}^{c}\sigma_{i,disp}\mathbf{v}_{i,disp} + {}^{c}\sigma_{i,vel}\mathbf{v}_{i,vel} + {}^{c}\tilde{\tilde{Q}}_{i}\mathbf{c}_{ii} \tag{3.57} $$

The modal forces used to form the matrices ${}^{a}\tilde{\tilde{Q}}_{i}$, ${}^{b}\tilde{\tilde{Q}}_{i}$ and ${}^{c}\tilde{\tilde{Q}}_{i}$ are all computed using the POMs ${}^{a}U$. The terms $\mathbf{v}_{i,disp}$ and $\mathbf{v}_{i,vel}$ are POC histories for calculating the response to initial displacements and velocities, respectively. The term $\mathbf{c}_{ii}$ may be considered a discretized modal impulse response function. We wish to solve for $\mathbf{v}_{i,disp}$, $\mathbf{v}_{i,vel}$, and $\mathbf{c}_{ii}$ as they will allow us to predict system responses to new initial displacements, initial

velocities, and loads, respectively. However, Eqs. (3.55) - (3.57) represent only three matrix equations and there are nine matrix unknowns.

Additional equations may be found by considering the initial displacement and velocity profiles used to generate ${}^{a}W$, ${}^{b}W$ and ${}^{c}W$. We can compute the ratio of two displacement related POVs as

$$\frac{{}^{a}\sigma_{i,disp}}{{}^{b}\sigma_{i,disp}} = \frac{\left({}^{a}\mathbf{u}_i^T\right)\left({}^{a}\mathbf{w}_0\right)/\nu_{i,0,disp}}{\left({}^{a}\mathbf{u}_i^T\right)\left({}^{b}\mathbf{w}_0\right)/\nu_{i,0,disp}} = \frac{\left({}^{a}\mathbf{u}_i^T\right)\left({}^{a}\mathbf{w}_0\right)}{\left({}^{a}\mathbf{u}_i^T\right)\left({}^{b}\mathbf{w}_0\right)} \tag{3.58}$$

Similarly, the remaining displacement POV ratio and the velocity POV ratios can be computed as

$$\frac{{}^{a}\sigma_{i,disp}}{{}^{c}\sigma_{i,disp}} = \frac{\left({}^{a}\mathbf{u}_i^T\right)\left({}^{a}\mathbf{w}_0\right)}{\left({}^{a}\mathbf{u}_i^T\right)\left({}^{c}\mathbf{w}_0\right)} \tag{3.59}$$

$$\frac{{}^{a}\sigma_{i,vel}}{{}^{b}\sigma_{i,vel}} = \frac{\left({}^{a}\mathbf{u}_i^T\right)\left({}^{a}\dot{\mathbf{w}}_0\right)}{\left({}^{a}\mathbf{u}_i^T\right)\left({}^{b}\dot{\mathbf{w}}_0\right)} \tag{3.60}$$

$$\frac{{}^{a}\sigma_{i,vel}}{{}^{c}\sigma_{i,vel}} = \frac{\left({}^{a}\mathbf{u}_i^T\right)\left({}^{a}\dot{\mathbf{w}}_0\right)}{\left({}^{a}\mathbf{u}_i^T\right)\left({}^{c}\dot{\mathbf{w}}_0\right)} \tag{3.61}$$

The final two equations are obtained by recalling the orthonormality of POC histories:

$$\mathbf{v}_{\mathrm{i,disp}}^T\mathbf{v}_{i,disp} = 1 \tag{3.62}$$

$$\mathbf{v}_{\mathrm{i,vel}}^T\mathbf{v}_{i,vel} = 1 \tag{3.63}$$

Eqs. (3.55) - (3.63) represent a system of linear equations that may be solved to obtain $\mathbf{v}_{i,disp}$, $\mathbf{v}_{i,vel}$, and $\mathbf{c}_{ii}$ for i = 1, 2, …, k. Once these quantities are obtained they may be used as explained in the previous sections to predict the response of the system to any combination of initial displacements or applied loads.

If mixed response data are used to predict the response to initial velocities then the method given in Section 3.2.1 must be modified slightly. In Section 3.2.1 the initial time derivative of each POC history was calculated from Equation (3.18). If mixed response data are used to identify $\mathbf{v}_{i,vel}$ then the initial time derivative $\dot{v}_{i,0,vel}$ can not be calculated in the same way because there are no POVs directly corresponding to $\mathbf{v}_{i,vel}$. In this case, however, we can approximate $\dot{v}_{i,0,vel}$ a

$$\dot{v}_{i,0,vel} \approx \frac{v_{i,vel}(t_2) - v_{i,vel}(t_1)}{\Delta t} \tag{3.64}$$

The MR method is described in a flowchart in Fig. 3.6 below.

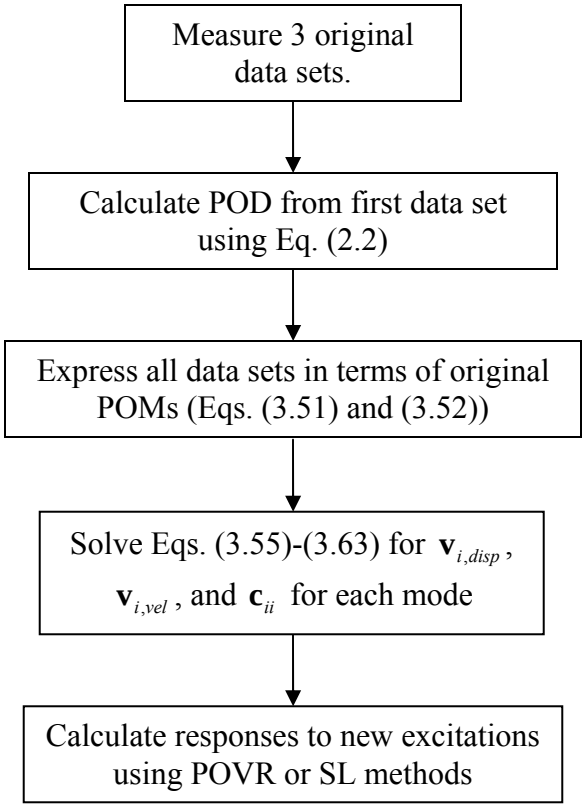

Fig. 3.6 Flowchart for MR Method

3.5 Deconvolution and Least Squares Methods

The methods given in Sections 3.3 and 3.4 for forced and mixed responses both involve solving deconvolution problems. This section reviews the difficulties associated with the deconvolution of noisy signals and describes the total least squares method for calculating acceptable solutions in the presence of noise. Although the existing literature does not discuss a matrix-vector deconvolution problem (such as exists in Eq. (3.48)), all of the principles discussed in this section apply equally well to a matrix-vector deconvolution. An excellent review of deconvolution theory is given in [59]; this section will provide a summary of the theory and its associated difficulties and then introduce the total least squares method as an appropriate solution technique.

The convolution of two signals $h(t)$ and $x(t)$ in the time domain is given by

$$y(t) = \int_0^t h(t-\tau)x(\tau)d\tau = \int_0^t x(t-\tau)h(\tau)d\tau \tag{3.65}$$

and is usually symbolized by the '*' operator:

$$y(t) = h(t) * x(t) = x(t) * h(t) \tag{3.66}$$

Deconvolution is the procedure of determining $h(t)$ from knowledge of $x(t)$ and $y(t)$. Deconvolution has no direct mathematical definition in the time domain other than being the inverse of Eq. (3.65). In the frequency domain, however, convolution is expressed as multiplication

$$Y(j\omega) = H(j\omega)X(j\omega) \tag{3.67}$$

and deconvolution is performed by division of frequency spectra:

$$H(j\omega) = \frac{\mathrm{Y}(j\omega)}{\mathrm{X}(j\omega)} \tag{3.68}$$

With exact knowledge of $x(t)$ and $y(t)$, deconvolution is possible and $h(t)$ can be determined exactly in the frequency domain from Eq.. (3.52) or in the time domain by solving a system of linear equations as in Eq. (3.43). In practice, however, $x(t)$ and $y(t)$ are not known exactly, but are obtained from noisy measurements. The measured signals, denoted $x_w(t)$ and $y_w(t)$, can be expressed as

$$x_w(t) = x(t) + x_e(t) \tag{3.69}$$

$$y_w(t) = y(t) + y_e(t) \tag{3.70}$$

where $x_e(t)$ and $y_e(t)$ are unknown error components. Expressing the true signals in terms of measured and error components into Eq. (3.67) yields

$$Y_w(j\omega) - Y_e(j\omega) = H(j\omega)\left[X_w(j\omega) - X_e(j\omega)\right] \tag{3.71}$$

Eq. (3.71) cannot be solved for $H(j\omega)$ because the error components are unknown. Instead, we solve for

$$H_w(j\omega) = \frac{\mathrm{Y_w}(j\omega)}{\mathrm{X_w}(j\omega)} \tag{3.72}$$

which may or may not be a good approximation to $H(j\omega)$. In fact, we can examine the approximation by rewriting Eq. (3.71) and comparing it with Eq. (3.72). The approximation is

$$H(j\omega) = \frac{\mathrm{Y}(j\omega)}{\mathrm{X}(j\omega)} = \frac{\mathrm{Y_w}(j\omega) - \mathrm{Y_e}(j\omega)}{\mathrm{X_w}(j\omega) - \mathrm{X_e}(j\omega)} \approx \frac{\mathrm{Y_w}(j\omega)}{\mathrm{X_w}(j\omega)} = H_w(j\omega) \tag{3.73}$$

Unfortunately, there are several situations where this approximation fails, resulting in a very poor estimate of $H(j\omega)$. First, there are regions where $X(j\omega)$ may be very small (and, from Eq. (3.67), $Y(j\omega)$ is small as well). The resulting approximations that $X(j\omega) \approx X_w(j\omega)$ and $Y(j\omega) \approx Y_w(j\omega)$ are then likely to be inaccurate and the ratio $Y_w(j\omega)/X_w(j\omega)$ may be orders of magnitude off [59]. Another special case is where

$X(j\omega) = -X_e(j\omega)$, resulting in infinite values for $H_w(j\omega)$. These errors in $H_w(j\omega)$ may dominate the entire behavior of the time-domain signal, obscuring all meaningful details of $h_w(t)$[59].

Although this description has utilized the frequency-domain form of deconvolution in Eq. (3.68) for explanation, the same errors exist when deconvolution is performed entirely in the time domain [59]. Due to these errors, the deconvolution problem cannot be solved uniquely and is therefore often referred to as "ill-conditioned" or "ill-posed" [60]. It is possible, however, to calculate an acceptable estimate for $h_w(t)$ using least squares methods [58].

We recall that the deconvolution problem for single- and multiple-load methods can be solved by solving the linear systems in Eqs. (3.27) and (3.32), respectively. A general system of linear equations may be written as

$$A\underline{x} = \underline{b} \tag{3.74}$$

where $A \in \Re^{n \times n}$ is called the data matrix $\underline{b} \in \Re^{n \times 1}$ is typically known as a vector of observations. If the system represents the structural deconvolution problems in Eqs. (3.43) and (3.48), then A corresponds to a modal force and $\underline{b}$ corresponds to a POC history, which is calculated from measured displacements. Therefore, uncertainty in force and displacement measurements result in errors in A and $\underline{b}$, respectively.

The least squares approach to deconvolution considers only errors in $\underline{b}$ and may be cast in terms of calculating $\underline{x}_{LS}$ [58] such that

$$A\underline{x}_{LS} = \underline{b} + \underline{r} \tag{3.75}$$

where we minimize $\|\underline{r}\|_2$ subject to the constraint that $\underline{b} + \underline{r} \in Range(A)$. In other words, we allow $\underline{b}$ to vary the minimum amount required so that it falls in the column space of A. The solution may be computed as

$$\underline{x}_{LS} = \left(A^T A\right)^{-1} A^T \underline{b} = A^+ \underline{b} \tag{3.76}$$

where A^+ is the Moore-Penrose pseudoinverse of A. If measurement errors are present in the displacements only and the applied is known exactly then a least-squares estimate will yield an accurate response prediction [58].

The total least squares method is designed for application when errors in both A and $\underline{b}$ are significant and can be posed as solving for $\underline{x}_{TLS}$ such that

$$(A + E)\underline{x}_{TLS} = \underline{b} + \underline{r} \tag{3.77}$$

and for which we minimize $\|[E\,|\,\underline{r}]\|_F$ subject to $\underline{b} + \underline{r} \in Range(A + E)$, where $\|\cdot\|_F$ signifies the Frobenius norm. The total least squares problem is "equivalent to the problem of solving a nearest least squares problem of minimizing $\|(A + E)\underline{x} - (\underline{b} + \underline{r})\|_2$

where nearness is measured by the…Frobenius norm" [58]. We may calculate $\underline{x}_{TLS}$ by first forming an augmented matrix C:

$$C = \left[A \middle| \underline{b}\right] \tag{3.78}$$

Reference [58] shows that if the singular value decomposition of C is computed as

$$C = U_C \Sigma_C V_C^T \tag{3.79}$$

then a total least squares solution may be calculated from the *r* most dominant right singular vectors of C:

$$\underline{x}_{TLS} = \frac{\left(\sum_{i=1}^{r} V_{C,n+1,i} \begin{bmatrix} V_{C,1,i} & V_{C,2,i} & \cdots & V_{C,n,i} \end{bmatrix}^T \right)}{\left(1 - \sum_{i=1}^{r} V_{C,n+1,i}^2 \right)} \tag{3.80}$$

Reference [58] gives a method for choosing a value for *r* based on the signal-to-noise ratio of the measured data.

Finally, we note that the proposed algorithm for total least squares from [58] assumes that weighting matrices for the problem are equal to the identity matrix. A more general total least squares method is formulated by solving Eqn. (3.77) while minimizing $\left\| D\left[E \middle| \underline{r} \right] T \right\|_F$, where D and T are diagonal weighting matrices with positive diagonal terms. It is possible, perhaps even probable, that non-identity weighting matrices will yield a more accurate solution, but this topic is left for future research.

3.6 Sources of Error

Several types of error will be present in predictions made with the POD-based methods presented in this section. This section discusses four probably sources of error, namely projection error, diagonalization error, linearization error, and deconvolution error.

The first type of error is called “projection” error because the original problem is projected onto a reduced subspace spanned by a limited set of dominant POMs. Because of this projection, the model can only accurately predict a response matrix that may be spanned by the original set of POMs. If a new excitation is introduced that generates a response that cannot be expressed by the original POMs then the prediction will be inaccurate. An extreme example arises when a model constructed from a response that is restricted to one plane is used to predict the response an excitation that excites motion that is restricted to a perpendicular plane. In this case, the measured POMs are entirely unable to represent the responses to these new initial conditions and the method predicts no response at all. Therefore, when constructing the model it is desirable to use a response to that exhibits a wide variety of motion in order to generate POMs that can represent responses to a large selection of new excitations.

Projection error is also encountered when a limited set of POMs is used as a basis for model reduction (linear or nonlinear). Despite the presence of this error, POMs are often used for model reduction and it is assumed that the error will be low. Currently there is no satisfactory method for estimating this error ahead of time, although an attempt has been made in [46]. Their method estimates an upper bound for the projection error, but

they assume that the new excitation is similar to the original one and admit that the method is invalid for excitations that are substantially different. Because there is no indication of how similar is similar enough, the method has no guarantee of accuracy.

Another source of error for several of the methods lies in the assumption that the matrices $\Phi_{11}(t)$, $\Phi_{12}(t)$, and $C(t)$ are diagonal. In reality, structures will not generally meet the conditions required for these matrices to be diagonal and the resulting error is called "diagonalization" error. The mass matrix of almost any real structure will not be proportional to the identity matrix (e.g. even the mass matrix for a beam element is not diagonal). The damping of a system may also be heavy and the damping matrix is generally not proportional to a linear combination of the mass and stiffness matrices. When the conditions are not met exactly then the accuracy of the method will suffer. However, the damping may be light and the mass matrix may be diagonally dominant with diagonal terms that are similar even if they are not identical. In these cases the solution may be accurate enough that it may be appropriate to use methods that assume diagonal $\Phi_{11}(t)$, $\Phi_{12}(t)$, and $C(t)$ matrices.

When the methods are applied to nonlinear systems, a linear time-varying model is obtained that will match the measured nonlinear response exactly. For nonlinear systems, a new excitation can result in a significant change in the natural frequencies of the system and/or cause the system exhibit new behaviors [10, 11]. The model constructed from these linear methods will be unable to predict these new effects and we call the resulting error "linearization" error. However, the model may be used to accurately predict the

structure's response to an excitation that is "nearby" the original one. This error is inherent in using linear methods to identify nonlinear systems, but may be acceptable when nonlinear methods cannot be applied due to difficulties described in Chapter 2.

Another manifestation of linearization error occurs when multiple data sets are used to construct the model. When these methods are applied to identify a linear time-varying system, each data set results from a system that varies with time in the same way over time, i.e. the time variance repeats itself in each data set. Nonlinear systems will exhibit different time-varying behaviors in each data set and therefore all of the data sets cannot be represented by the same linear time-varying system. The methods, then, will identify an "average" linear time-varying system in the sense that it contains characteristics from each measured response and can reconstruct all of the original responses accurately (as long as they can be accurately expressed by the chosen POMs). When the methods are applied to predict the response to a new excitation, amplitude errors may present that result from a combination of periodic signals of varying frequencies. Due to the differences in frequencies, each signal will move in and out of phase with the others and the combined signal will exhibit amplitude distortions as a result (this is analogous to averaging two sine waves of slightly different frequencies). This error will grow with the strength of the nonlinearities in the system because the frequency content in each data set will differ more in the presence of strong nonlinearities than weak ones.

Finally, as explained in the previous section, the deconvolution operations in the forced and mixed response methods cannot be performed exactly when noise is present in the

data. The magnitude of this error will depend on the quality of the data and is likely to be very high if the data are very noise. As with linearization error for multiple data sets, an interesting compromise arises because of the deconvolution and projection error. In order to minimize projection error, one may desire to use a large number of POMs in the identification methods. Unfortunately, this will generally lead to higher deconvolution error because the noise level is higher in the lower POMs and POC histories.

3.7 Summary

This chapter has explained the theory behind five methods for identification of linear time-varying systems. The methods extend the capabilities beyond other existing methods in that they may be applied to multiple-input multiple-output systems, they require only a small number of data sets, and no knowledge regarding the form of the time variance in the structure is necessary to obtain a predictive model.

The methods are summarized in Table 3.1 below. The methods are referred to as POVR, MDS, SL, ML, and MR for the Proper Orthogonal Value Recalculation", "Multiple Data Set", "Single-Load", "Multiple-Load", and "Mixed Response" methods, respectively. The table shows the excitation type each method is valid for, and types of error that are expected to be present in the methods' predictions for linear systems (other than errors related to noise in the data). These error types are abbreviated as "Proj" for projection error and "Diag" for diagonalization error. The table also shows the number of data sets (NDS) required be each method, as well as any assumptions made by the method other than that the system is linear.

Table 3.1 Summary of Proposed System Identification Methods

Method	**Excitation Type**	**Error**	**NDS**	**Assumptions**
POVR	Initial Conditions	Proj, Diag	1	Diagonal $\Phi_{11}(t)$ or $\Phi_{12}(t)$
MDS	Initial Conditions	Proj	*k*	None
SL	Loads	Proj, Diag	1	Diagonal $C(t)$
ML	Loads	Proj,	*k*	None
MR	Both	Proj, Diag	3	Diagonal $C(t)$, $\Phi_{11}(t)$ and $\Phi_{12}(t)$

4. Numerical Examples

This chapter applies the methods described in Chapter 3 to three beam models and a satellite truss model. The strengths and weakness of each method when applied to various types of systems are then discussed at the end of the chapter.

4.1 Beam Models

The three beam models are shown in Fig. 4.1. The first model is a linear time-invariant (LTI) undamped cantilever beam. Next, a time-varying tip mass is attached to the tip of the beam to convert it to a linear time-varying (LTV) system. The LTI beam is also converted to a nonlinear (NL) system by attaching a cubic spring to the tip. A dashpot is also attached to the nonlinear beam to simulate damping. All of the beam models were made of steel ($E = 29\times10^6$ psi, ρ = 500 lbm/ft^3) and had dimensions of 24 x 1 x 0.75 inches. Finite element (FE) models were created for each beam using 24 beam elements. The spring force (over the tip displacement range seen in simulations) for the nonlinear beam is shown in Fig. 4.2 and the time variance in the tip mass for the second beam is shown in Fig. 4.3 along with their respective governing equations. The value of the dashpot was 0.2 lbf-s/in.

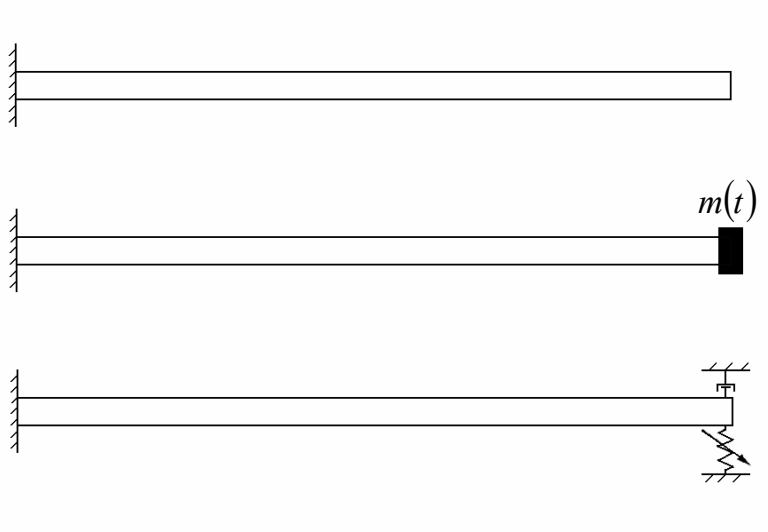

Fig. 4.1 LTI (top), LTV (middle), and NL (bottom) Beam Models

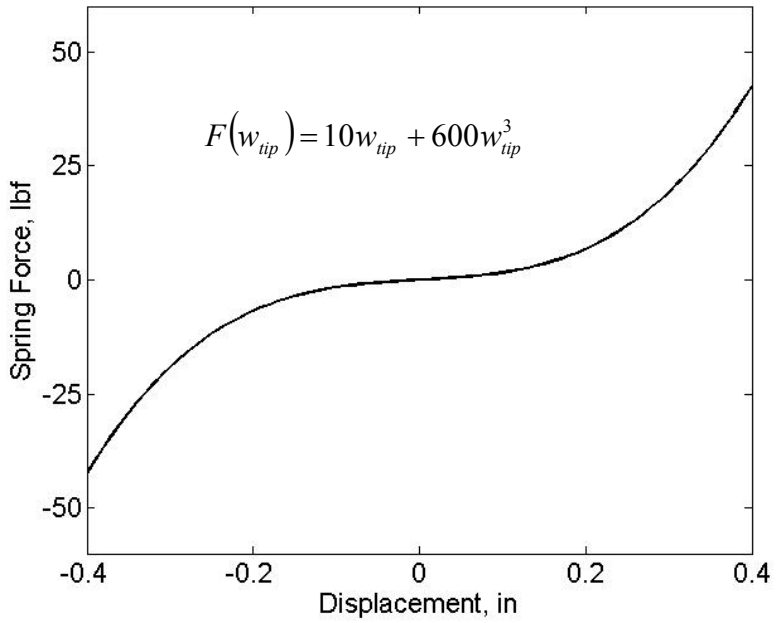

Fig. 4.2 Cubic Spring Force for Nonlinear Beam Model

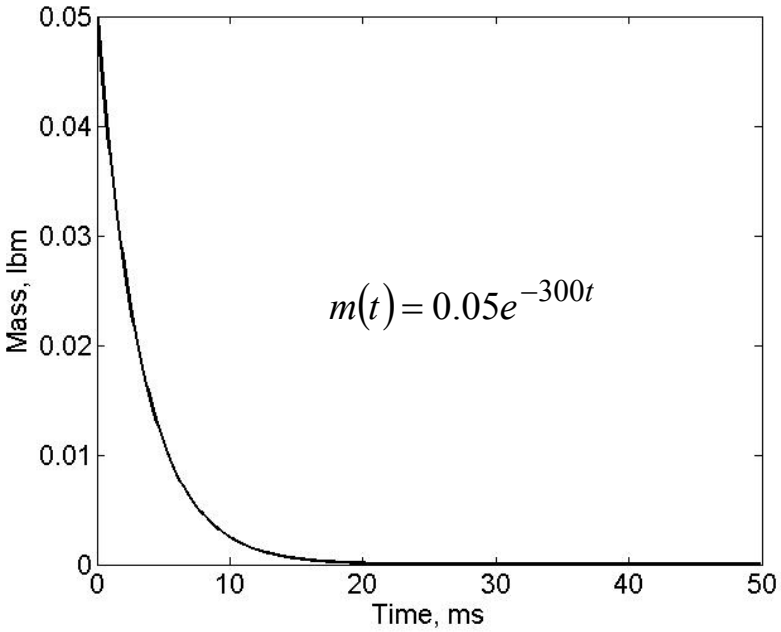

Fig. 4.3 Time Variation of Tip Mass for LTI Beam Model

The Newmark method [61] was applied to simulate the exact response of each beam model to various excitations and the appropriate methods were applied to predict the response of the beam to new free, forced, or mixed responses as shown in the respective following sections.

4.1.1 Free Response

The FE models were used to simulate the exact response of each model beam model to four initial displacement profiles, shown in Fig. 4.4. Each displacement profile was generated by applying static loads to the LTI beam. The displacement profile $\mathbf{w}_0$ was generated by applying static loads of 300, 200, and -260 lbf at locations 17, 18, and 24 inches from the root of the beam. Profiles $\mathbf{w}_1$ and $\mathbf{w}_2$ were formed by applying static loads of 100 and -300 lbf at locations 24 and 8 inches from the root of the beam,

respectively. Finally, the initial displacement profile $\mathbf{w}_3$ was formed by applying loads of 2000 and -1300 lbf at locations 14 and 18 inches from the beam root. The free responses of each model to each initial displacement were simulated for 0.05 seconds (approximately twice the fundamental period of 0.0238 seconds for the linear beam) and the vertical displacements at 25 points were captured at every time step (0.1 milliseconds) to form W. Thus the dimensions of W were (25 x 500) for both models.

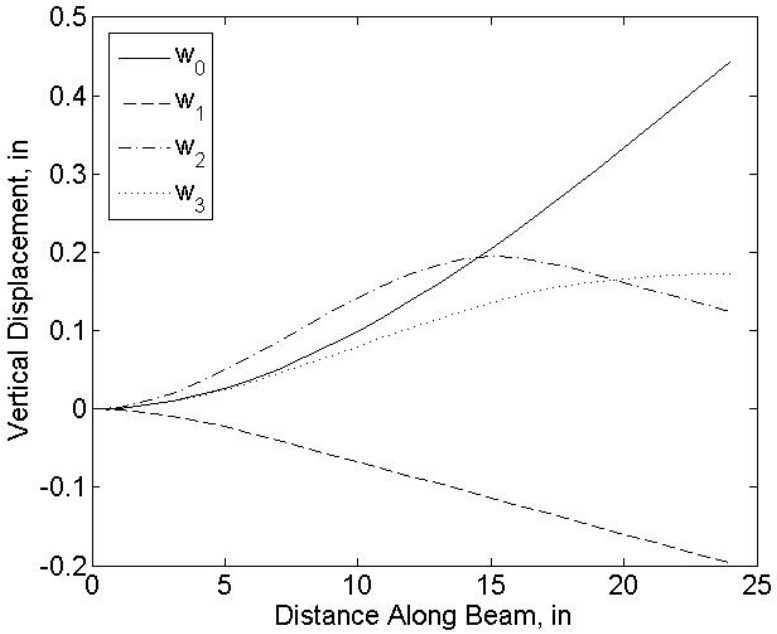

Fig. 4.4 Applied Initial Displacement Profiles

Next, the POD was computed from each beam's response to $\mathbf{w}_0$ and the method of POV recalculation (POVR) was applied to simulate the responses of each of the beams to initial displacement profile $\mathbf{w}_3$. The free response method using multiple data sets (MDS) was also applied to predict the response to $\mathbf{w}_3$ using the responses to initial displacement profiles $\mathbf{w}_1$ and $\mathbf{w}_2$ as supplementary data sets. The responses were simulated using the first three POMs, which corresponded to 99% of the signal energy in the LTI beam's

response to $\mathbf{w}_0$. The three most dominant original POVs (calculated from the measured response to $\mathbf{w}_0$) and recalculated POVs (for the response to $\mathbf{w}_3$) are shown in Fig. 4.5 for the LTI beam. The "index" on the horizontal axis simply denotes the order of each POV in dominance (i.e. the largest POV is first, the second-largest POV is second and so on). The original POVs drop off very quickly, showing that only a few POMs are necessary to represent the measured response accurately. This figure also illustrates how the significance of each mode changes in response to the different initial displacement profiles. For example, the first POV for both beams is larger in response to $\mathbf{w}_0$ than to $\mathbf{w}_3$, indicating that the first POM is more active in the response to $\mathbf{w}_0$ than to $\mathbf{w}_3$. The original and recalculated POVs for the LTV and NL beams show similar behaviors and are not shown.

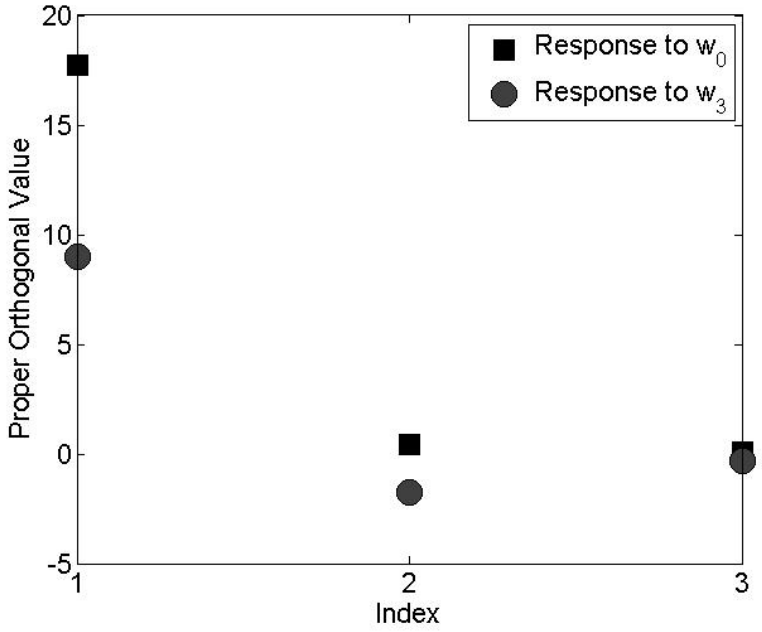

Fig. 4.5 Original and Recalculated POVs for Linear Beam Model

In order to represent the displacement of every point at each time step, a displacement norm is defined as:

$$\|\mathbf{w}[t_i]\|_2 = \sqrt{\mathbf{w}[t_i]^T \mathbf{w}[t_i]} \tag{4.1}$$

Direct comparison of time-series data is generally considered a very strict validation metric for a model, but is useful in this case because it can be used to express all of the prediction data in a single plot for easy comparison with 'exact' results from a finite element model. The displacement norms at each time step calculated by the FE models and the POVR and MDS methods for the linear beam responses to $\mathbf{w}_3$ are shown in Figs. 4.6 and 4.8 for the LTI and LTV beams, respectively. The percent errors in each prediction were calculated at each time step from the equation

$$PE[t_i] = 100\% \times \frac{\left| \|\mathbf{w}_{FE}[t_i]\|_2 - \|\mathbf{w}_{predicted}[t_i]\|_2 \right|}{\|\mathbf{w}_{FE}[t_i]\|_2} \tag{4.2}$$

and are shown in Figs. 4.7 and 4.9 for the LTI and LTV beams. These figures show that the MDS method predicts the displacements very accurately (nearly always < 5% error) for the linear beams in response to the new initial displacement profiles. Small inaccuracies exist in the MDS prediction are attributed to projection error, i.e. the POMs from the response to $\mathbf{w}_0$ are not optimal for predicting the response to $\mathbf{w}_3$. The percent error is relatively high at locations where the displacement norm of the FE model is close to zero, resulting in a very small number in the denominator of Eq. (4.2). The POVR method works very well for the LTI beam, although it is not as accurate as the MDS method due to the diagonalization error described in Section 3.6. For the LTV beam,

however, the POVR method does not provide an accurate prediction. The diagonalization error for the LTV beam is expected to be much greater because the large value of the tip mass results in a mass matrix with diagonal terms that are not close in value.

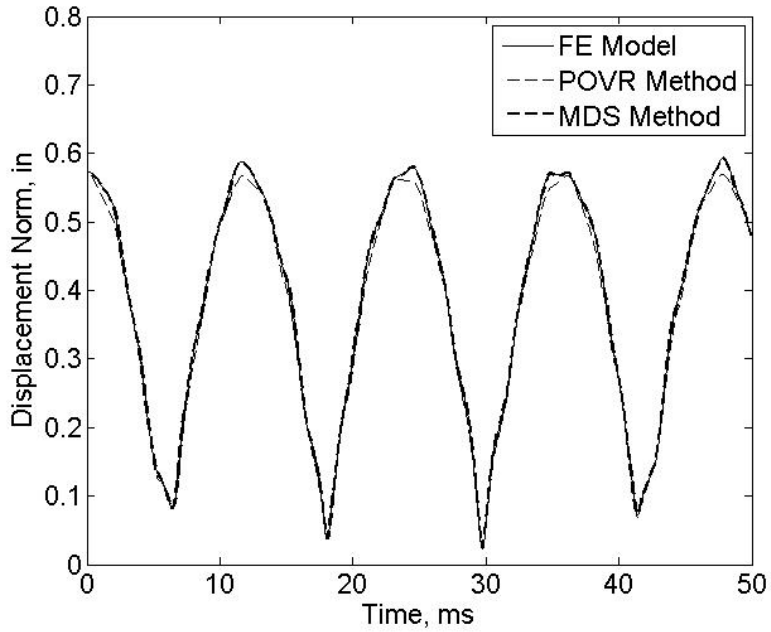

Fig 4.6 Displacement Norms for LTI Beam Model in Response to $\mathbf{w}_3$

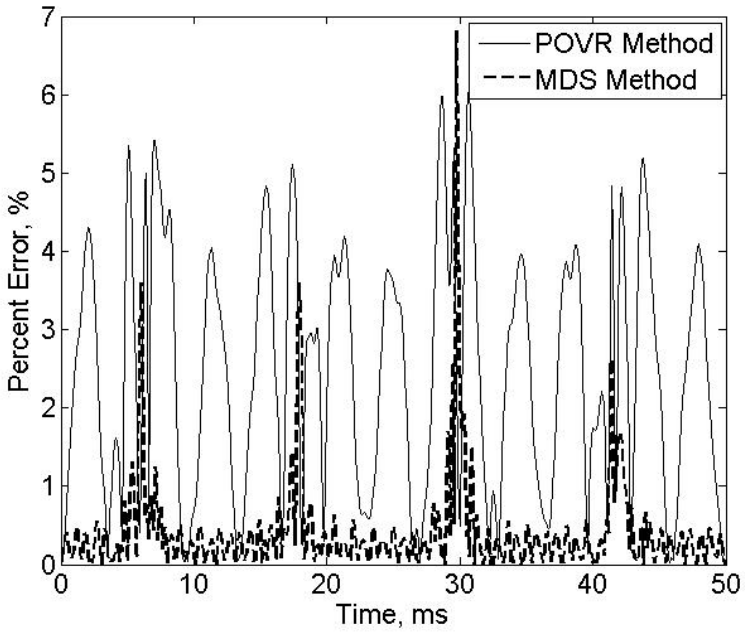

Fig. 4.7 Percent Error of Displacement Norms for LTI Beam Model in Response to $\mathbf{w}_3$

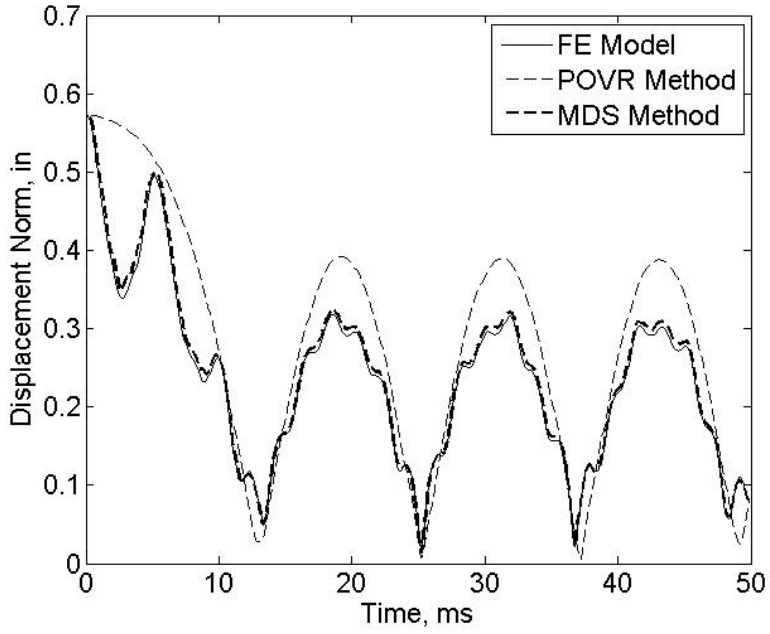

Fig. 4.8 Displacement Norms for LTV Beam Model in Response to $\mathbf{w}_3$

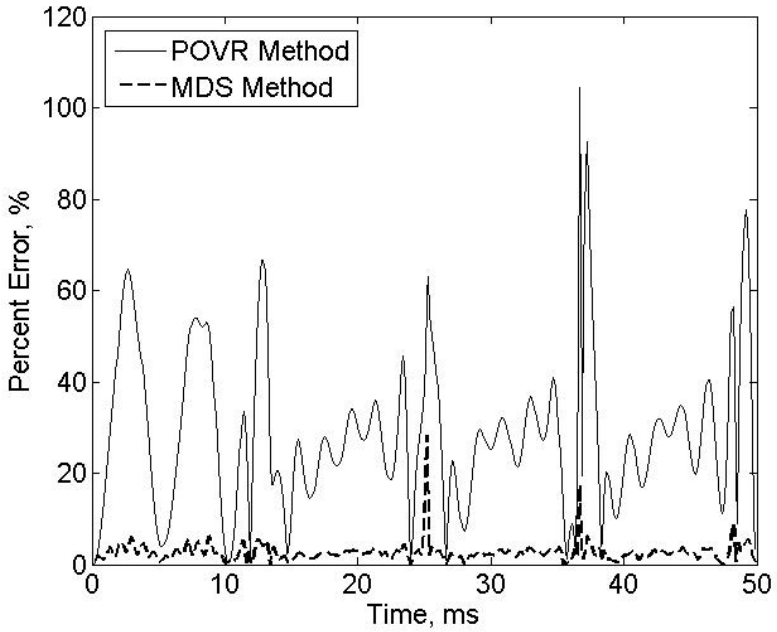

Fig. 4.9 Percent Error of Displacement Norms for LTV Beam Model in Response to $\mathbf{w}_3$

The displacement norms and corresponding percent errors for the nonlinear beam's response to $\mathbf{w}_3$ are shown in Figs. 4.10 and 4.11. It is very apparent that, in this case, significant errors exist in the predictions generated by both the POVR and MDS methods. Frequency errors exist in both predicted responses, and significant amplitude errors are present in the MDS method's response. The frequency errors result in phase shifts that increase with time and are visible in the percent error plots as the error increases in magnitude over time. Both the frequency and amplitude discrepancies are most likely manifestations of linearization error, i.e., they can be attributed to the fact that the natural frequencies of the nonlinear beam change with each new initial condition and the POD-based methods are unable to reproduce (POVR and MDS methods) or interpret (MDS method) the changing frequencies appropriately. The significant amplitude errors in the response predicted by the MDS method result from the method attempting to create an

"average" time-varying model from periodic signals of different frequencies. The various responses are out of phase with each other and their combination results in the amplitude distortions that are present. For this model and the corresponding excitation sets, the POVR method is actually more accurate than the MDS method. Projection error (for both methods) and diagonalization error (for the POVR method) are both present as well, but they are dwarfed by the linearization error.

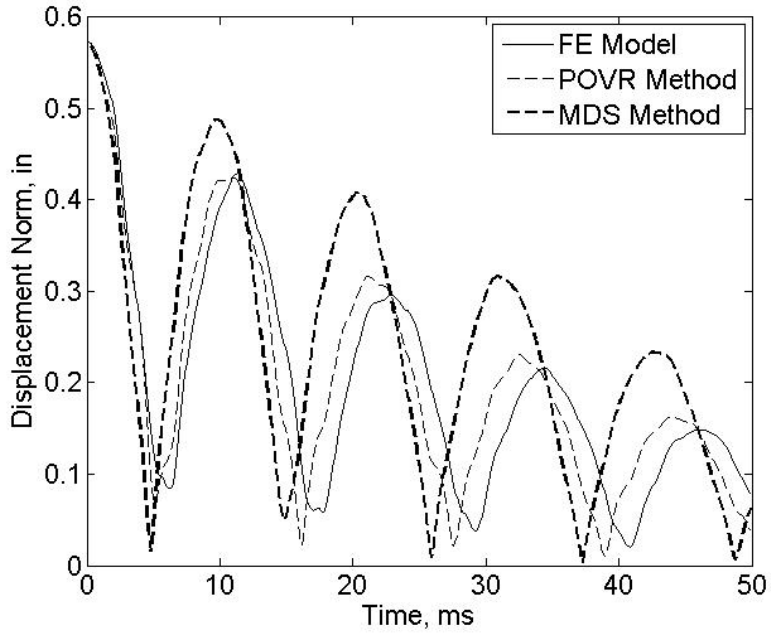

Fig. 4.10 Displacement Norms for NL Beam Model in Response to $\mathbf{w}_3$

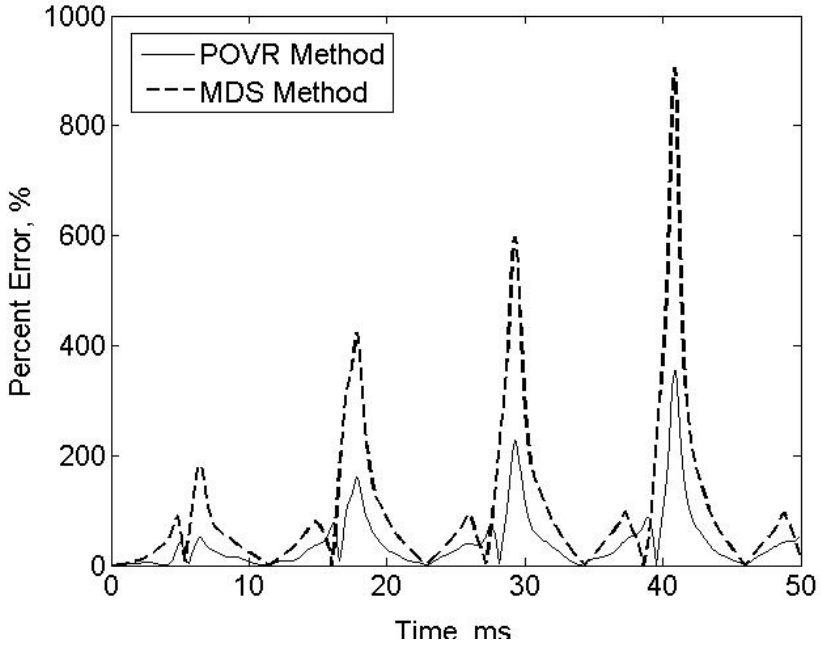

Fig. 4.11 Percent Error of Displacement Norms for NL Beam Model in Response to $\mathbf{w}_3$

Next, we applied the methods described in Section 3.2 to the three beam models (Fig. 4.1) to predict the initial velocity response of each beam. As with the initial displacement example, FE models for each beam were used to simulate the exact response of each beam to multiple initial velocity profiles, shown in Fig. 4.12. The initial velocity profiles were constructed by applying 1000-lbf impulses to locations 19, 15, 11, 7, and 3 inches from the root of the LTI beam and measuring the resulting velocity changes. Four POMs and POC histories (capturing 99% of the original signal energy) were obtained from the response of each model to the initial velocity profile $\dot{\mathbf{w}}_0$ and used to predict responses to $\dot{\mathbf{w}}_4$ for each beam using both the POVR and MDS methods. The maximum tip displacements of the nonlinear beam in response to $\dot{\mathbf{w}}_0$, $\dot{\mathbf{w}}_1$, $\dot{\mathbf{w}}_2$, $\dot{\mathbf{w}}_3$, and $\dot{\mathbf{w}}_4$ were 0.30, 0.26, 0.18, 0.10, and 0.03 inches, respectively, so that the nonlinear spring was excited at various levels of its nonlinear range.

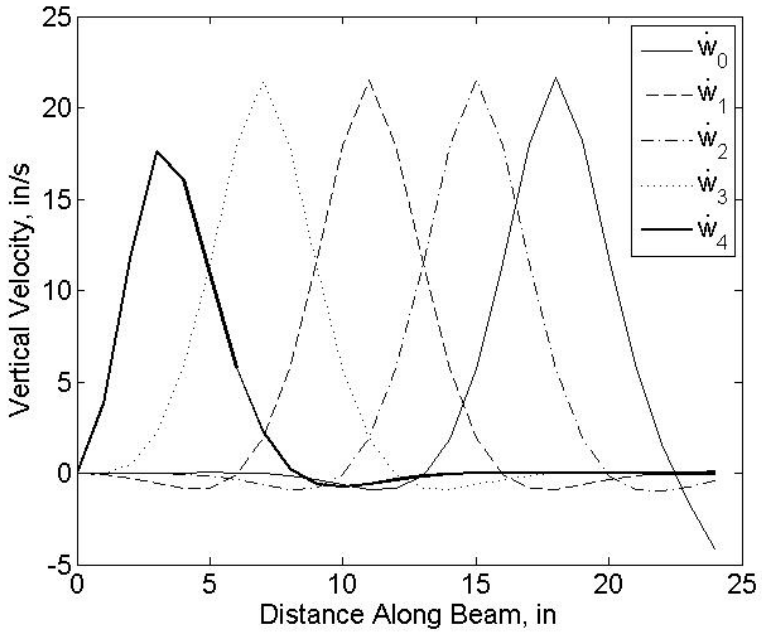

Fig. 4.12 Applied Initial Velocity Profiles

The displacement norms and error percentages (compared with FE model results) in predicted by the POD methods are plotted in Figs. 4.13 and 4.14 for the LTI beam. These figures show the same trend that was visible for in the LTI beam's response to initial displacements: the MDS method is more accurate than the POVR method because the mass matrix for the LTI beam is not proportional to the identity matrix. Overall, however, the errors are higher than was observed for initial displacements. This error increase is attributed to an increase in projection error, e.g. the POMs that comprise 99% of the energy in response to $\dot{\mathbf{w}}_0$ are insufficient to predict the response to $\dot{\mathbf{w}}_4$ with greater accuracy than shown in Fig. 4.13.

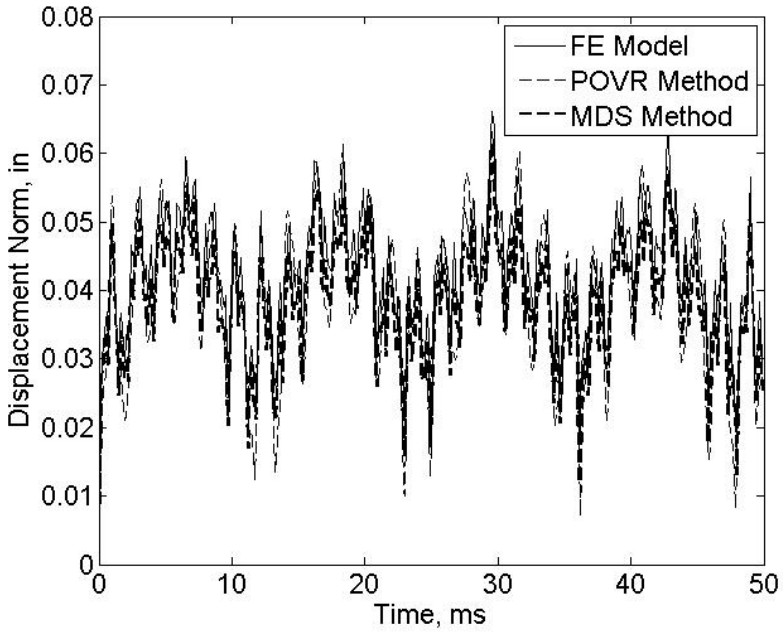

Fig. 4.13 Displacement Norm for LTI Beam Model in Response to $\dot{\mathbf{w}}_4$

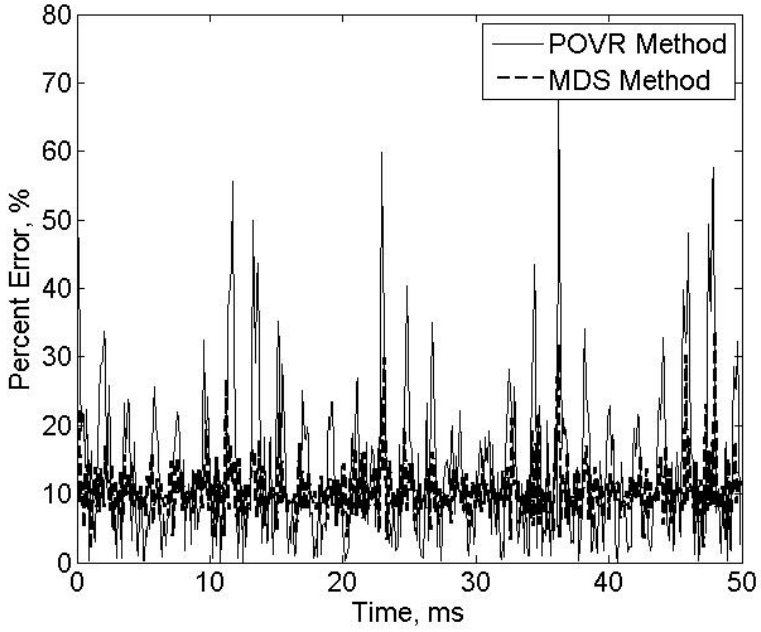

Fig. 4.14 Percent Error of Displacement Norms for LTI Beam Model in Response to $\dot{\mathbf{w}}_4$

Figs. 4.15 and 4.16 show the response predictions and percent errors for the LTV beam. Again, the error is higher using the POVR method than the MDS method, likely because

the large mass at the tip of the beam increases the diagonalization error. The level of error for the MDS method in this response is approximately the same as for the LTI beam, and is attributed to projection error.

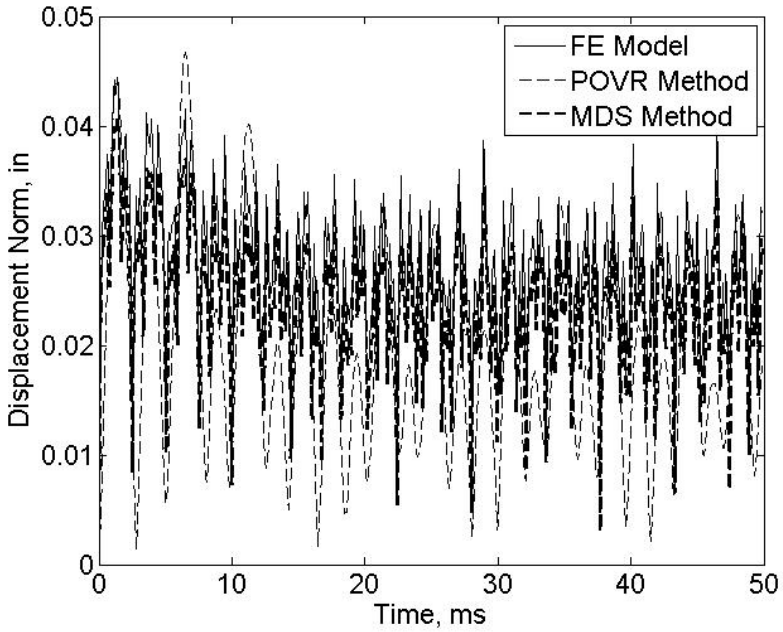

Fig. 4.15 Displacement Norm for LTV Beam Model in Response to $\dot{w}_4$

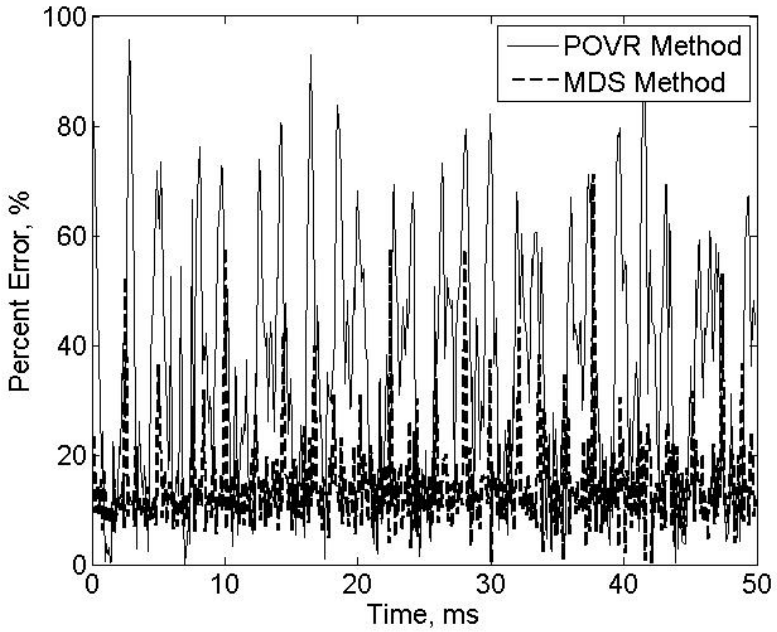

Fig. 4.16 Percent Error of Displacement Norms for LTV Beam Model in Response to $\dot{\mathbf{w}}_4$

The response predictions generated by the POVR and MDS methods for the nonlinear beam are compared with finite element model predictions in Figs. 4.17 and 4.18 below. Both response predictions exhibit a slight frequency error (the increasing phase difference between signals is visible in the percent error plot for the MDS method as the error increases over time) and is assumed to be a result of linearization effects. The linearization error is also present for the POVR method but it is difficult to see in the percent error plot because errors associated with diagonalization are also present.

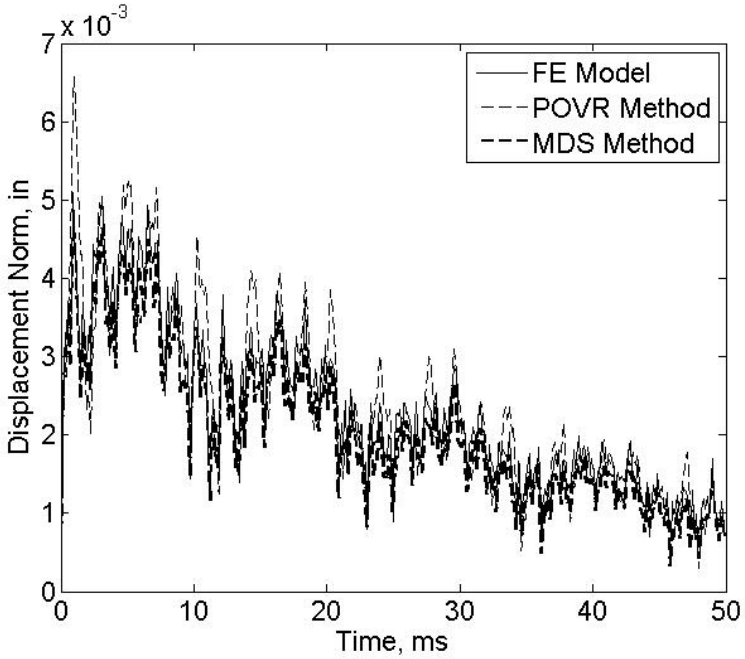

Fig. 4.17 Displacement Norm for NL Beam Model in Response to $\dot{\mathbf{w}}_4$

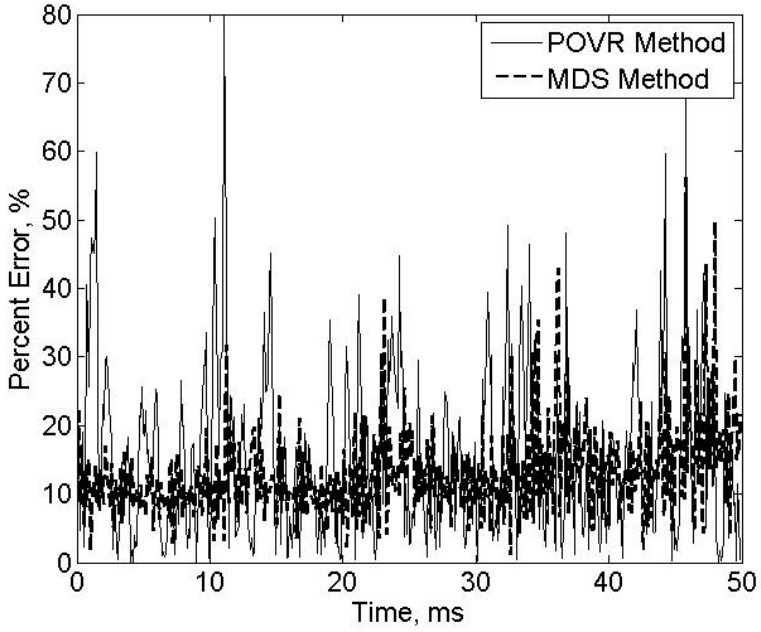

Fig. 4.18 Percent Error of Displacement Norms for NL Beam Model in Response to $\dot{\mathbf{w}}_4$

4.1.2 Forced Response

This section describes the application of both the single- and multiple-load methods (see Section 3.2) to numerical models of the beams in Fig. 4.1. First, finite element models of the beams were used to simulate the exact response of each beam to a 500-lb vertical 0.5-millisecond pulse (see Fig. 4.19) applied at locations 2, 7, 11, 16, and 23 inches from the root of the beam, shown approximately as locations 1, 2, 3, 4, and 5 in Fig. 4.20. The pulse applied at point 1 is called load 1, the pulse applied at point 2 is called load 2, and so on for all five loads. The responses of each model to each force were simulated for 0.05 seconds and the vertical displacements at 25 points were captured every 0.1 milliseconds to form W. Thus the dimensions of W were (25 x 500) for all three beam models.

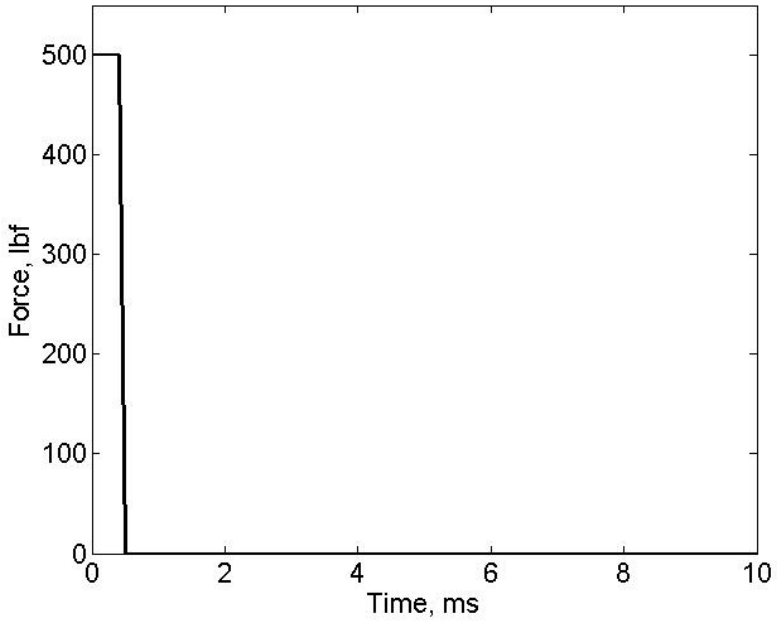

Fig. 4.19 Pulse Load Applied to Beam Models

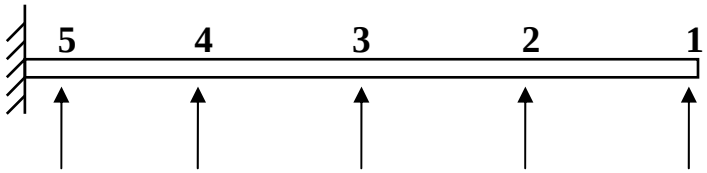

Fig. 4.20 Five Locations of Pulse Load Application

Next, the POD was computed for each beam from the response to load 1 and both the single-load (SL) and multiple-load (ML) methods were applied to simulate the responses of each beam to load 5. The first four POMs were considered, corresponding to 99% of the original signal energy. For the ML method, responses to loads 2, 3, and 4 were used as supplementary loads to solve for off-diagonal elements of $C(t)$.

The displacement norm at each time step was calculated for the FE results and the predictions obtained using the single-load (SL) and multiple-load (ML) methods. Fig. 4.21 shows the displacement norms for the LTI beam's response to load 5, and Fig. 4.22 shows the percent errors for displacement norms of the SL and ML methods. The figures show that while both methods are able to predict the displacement of the LTI beam accurately when compared with the FE model, the ML method is more accurate than the SL method. This accuracy difference is attributed to the fact that the beam does not have a mass matrix proportional to the identity matrix as the SL method assumes.

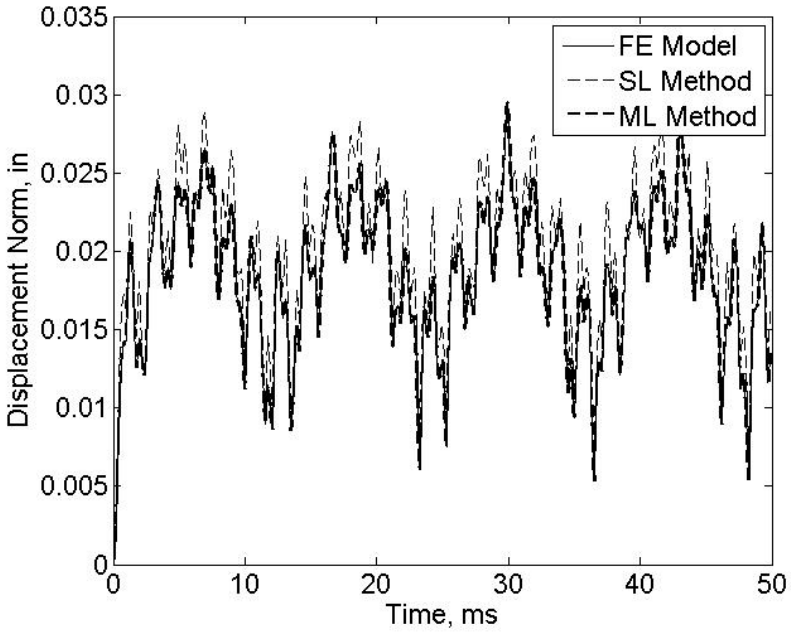

Fig 4.21 Displacement Norms for LTI Beam Response to Load 5

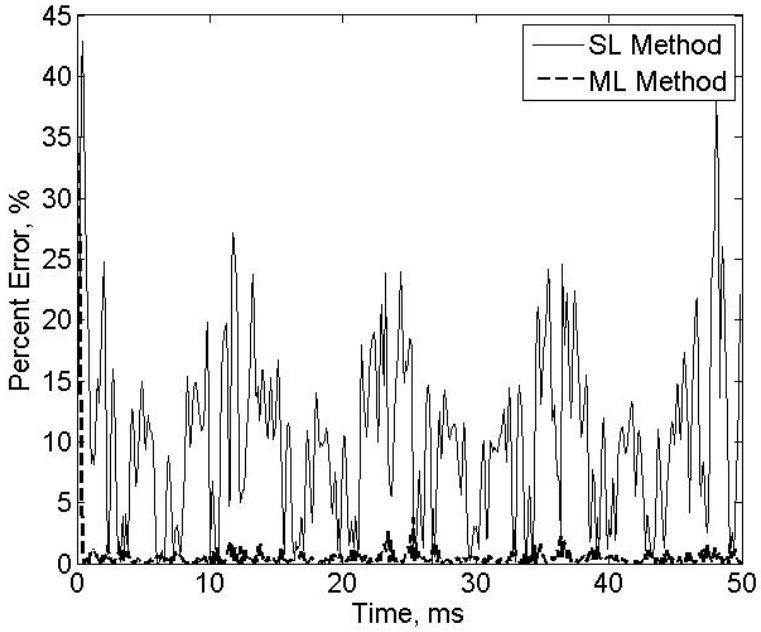

Fig. 4.22 Percent Error of Displacement Norms for LTI Beam Response to Load 5

The displacement norms and percent errors for the LTV beam are shown in Figs. 4.23 and 4.24 for both SL and ML methods. The figures show that although the ML method is

able to predict the displacement of the LTV beam very accurately when compared with the FE model, the SL method is terribly inaccurate. The large tip mass that is present in the LTV beam likely leads to very high diagonalization error when the SL method is applied.

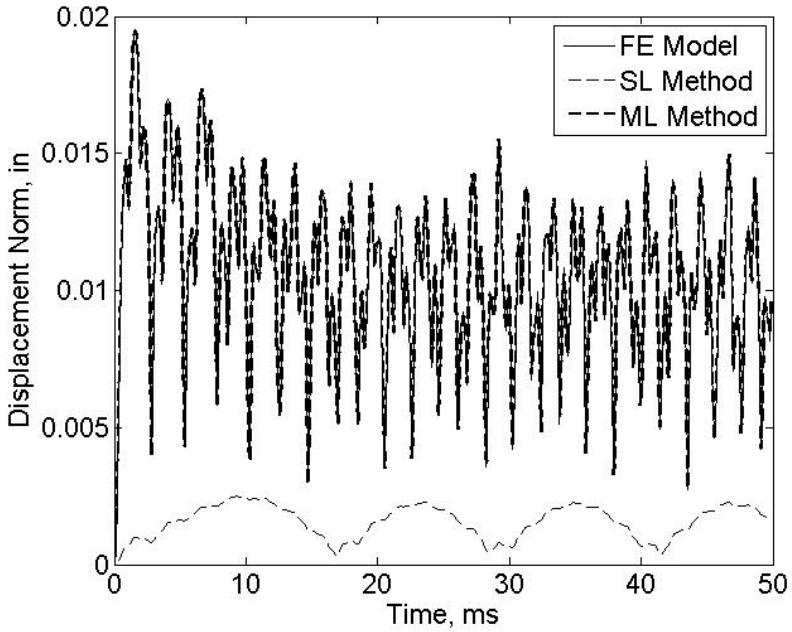

Fig 4.23 Displacement Norms for LTV Beam Response to Load 5

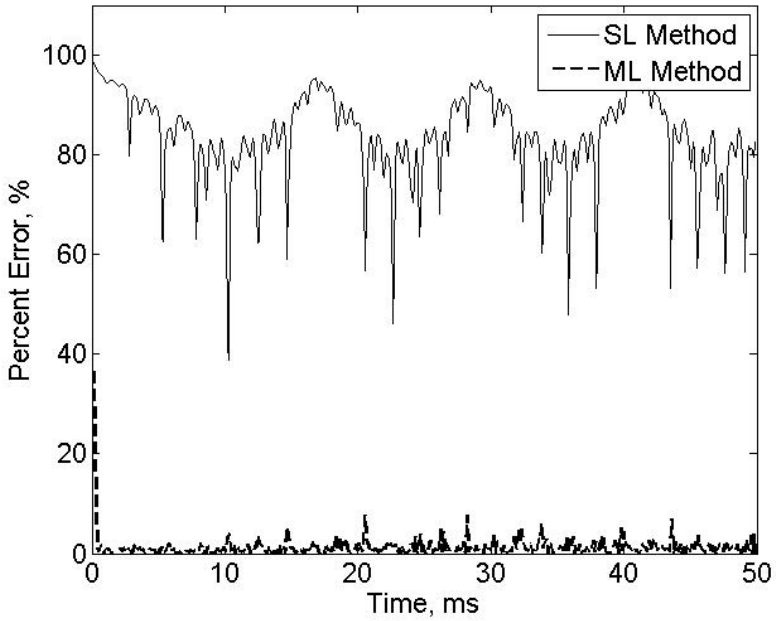

Fig. 4.24 Percent Error of Displacement Norms for LTV Beam Response to Load 5

The displacement norms for response of the NL beam are shown in Fig. 4.25, and the percent errors for both the SL and ML methods are shown in Fig. 4.26. The amplitude of the displacement norm decreases over time due to the damping effect of the dashpot. Again, the ML method provides a better prediction than the SL method because it does not assume a diagonal $C(t)$ matrix. The percent error for the ML method increases over time due to linearization error. Linearization error is, of course, also present for the SL method, but it is combined with diagonalization error and is more difficult to visualize in Fig. 4.26.

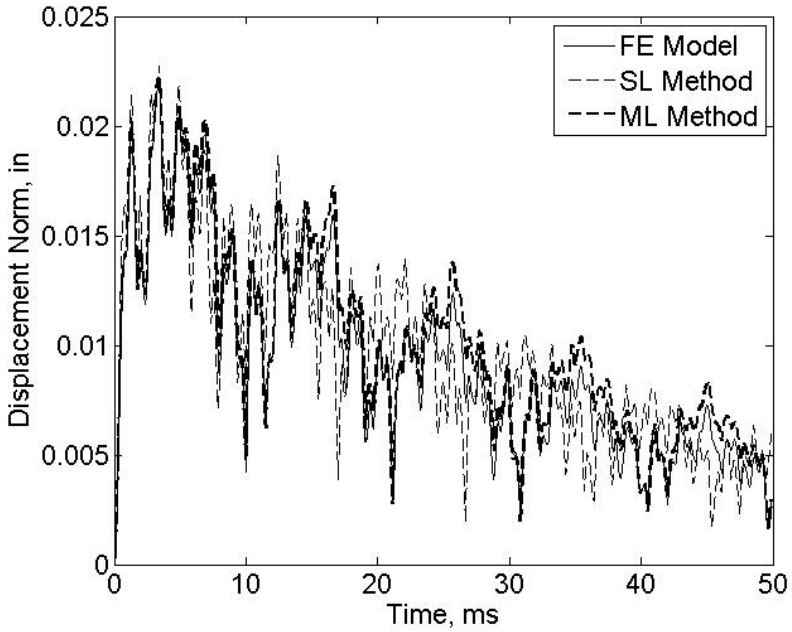

Fig 4.25 Displacement Norms for NL Beam Response to Load 5

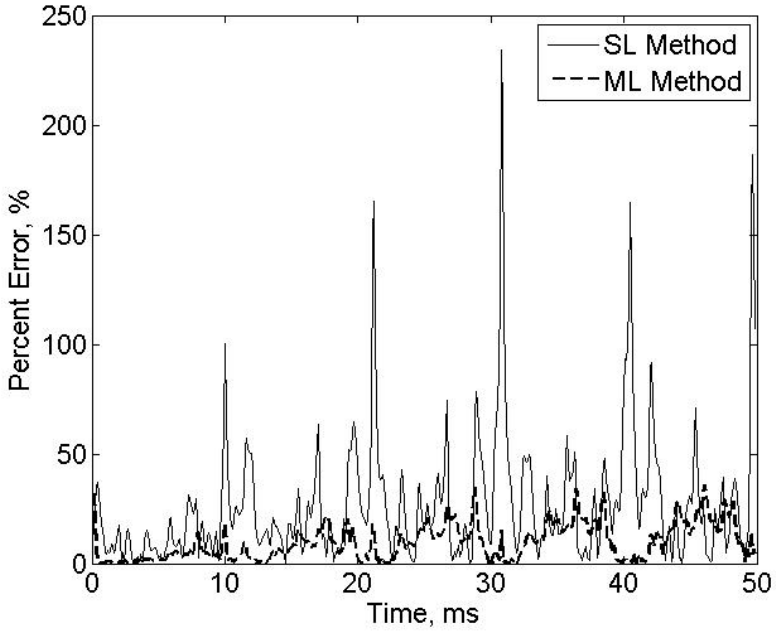

Fig. 4.26 Percent Error of Displacement Norms for NL Beam Response to Load 5

4.1.3 Mixed Response

This section applies the mixed response (MR) method described in Section 3.4 to the beam models in Fig. 4.1. The Newmark method was used to simulate the exact response of each model to three excitation sets consisting of initial displacements and velocities and an applied force. The initial displacement and velocity profiles for the beams are shown in Figures 4.27 and 4.28, respectively, and a 500-lb vertical pulse was applied for 0.5 millisecond (see Fig. 4.19) at locations 21, 12, and 3 inches from the beam root for respective excitation sets a, b, and c. The responses of each beam model to each excitation set were simulated for 50 milliseconds and the vertical displacements at 25 points along each beam were captured every 0.1 milliseconds to form W. Thus the dimensions of ${}^{a}W$, ${}^{b}W$ and ${}^{c}W$ were (25 x 500) for all beam models.

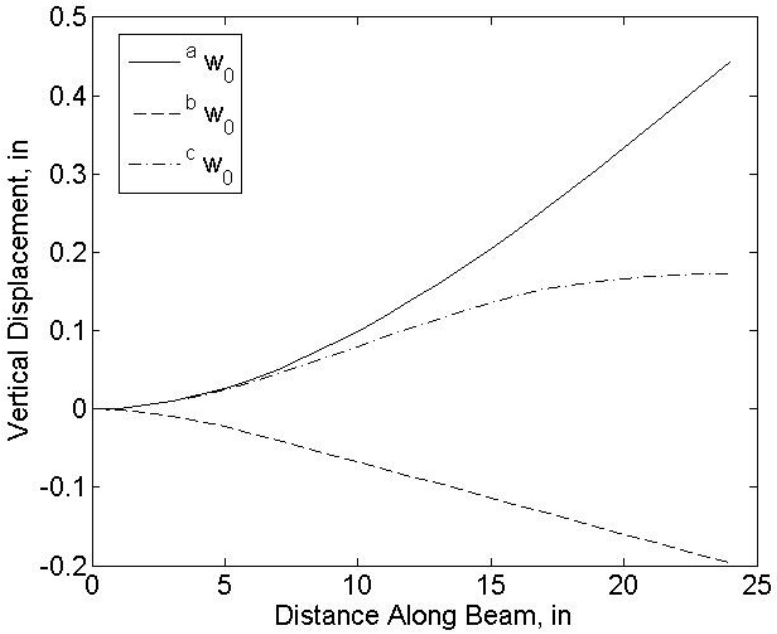

Fig. 4.27 Initial Displacements in Excitation Sets a, b, and c

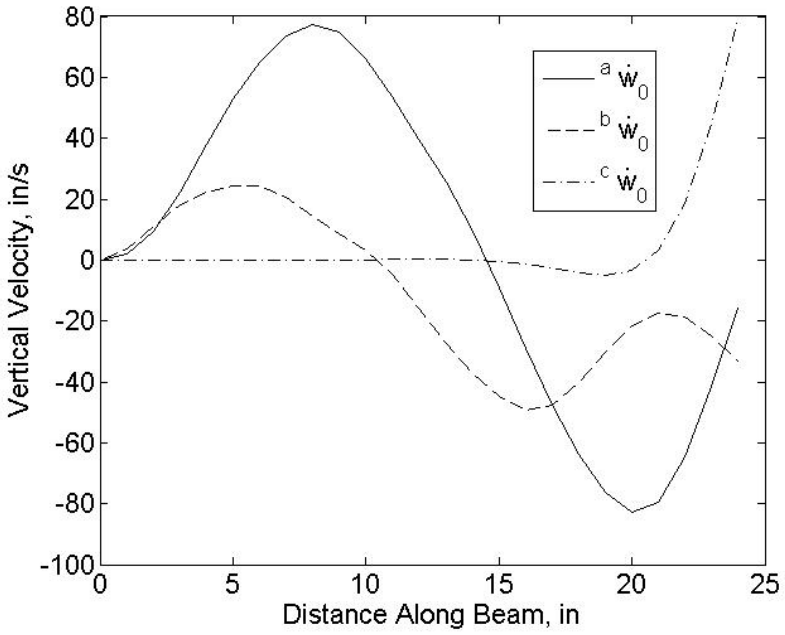

Fig. 4.28 Initial Velocities in Excitation Sets a, b, and c

Next, the POD was computed for each beam's response to the first excitation set and the MR method described in Section 3.4 was applied to identify $\mathbf{v}_{i,disp}$, $\mathbf{v}_{i,vel}$, and $\mathbf{c}_{ii}$ for each beam. These quantities were used to simulate the response of both systems to a new initial displacement $\tilde{\mathbf{w}}_0$, a new initial velocity $\dot{\tilde{\mathbf{w}}}_0$, and a new applied load $\tilde{F}(t)$, shown in Figures 4.29, 4.30, and 4.31, respectively. The responses were simulated using the first four POMs, which corresponded to 99% of the signal energy.

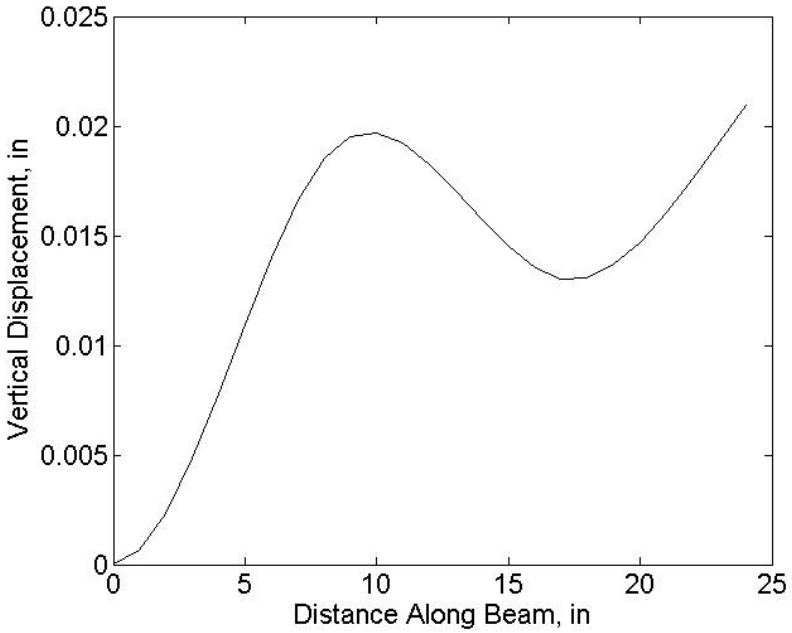

Fig. 4.29 New Initial Displacement Profile $\tilde{w}_0$

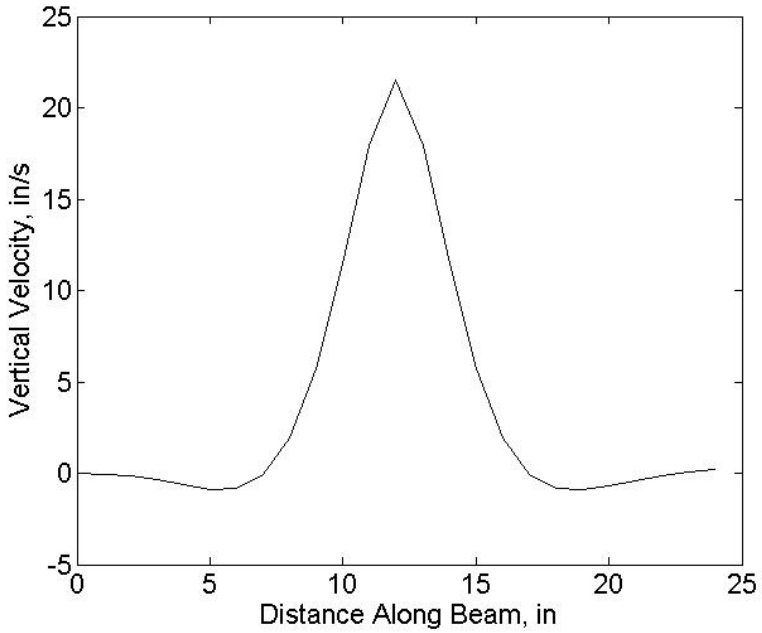

Fig. 4.30 New Initial Velocity Profile $\dot{\tilde{w}}_0$

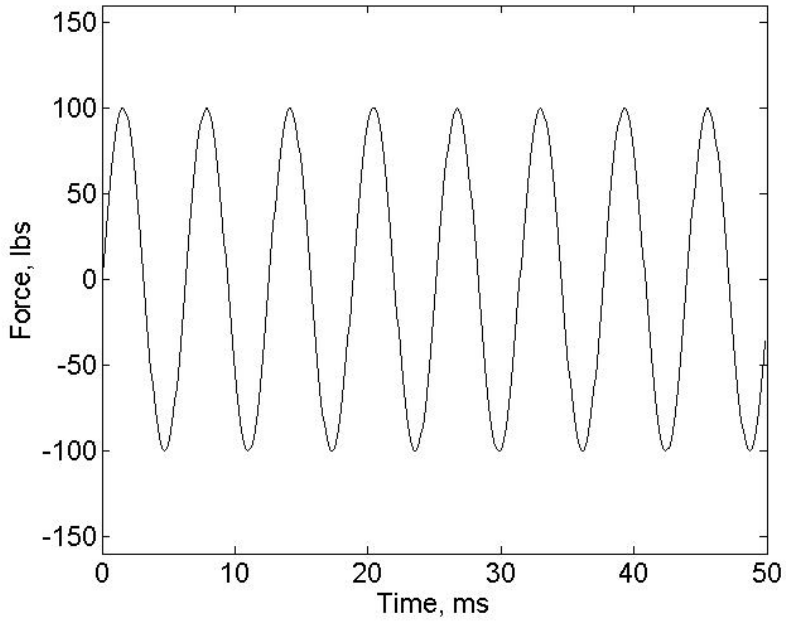

Fig. 4.31 New Load Applied Vertically at Beam Tip

The displacement norms at each time step calculated by the FE model and the MR method for response of the LTI beam to each excitation are shown in Figs. 4.32, 4.34 and 4.36, with respective error percentages in Figs. 4.33, 4.35, and 4.37. All six figures show that the POD-based model predicts the displacements satisfactorily (generally less than 20% error) for the LTI beam, but the errors are significant. The errors are attributed to a combination of projection and diagonalization error.

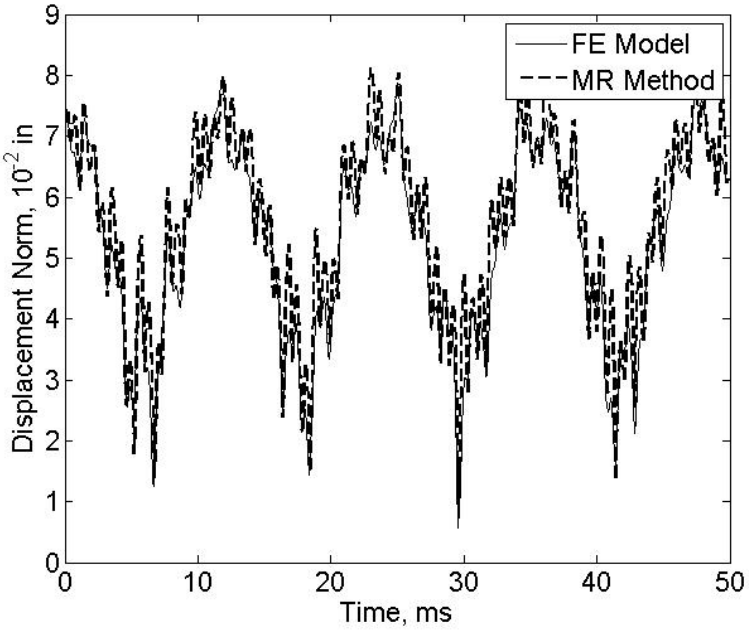

Fig. 4.32 Displacement Norms for LTI Beam in Response to $\tilde{\mathbf{w}}_0$

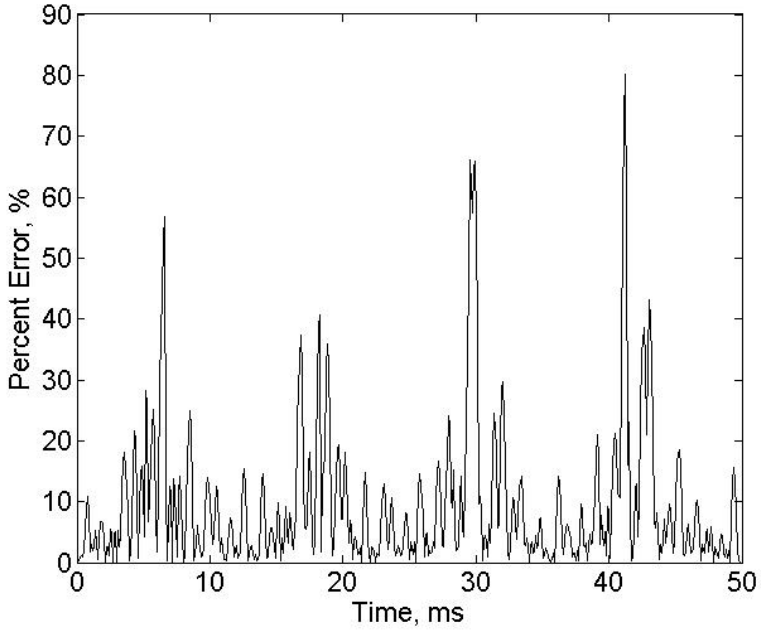

Fig. 4.33 Percent Error of Displacement Norms for LTI Beam in Response to $\tilde{\mathbf{w}}_0$

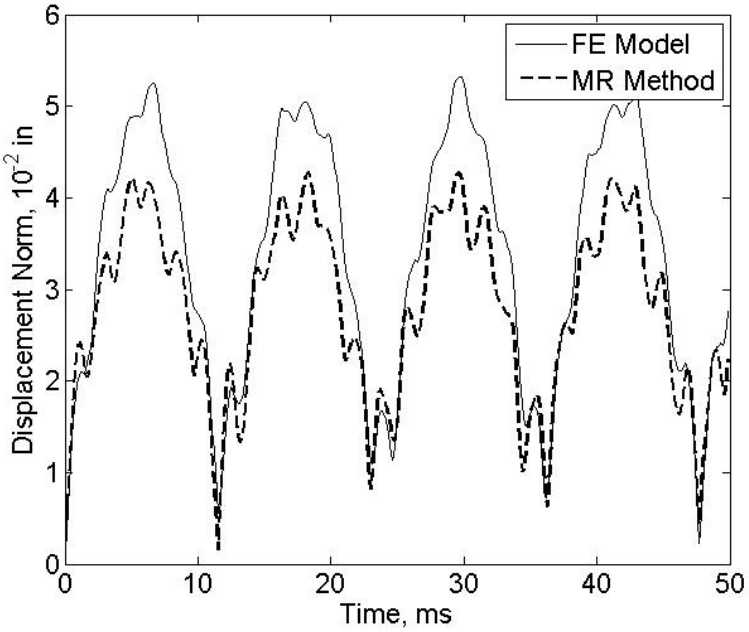

Fig. 4.34 Displacement Norms for LTI Beam in Response to $\dot{\tilde{\mathbf{w}}}_0$

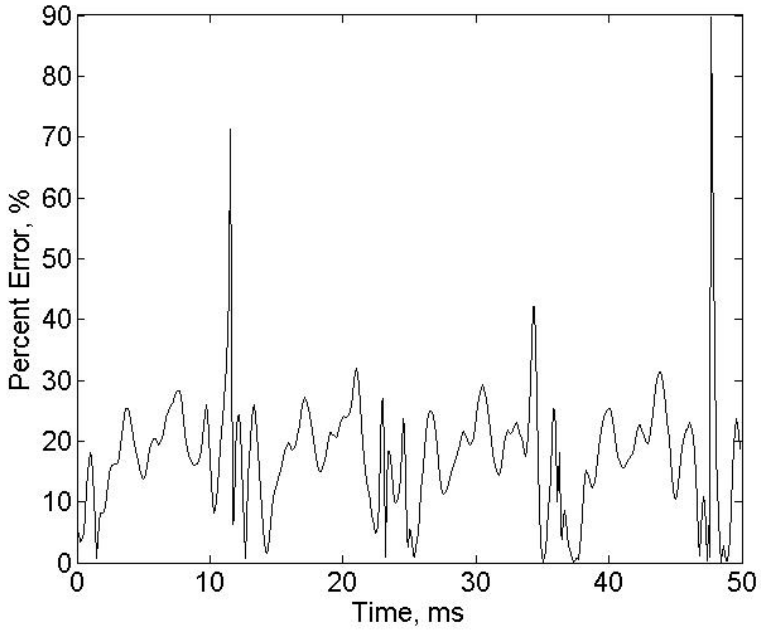

Fig. 4.35 Percent Error of Displacement Norms for LTI Beam in Response to $\dot{\tilde{\mathbf{w}}}_0$

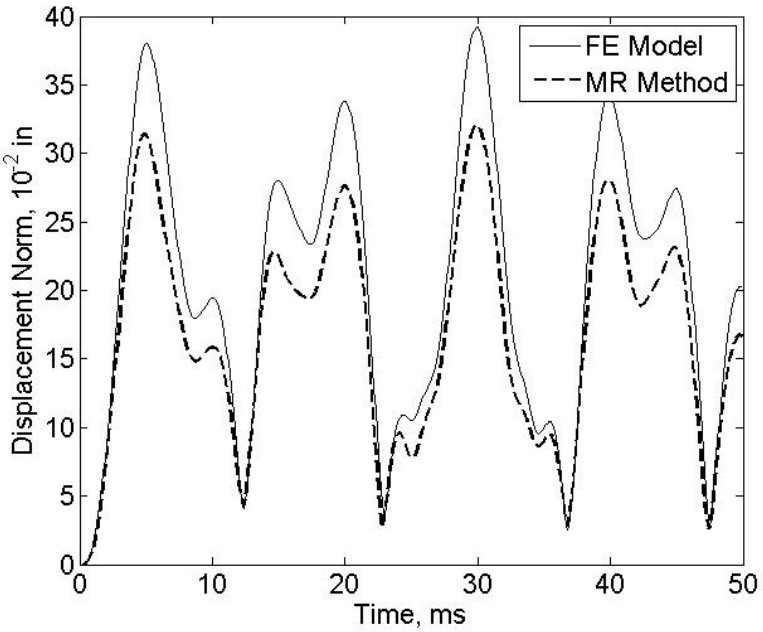

Fig. 4.36 Displacement Norms for LTI Beam in Response to $\widetilde{F}(t)$

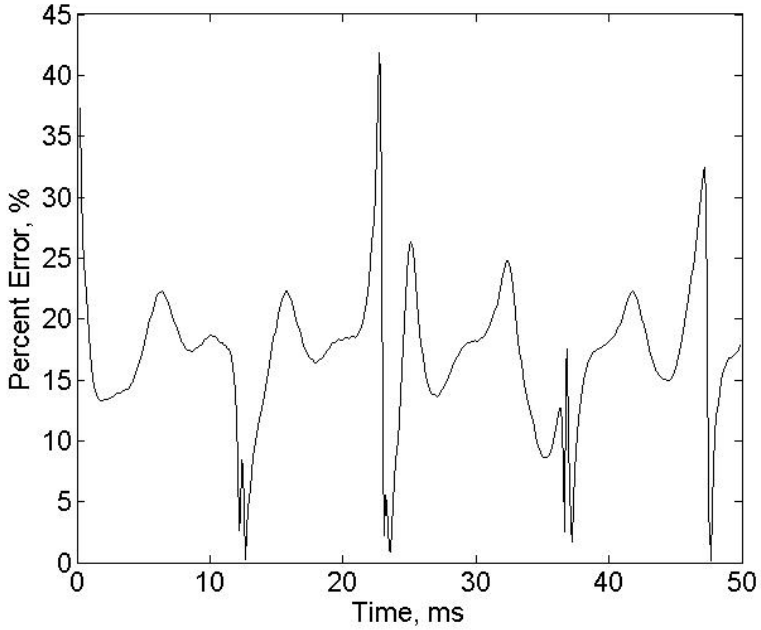

Fig. 4.37 Percent Error of Displacement Norms for LTI Beam in Response to $\widetilde{F}(t)$

The displacement norms at each time step calculated by the FE model and the MR method for the LTV beam are shown in Figs. 4.38, 4.40, and 4.42 for the responses to the initial displacement, initial velocity, and load, respectively. The corresponding error percentages are shown in Figs. 4.39, 4.41, and 4.43. The figures show that MR method does not provide good predictions for the LTV beam model for any of the excitations, particularly the response to the initial velocity and applied load. These high errors are attributed to the fact that the tip mass causes high diagonalization error.

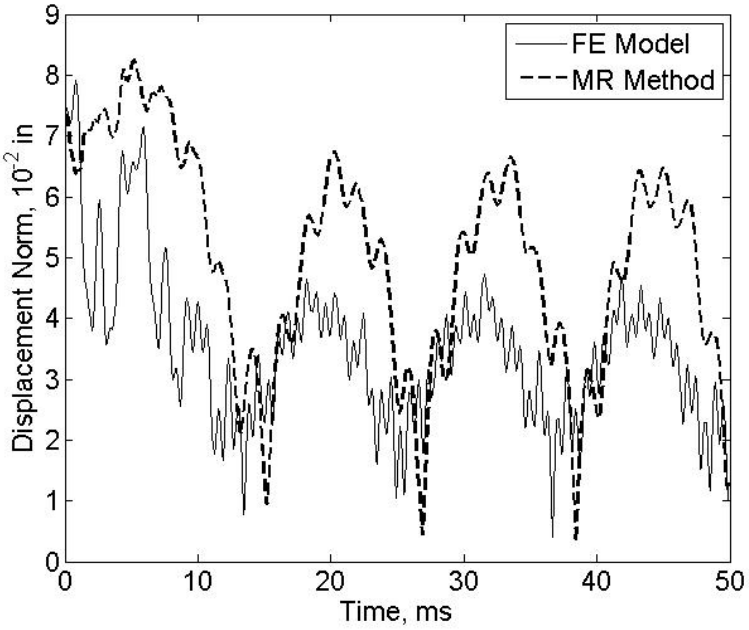

Fig. 4.38 Displacement Norms for LTV Beam in Response to $\widetilde{w}_0$

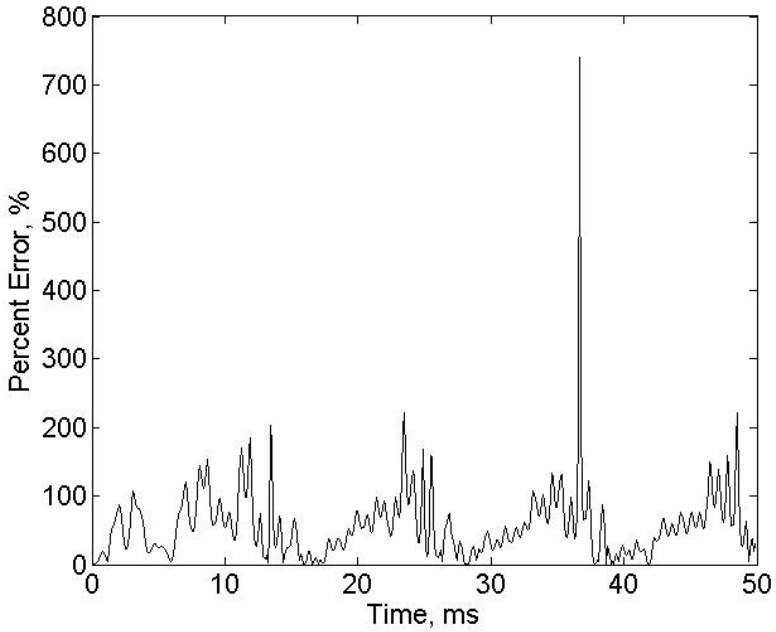

Fig. 4.39 Percent Error of Displacement Norms for LTV Beam in Response to $\tilde{\mathbf{w}}_0$

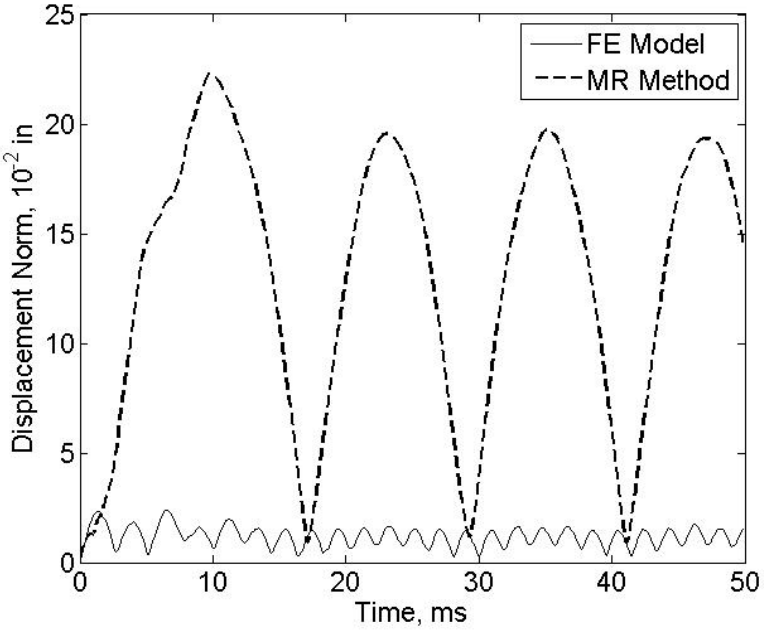

Fig. 4.40 Displacement Norms for LTV Beam in Response to $\dot{\tilde{\mathbf{w}}}_0$

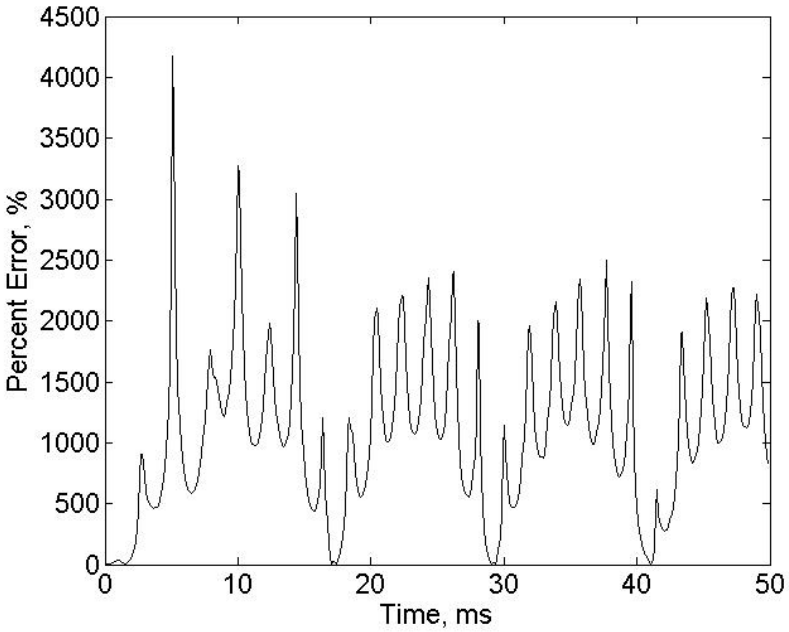

Fig. 4.41 Percent Error of Displacement Norms for LTV Beam in Response to $\dot{\tilde{\mathbf{w}}}_0$

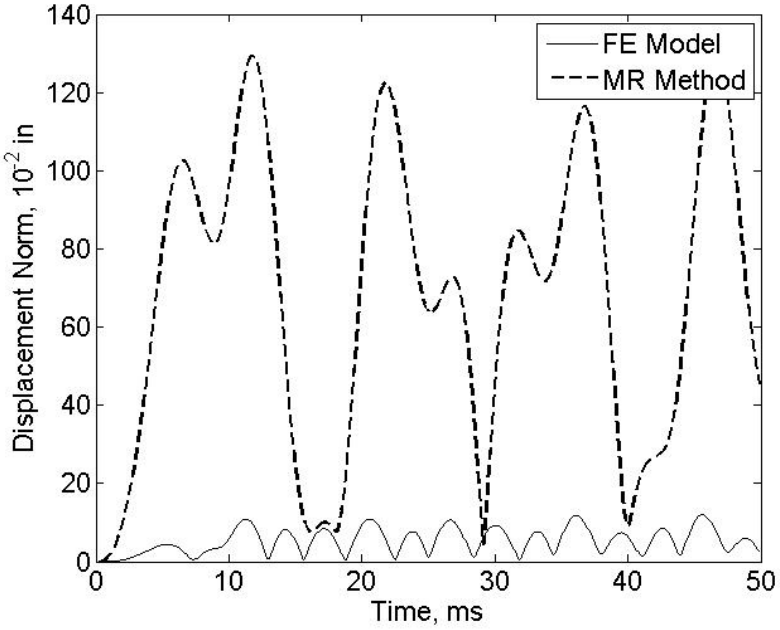

Fig. 4.42 Displacement Norms for LTV Beam in Response to $\tilde{F}(t)$

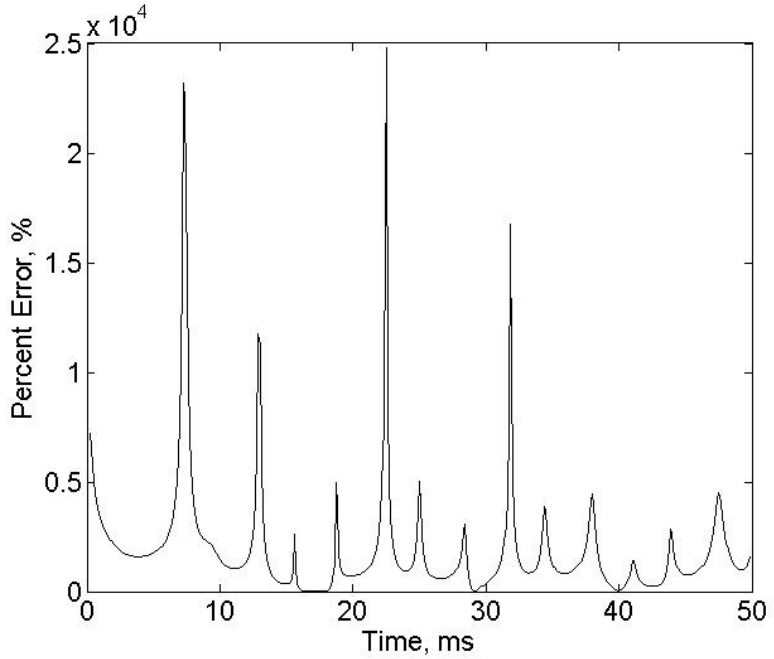

Fig. 4.43 Percent Error of Displacement Norms for LTV Beam in Response to $\widetilde{F}(t)$

The displacement norms for the NL beam are shown in Figs. 4.44, 4.46, and 4.48 for the three new excitations, with corresponding error percentages in Figs. 4.45, 4.47, and 4.49. In each figure the results obtained using the MR method are plotted with the exact results obtained by the FE models. The figures show that the MR method is capable of generating a reasonably accurate response prediction, although several sources of error are present. Projection errors and diagonalization errors are probably present, although diagonalization error is significantly lower than for the LTV beam because the model approximately meets the conditions for $C(t)$ to be diagonal. The response predictions for the NL beam contain additional linearization errors that show up as frequency and magnitude discrepancies in Figs. 4.44 and 4.46.

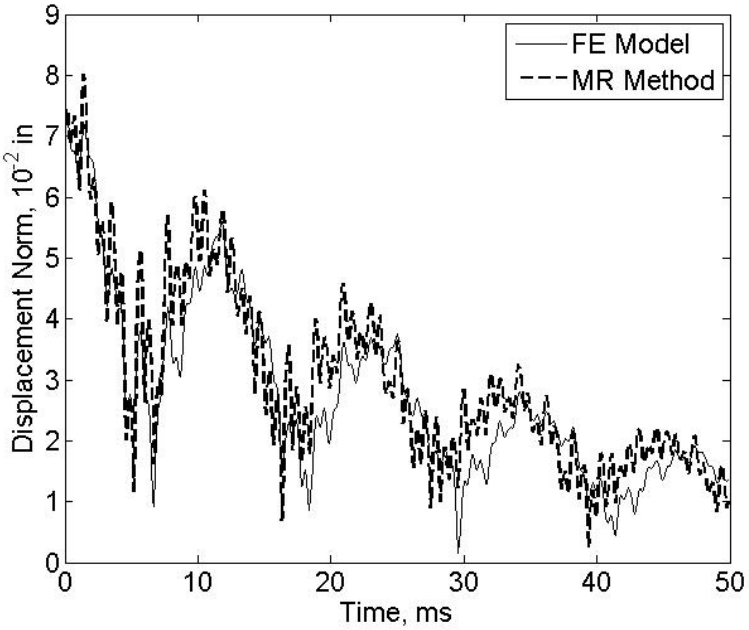

Fig. 4.44 Displacement Norms for NL Beam in Response to $\widetilde{\mathbf{w}}_0$

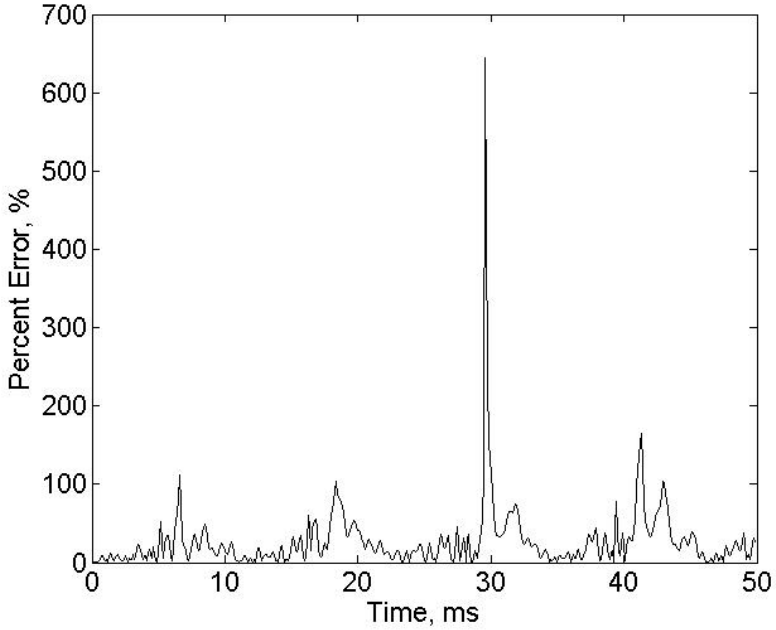

Fig. 4.45 Percent Error of Displacement Norms for NL Beam in Response to $\widetilde{\mathbf{w}}_0$

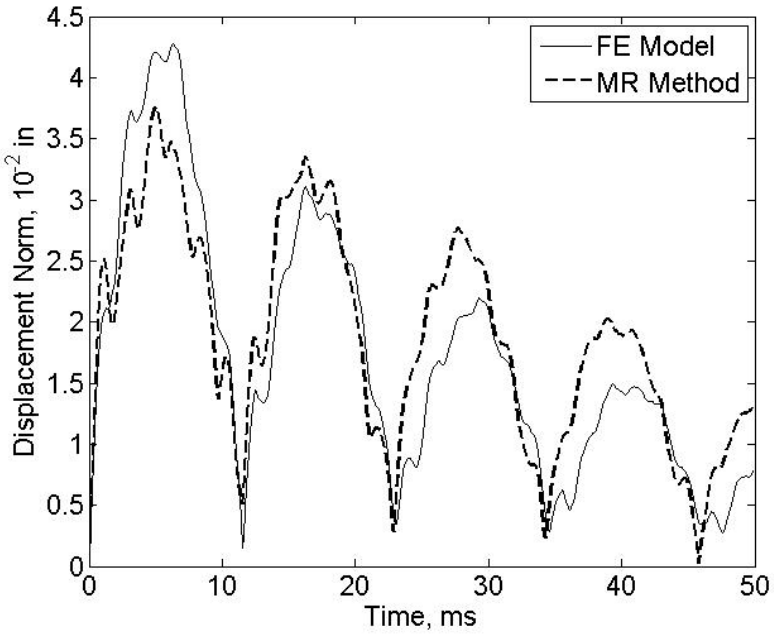

Fig. 4.46 Displacement Norms for NL Beam in Response to $\ddot{\tilde{w}}_0$

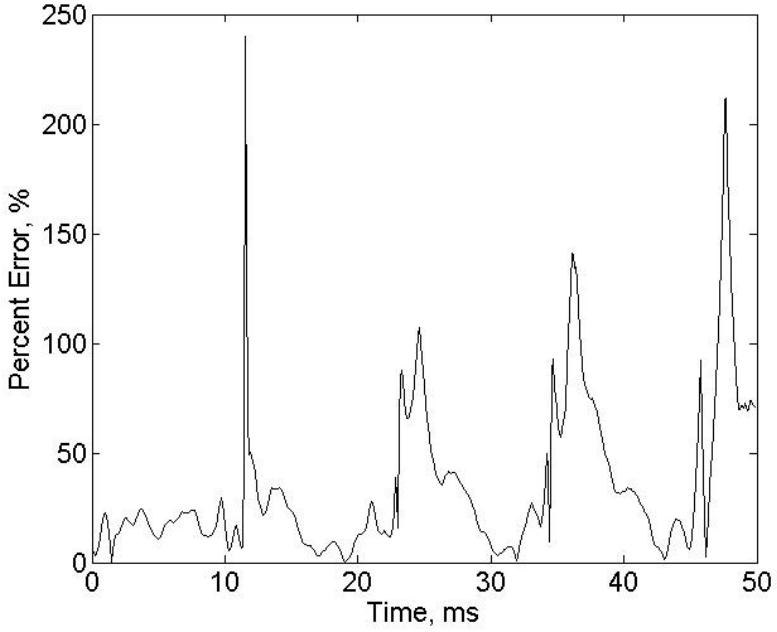

Fig. 4.47 Percent Error of Displacement Norms for NL Beam in Response to $\ddot{\tilde{w}}_0$

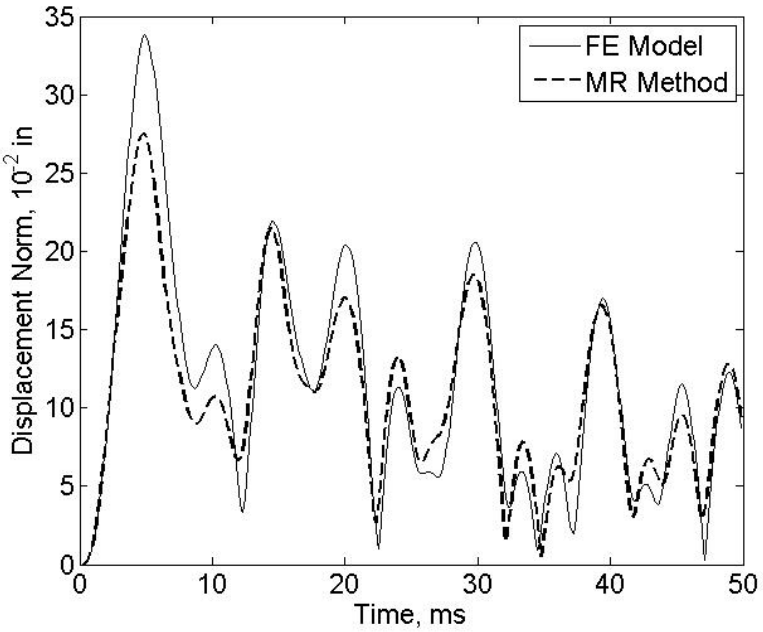

Fig. 4.48 Displacement Norms for NL Beam in Response to $\widetilde{F}(t)$

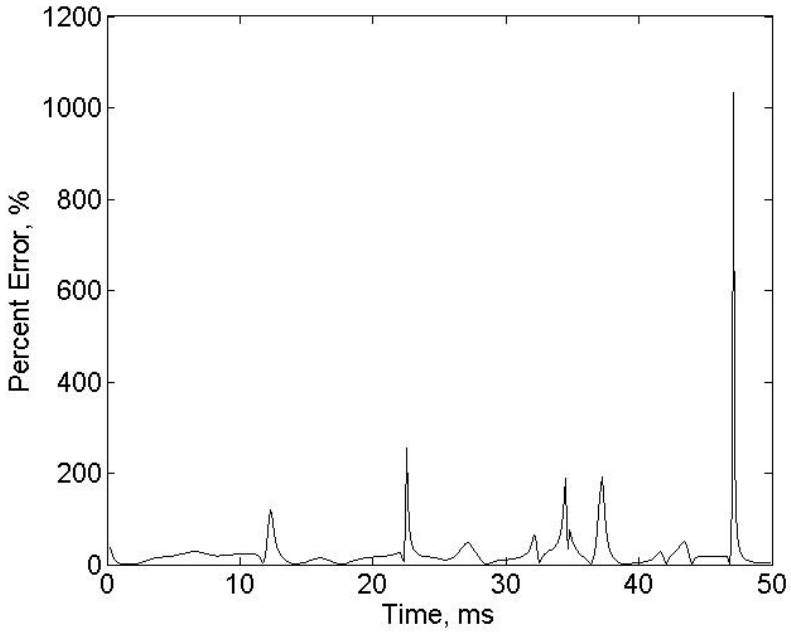

Fig. 4.49 Percent Error of Displacement Norms for NL Beam in Response to $\widetilde{F}(t)$

4.2 Satellite Truss Model

In this section, the POVR, MDS, SL, and ML methods from Sections 3.2 and 3.3 are applied to a satellite truss structure, one element of which is shown in Fig. 4.50. The MR method is not applied because the diagonalization error is anticipated to be very high based on the results from the POVR and SL methods.

The cross section of a truss element is an equilateral triangle as shown in Fig. 4.50, and the length of each side is 3 meters. Each element is constructed of 21 truss members, many of which share the same geometry and material properties (see Table 4.1). The members all have hollow circular cross sections and are joined by idealized pin joints.

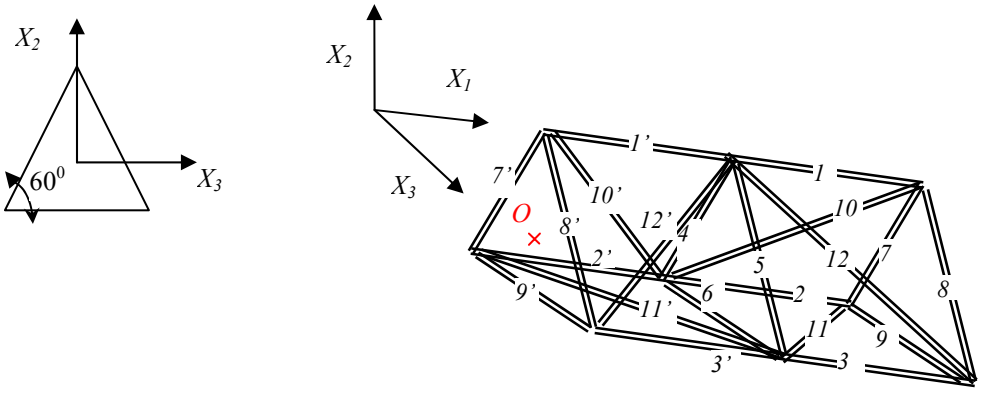

Fig. 4.50 Cross Section and Schematic View of a Single Truss Element [Courtesy Armaghan Salehian]

Table 4.1 Truss Member Geometry and Material Properties

Members	Length (ft)	Diameter (in)	Thickness (in)	Young's Modulus (psi)	Density (lbm/ft^3)
1,1',2,2',3,3'	9.8	3	0.04	1.00E+07	112.3
4,5,6,7,7',8,8',9,9'	9.8	1	0.02	1.00E+07	112.3
10,10',11,11',12,12'	13.9	1	0.02	1.00E+07	112.3

The motion of each truss element was described by nine coordinates that are defined in Fig. 4.51. Only motion in the X_1-X_2 plane is considered and the displacement of the three top joints is described by Δ_1, Δ_3, and Δ_5. The displacements of the two bottom joints at each cross-sectional face are assumed to be equal due to the symmetry of the truss structure and are described by Δ_2, Δ_4, and Δ_6. Rotation of the three cross-sectional faces about the X_3 axis is described by the coordinates Θ_1, Θ_2, and Θ_3. Fifty truss elements were assembled together lengthwise (the three boundary degrees of freedom at each truss segment boundary overlapped with the boundary degrees of freedom of the elements on either side) and pinned boundary conditions were applied to each end of the assembled truss structure. The dimension of the global mass and stiffness matrices with boundary conditions applied was therefore 299. After 3 seconds, the stiffness matrix for the 10^{th} truss element from the left boundary was removed from the global stiffness matrix to simulate a fracture (i.e. the 10^{th} truss element breaks off and disappears). As a result, the remaining truss sections on the right and left of the break are free to exhibit rigid-body rotation around each pinned end. The structure is therefore a linear time-varying system.

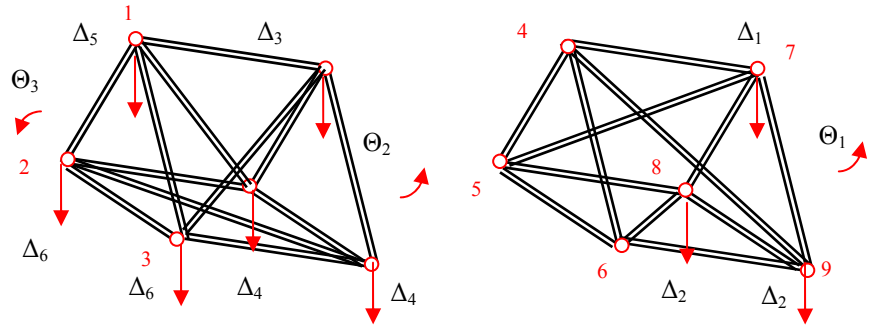

Fig. 4.51 Coordinates for Truss Element [Courtesy Armaghan Salehian]

4.2.1 Free Response

The POVR and MDS methods that were discussed in Section 3.2 for predicting responses to initial displacements and velocities are applied to the satellite truss structure in this section. First, six initial displacement profiles were formed by applying static loads as shown in Table 4.2. The responses to each initial displacement were simulated for 10 seconds using the FE model for the truss using the Newmark method with a time step of 0.05 s, so the dimensions of W were (299 x 200) for each response.

Table 4.2 Static Loads Applied to Generate Initial Displacements for Truss

	Force (lbf)	DOF	DOF Description
$\mathbf{w}_1$	11.3	140	Δ_2 on 23rd truss element from left boundary
$\mathbf{w}_2$	-16.9 22.5	50 80	Δ_2 on 8th truss element from left boundary Δ_2 on 13th truss element from left boundary
$\mathbf{w}_3$	-6.7	200	Δ_2 on 33rd truss element from left boundary
$\mathbf{w}_4$	67.4	290	Δ_2 on 48th truss element from left boundary
$\mathbf{w}_5$	18.0 -13.5	56 170	Δ_2 on 9th truss element from left boundary Δ_2 on 28th truss element from left boundary
$\mathbf{w}_6$	-89.9	20	Δ_2 on 3rd truss element from left boundary

Next, the POD was computed from the response to $\mathbf{w}_1$ and the POVR method was applied to predict the response to $\mathbf{w}_6$ with 5 POMs (99% of the original signal energy). The MDS method was also applied to predict the response to $\mathbf{w}_6$ and the responses to $\mathbf{w}_2$ - $\mathbf{w}_5$ were used as supplementary data sets. The displacement norms and percent errors for the response predictions are shown in Figs. 4.52 and 4.53, respectively. The relatively large displacements due to the rigid body rotation of the two truss segments after the break at 3 seconds are clearly visible in all of the displacement norms. The POVR method generated a less accurate prediction than the MDS method, probably due to diagonalization error, but the predicted responses for both methods are reasonably

accurate. Projection error is likely present in the predictions from both methods, but is quite small in this case (the MDS method has very low error).

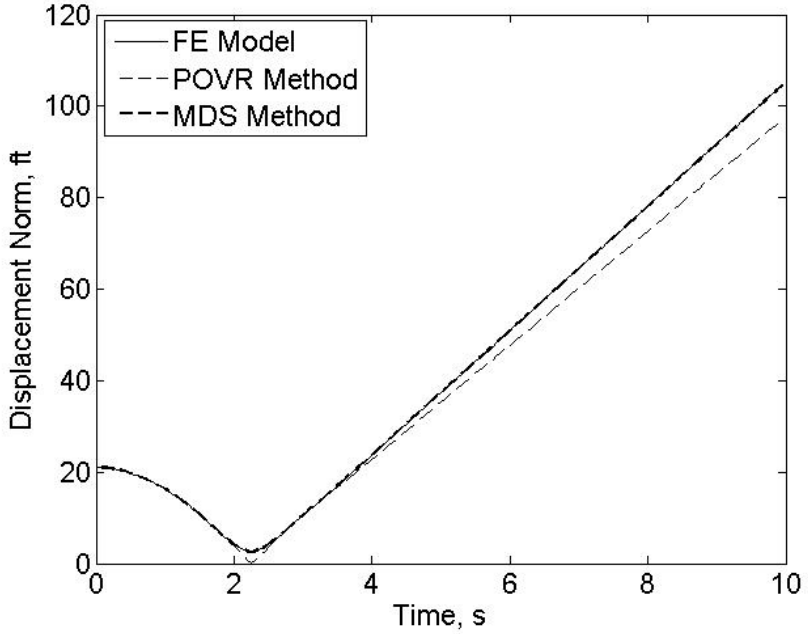

Fig. 4.52 Displacement Norms for Truss Model in Response to $\mathbf{w}_6$

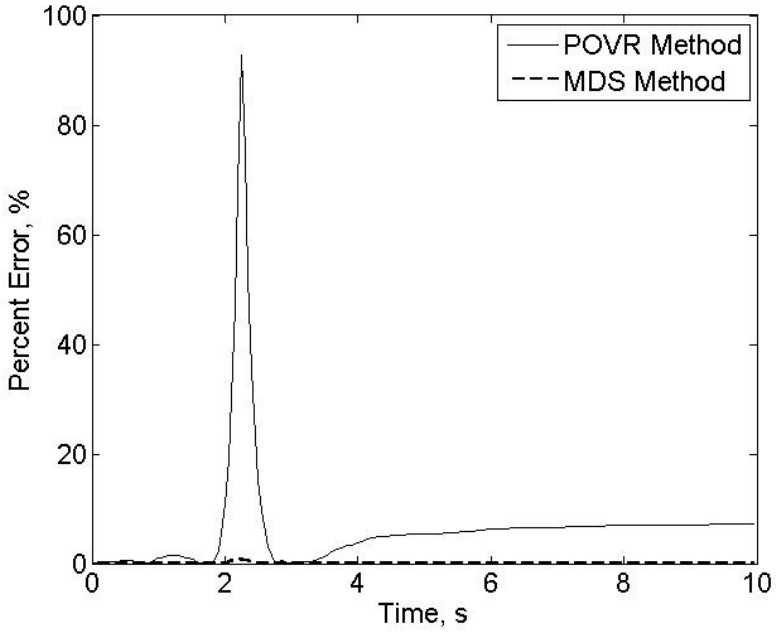

Fig. 4.53 Percent Error of Displacement Norms for Truss Model in Response to $\mathbf{w}_6$

Next, eight initial velocity profiles were generated by applying 1125-lbf impulses to various points along the truss and measuring the change in velocity. The locations of the impulsive loads are given in Table 4.3 below.

Table 4.3 Impulsive Loads Applied to Generate Initial Velocities for Truss

	Force (lbf)	DOF	DOF Description
$\dot{\mathbf{w}}_1$	1125	80	Δ_2 on 13th truss element from left boundary
$\dot{\mathbf{w}}_2$	1125	140	Δ_2 on 23rd truss element from left boundary
$\dot{\mathbf{w}}_3$	1125	170	Δ_2 on 28th truss element from left boundary
$\dot{\mathbf{w}}_4$	1125	50	Δ_2 on 8th truss element from left boundary
$\dot{\mathbf{w}}_5$	1125	20	Δ_2 on 3rd truss element from left boundary
$\dot{\mathbf{w}}_6$	1125	200	Δ_2 on 33rd truss element from left boundary
$\dot{\mathbf{w}}_7$	1125	230	Δ_2 on 38th truss element from left boundary
$\dot{\mathbf{w}}_8$	1125	110	Δ_2 on 18th truss element from left boundary

The POD was computed from the response to $\dot{\mathbf{w}}_1$ and the POVR method for initial velocities was applied to predict the response to $\dot{\mathbf{w}}_8$ with 7 POMs (99% of the original signal energy). The MDS method was also applied to predict the response to $\dot{\mathbf{w}}_8$ and the responses to $\dot{\mathbf{w}}_2$ - $\dot{\mathbf{w}}_7$ were used as supplementary data sets. The displacement norms and percent errors for the response predictions are shown in Figs. 4.54 and 4.55, respectively. Again, the relatively large displacements due to the rigid body rotation of the two truss segments are clearly visible in the plots of the displacement norms. The error is higher than for the initial displacement case for both methods due to an assumed increase in projection error. In this case, the MDS method produced a satisfactory response prediction, but the accuracy of the POVR method is unacceptable due to what is assumed to be high diagonalization error. Although the same system was used for initial

displacements and velocities, the diagonalization error may change because it depends on the POMs, which are excitation-dependent.

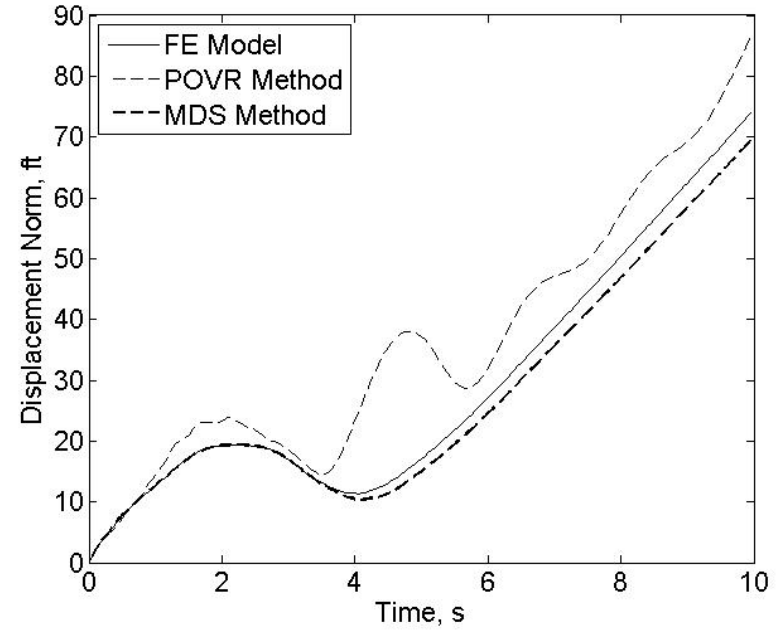

Fig. 4.54 Displacement Norms for Truss Model in Response to $\dot{w}_8$

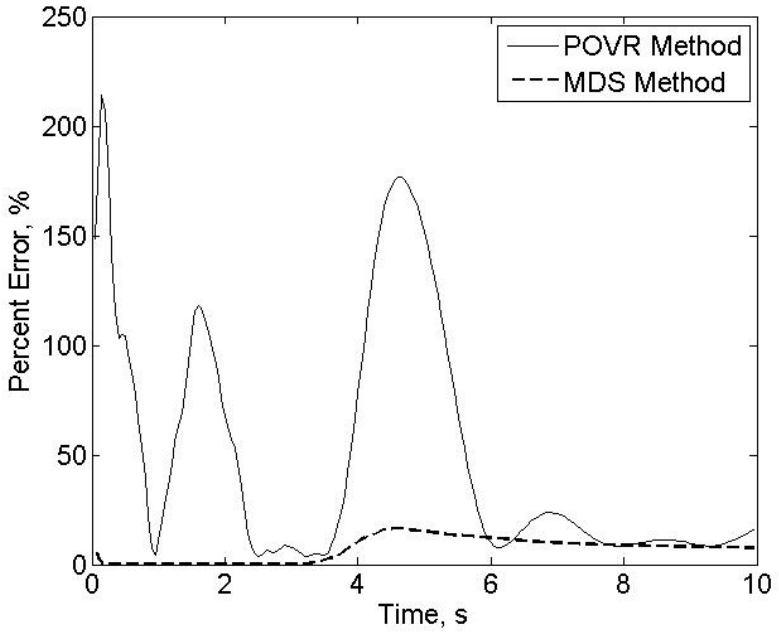

Fig. 4.55 Percent Error of Displacement Norms for Truss Model in Response to $\dot{w}_8$

4.2.2 Forced Response

This section applies the SL and ML methods from Section 3.3 to predict the forced response of the satellite truss structure. A 225-lbf pulse load (lasting 0.4 s) was applied to six points along the structure (see Fig. 4.56) and the Newmark method was applied to simulate the transient response of the system to each load for 10 seconds. The loads were applied at the Δ_2 DOF at truss elements numbers 23, 18, 33, 13, 8, and 38 (counting from the left boundary).

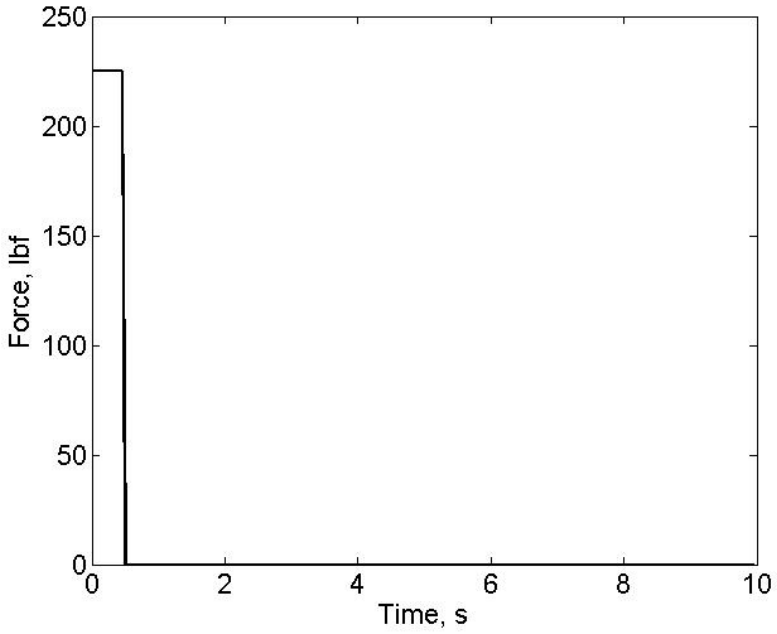

Fig. 4.56 Pulse Load Applied to Satellite Truss Model

The POD was computed from the response to the load applied at truss element 23, and the SL method was applied to predict the response of the structure to the load applied to element 38 with 5 POMs (99% of the original signal energy). The ML method was also applied and the responses to loads applied to truss elements 18, 33, 13, and 8 were used as supplementary loads. The displacement norms for both methods and the FE method

and the percent errors for the SL and ML methods when compared to the FE method are shown in Figs. 4.57 and 4.58, respectively.

The plots show that the ML method produces a very accurate prediction, but that there are significant errors in the prediction generated by the SL method. Again, the large errors in the SL method's prediction are attributed to diagonalization error. Projection error likely affects the accuracy of both methods slightly and can be visualized in the ML method's response prediction.

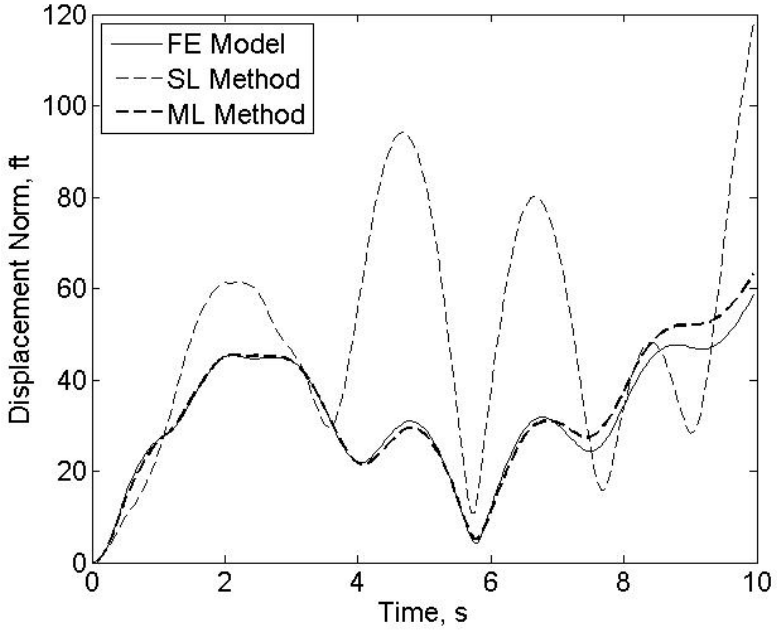

Fig. 4.57 Displacement Norms for Truss Model in Response to Load

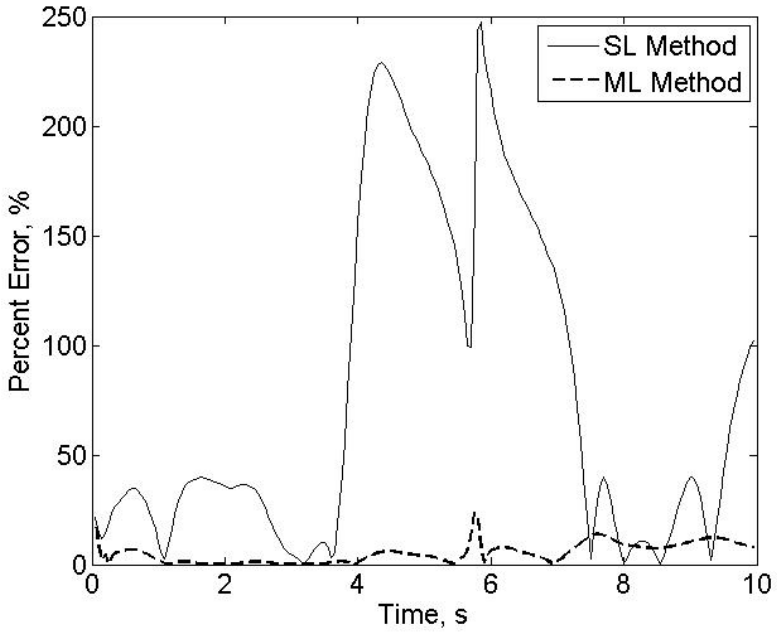

Fig. 4.58 Percent Error of Displacement Norms for Truss Model in Response to Load

4.3 Concluding Remarks

This chapter has applied the system identification methods described in Chapter 3 to four systems: linear time-invariant (LTI) and linear time-varying (LTV) beams, a nonlinear (NL) beam, and a linear time-varying satellite truss model. The errors that were visible in the response predictions for the various models are attributed to the sources described in Section 3.6. For linear (both LTI and LTV) beam examples, the MDS and ML methods produced accurate predictions with percent error generally less than 10% for initial displacements and loads and 20% for initial velocities (the projection error was higher for initial velocity responses). The POVR, SL, and MR methods also produced satisfactory predictions for the beams with a reasonably uniform and diagonally dominant mass matrix, e.g. the LTI beam. For other models (such as the LTV beam) that did not meet these requirements, the error was extremely high in many cases.

The methods' application to the NL beam highlighted the strengths and weaknesses of a linear time-varying approach to nonlinear system identification. The methods were able to construct a predictive model for a nonlinear system without requiring any knowledge about the form of the nonlinearity. In addition, the methods are formulated so that they are able to accurately reconstruct the nonlinear responses in the original data. The methods must be used with caution, however, as several of the drawbacks of using a linear time-varying method for identification of nonlinear systems were highlighted in the predictions for the NL beam. In several cases, linearization error manifested itself as frequency and/or amplitude discrepancies between the response predicted by the methods and a finite element model prediction. These errors are a result of imposing a linear

framework onto a nonlinear system. However, the methods will predict the response of a nonlinear system to a new excitation accurately if it is 'nearby' the response(s) in the original data set(s).

Finally, the POVR, MDS, ML and SL methods were applied to a satellite truss model to assess the effectiveness of the methods when they are applied to models that are more complex than simple beam models. The predictions generated for the truss model indicate that the methods may be applied to complex structures and achieve results with the same accuracy as for the simple beam models, i.e. the results indicate that the complexity of the satellite model did not present any additional problems at all for the methods.

5. Experimental Verification

The forced and mixed response methods described in Chapter 3 all involve performing the deconvolution of two or more signals. As explained in Ssection 3.5, the deconvolution problem can be difficult to solve when noise is present in the data. The total least squares method was introduced in Section 3.5 in order to calculate an acceptable estimate of the deconvolved signal. In this section, the single-load (SL) and multiple-load (ML) methods are applied two experimental data from a linear beam and a nonlinear beam and the total least squares method is applied to perform the deconvolution of the data. Sections 5.1 and 5.2 describe the experiments and results for the linear and nonlinear beams, respectively, and Section 5.3 presents some concluding remarks about the effectiveness of the total least squares method.

5.1 Linear Beam

This section applies the system identification methods from Section 3.3 to experimental data obtained from the linear cantilever beam shown in Fig. 5.1. Although the beam is a simple system, it is sufficient for verifying that the methods presented in this paper can be used with experimental data. The beam is constructed from aluminum and is 20 inches long with a 1” x 0.125” cross-section. A Ling Dynamical Systems permanent magnet shaker was set up next the beam as shown in Fig. 5.2 and excited with a single rectangular pulse so that the sting struck the beam impulsively and a PCB 208C02 load cell measured the force applied to the beam at the striking location. Loads were applied in this manner at locations 4, 8, and 12 inches from the root of the beam. Although double

or triple impacts occurred for all of the load cases, the system identification methods are valid for any applied load and the extra hits do not interfere as long as they are measured.

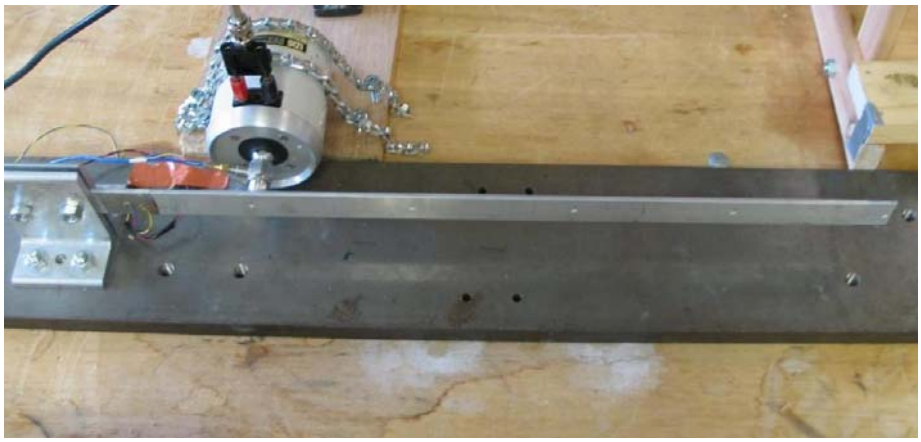

Fig. 5.1 Experimental Setup

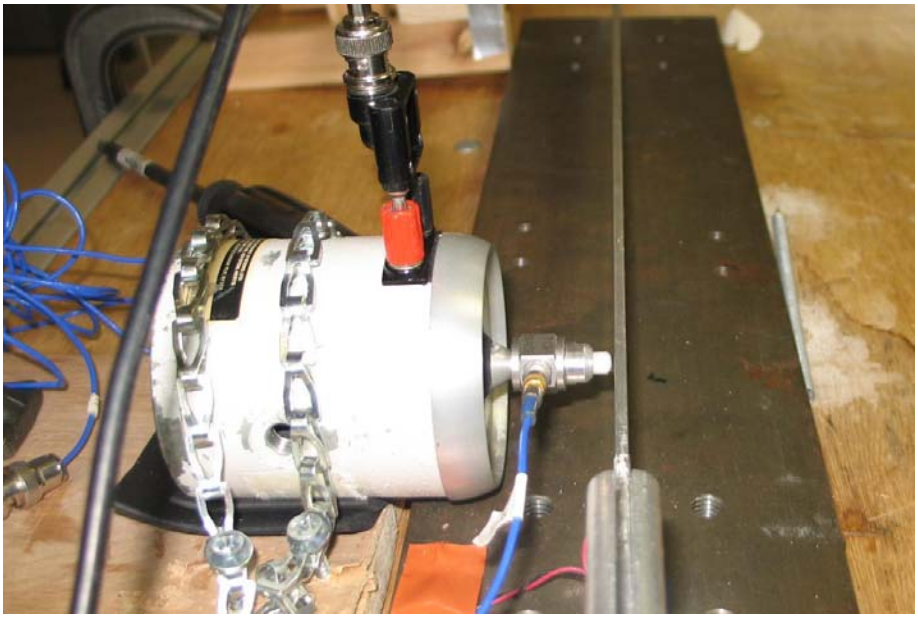

Fig. 5.2 Application of Impulsive Load via Shaker Strike

For each load case, a Polytec OFV-303 laser vibrometer was set up to measure the transverse displacement of the beam at different locations 0, 4, 8, 12, 16, and 20 inches

from the root of the beam. The shaker was used in order to apply the same load six times while the laser vibrometer measured the displacement of one point each time. The force and displacement response data were sampled every 0.1 milliseconds for 10.24 seconds (equal to the fundamental period of 0.1024 s), so the dimensions of W were (6 x 1024).

The force data obtained from the load cell were composed of the actual force applied to the beam and the inertial force experienced by the load cell due to the rapid pulse. In order to identify the actual force applied to the beam, the shaker was pulsed without impacting the beam and the resulting inertial load was measured. The shaker was then pulsed so that it impacted the beam and the two signals were compared to identify the impulsive loads that are applied to the beam (see Fig. 5.3 for example). This procedure was repeated for all three load cases to extract the applied force data and the resulting forces are shown in Fig. 5.4. No other methods of noise removal were employed to filter the force or displacement data.

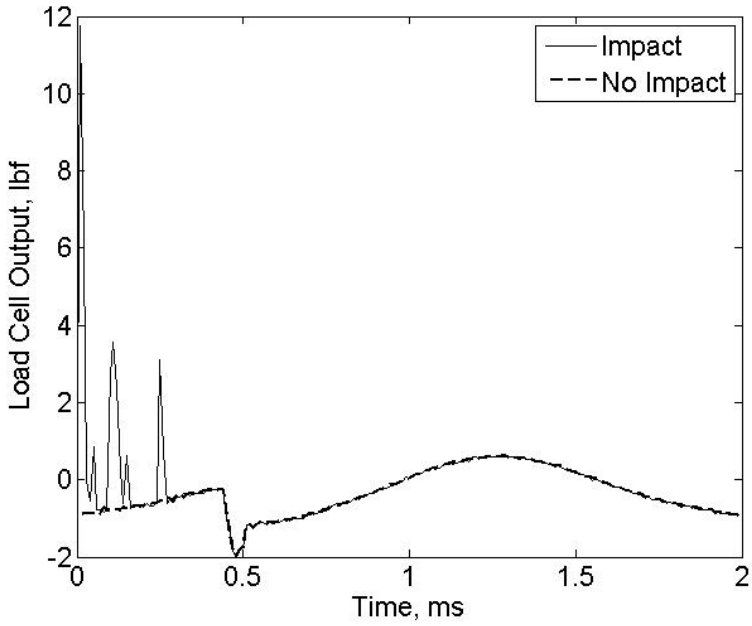

Fig. 5.3 Load Cell Output With and Without Beam Impact

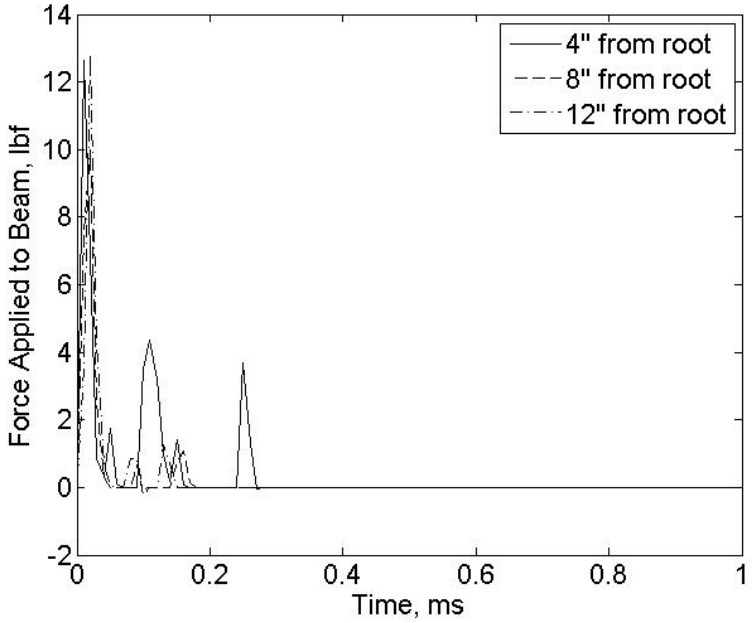

Fig. 5.4 Forces Applied to Various Beam Locations

Next, the POD was computed from the beam's response to the load applied 8" from the root. The first two POMs (shown in Fig. 5.5) were considered, corresponding to 90% of

the original signal energy. The first four POVs are shown in Fig. 5.6. Next, both the single-load (SL) and multiple-load (ML) methods were applied to simulate the response of the beam to the load 4" from the root. For the multiple-load method, the response to the load 12" from the root was used as a supplementary load to solve for off-diagonal elements of $C(t)$. Fig. 5.7 shows the displacement norms (see Eq. (4.1)) for the linear beam response to the load 4" from the root that were calculated by the SL and ML methods. Fig. 5.8 shows the percent errors (see Eq. (4.2)) for the displacement norms of the SL and ML methods compared with the measured data.

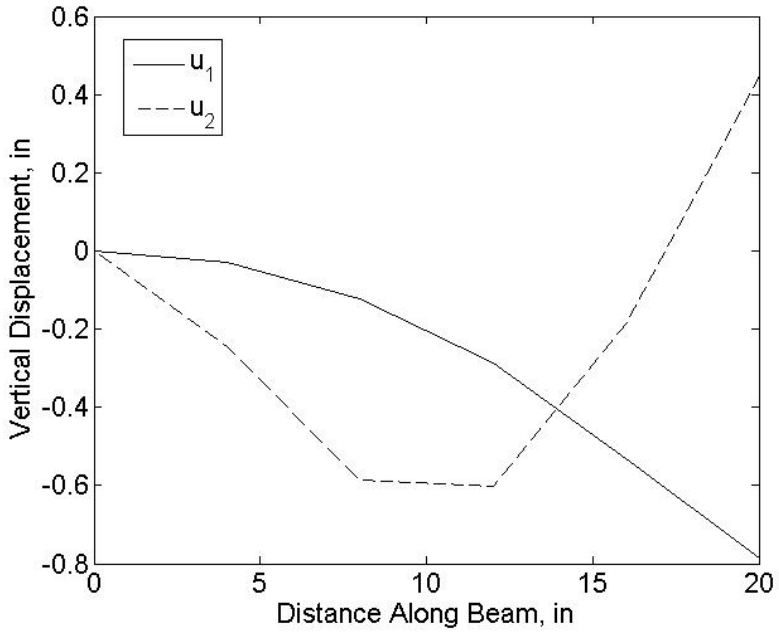

Fig. 5.5 Two Most Dominant POMs for Linear Beam

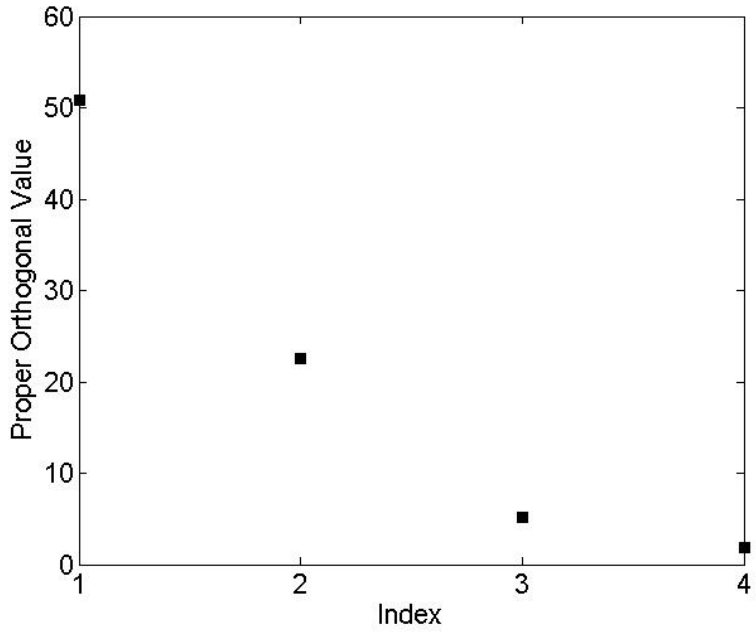

Fig. 5.6 POVs for Experimental Linear Beam

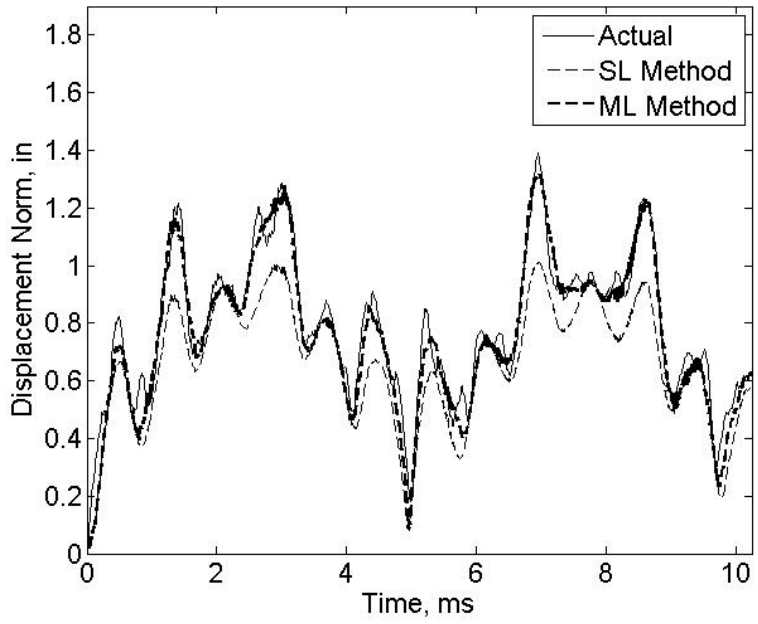

Fig. 5.7 Displacement Norms for Linear Experimental Beam Response to Load at 4”

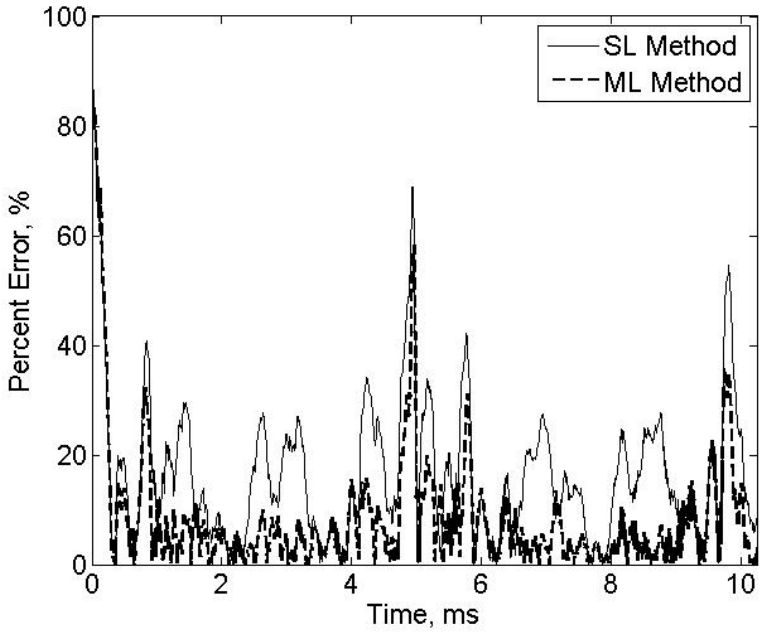

Fig. 5.8 Percent Error of Displacement Norms for Linear Experimental Beam Response

These figures show that while both the SL and ML methods are able to predict the displacement of the linear beam satisfactorily when compared with the measured response, the ML method is the more accurate of the two. The error is higher in the SL method's prediction because the method assumes that the mass matrix of the beam is proportional to the identity matrix, which is not true. The sharp increases in percent error near 0, 5, and 10 ms are due to the fact that the magnitude of the displacement norm is very low at those times and the percent error is calculated by dividing by a very small number.

5.2 Nonlinear Beam

This section describes the application of the forced response methods from Section 3.3 to a nonlinear experiment. A rubber band with stiffness of 0.12 lb/in was attached to the tip

of the linear beam from Section 5.1 (Fig. 5.1). The rubber band provides a nonlinearity for the system because it provides linear stiffness when the beam tip deflects away from where the rubber band is attached (see Fig. 5.9) but then provides zero stiffness when the beam tip deflects toward the rubber band attachment point (the rubber band buckles as shown in Fig. 5.10).

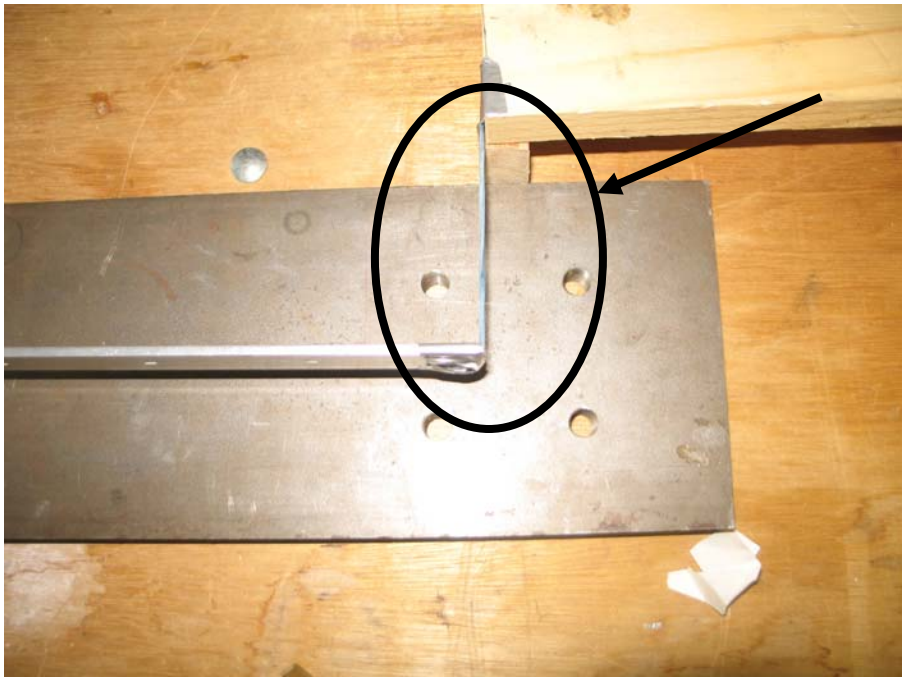

Fig. 5.9 Rubber Band Acting as Linear Spring

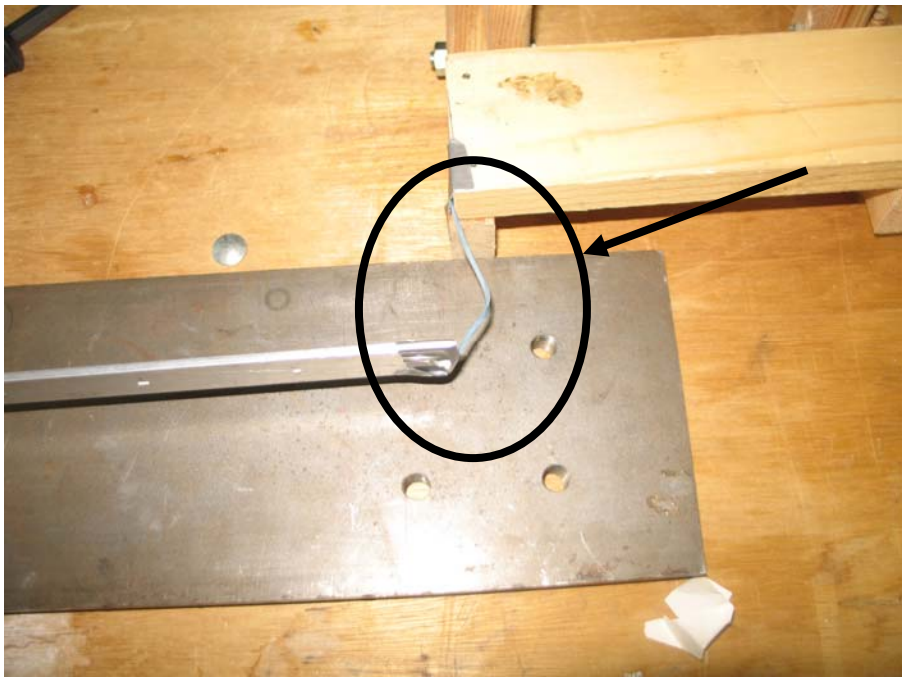

Fig. 5.10 Rubber Band Providing no Stiffness

In order to determine if the nonlinearity affected the response over the excitation range seen in the experiment, five impulses of increasing strength were applied to the point 4 inches from the root of the beam using the same shaker setup shown in Figs. 5.1 and 5.2. The five loads are shown in Fig. 5.11. The tip displacement of the beam in response to each impulse was measured and then scaled by the corresponding impulse magnitude. For a linear system, the principle of superposition dictates that the scaled tip displacements should be equal. Instead, the scaled tip displacements for this system, shown in Fig. 5.12, decrease as the impulse magnitude is increased, showing that the system does not satisfy superposition.

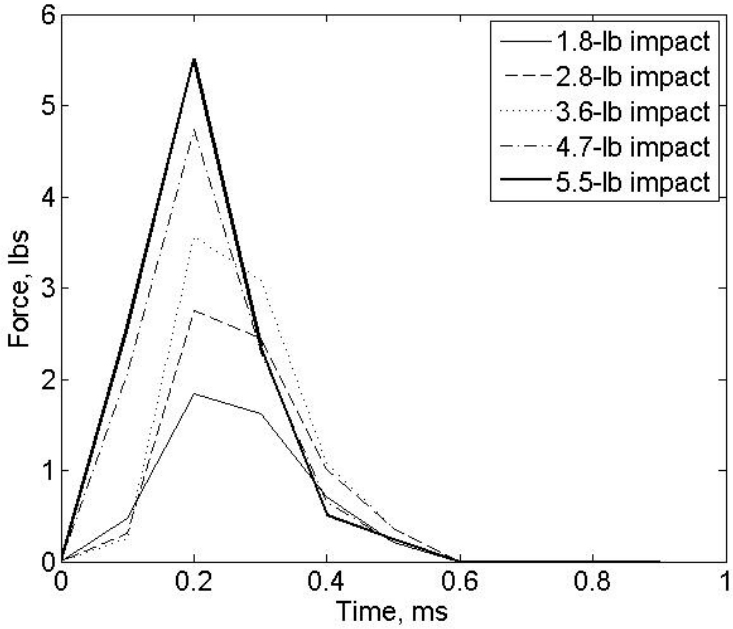

Fig. 5.11 Impulsive Loads Applied to Nonlinear Beam to Assess Nonlinear Activity

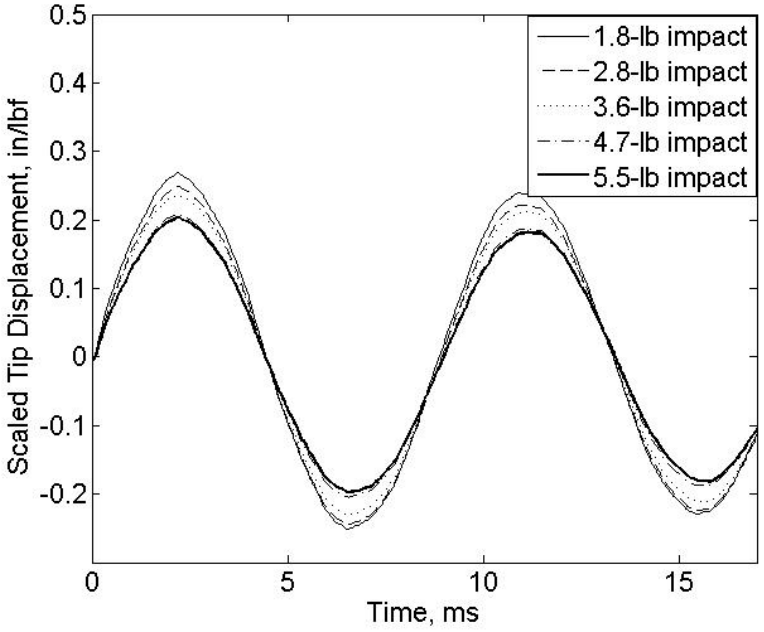

Fig. 5.12 Scaled Tip Displacements for Various Impulse Magnitudes

In addition to not satisfying superposition, the response of the nonlinear beam contains slightly different frequency content in the responses to various impulse magnitudes. The frequency discrepancies manifest themselves as phase differences in the signals that grow with time. The response to the 1.8-lb impulse was defined as a baseline and the phase lag of the other responses behind the baseline was measured at 500, 1000, 1500, and 2000 ms after impact. The phase lags are shown as percentages of the fundamental period of the reference linear beam (10.24 ms) for each of the impulse magnitudes in Fig. 5.13. From Fig. 5.13 we conclude that the lowest frequency of the system increases with the excitation magnitude, indicating that the nonlinearity is active in the beam response.

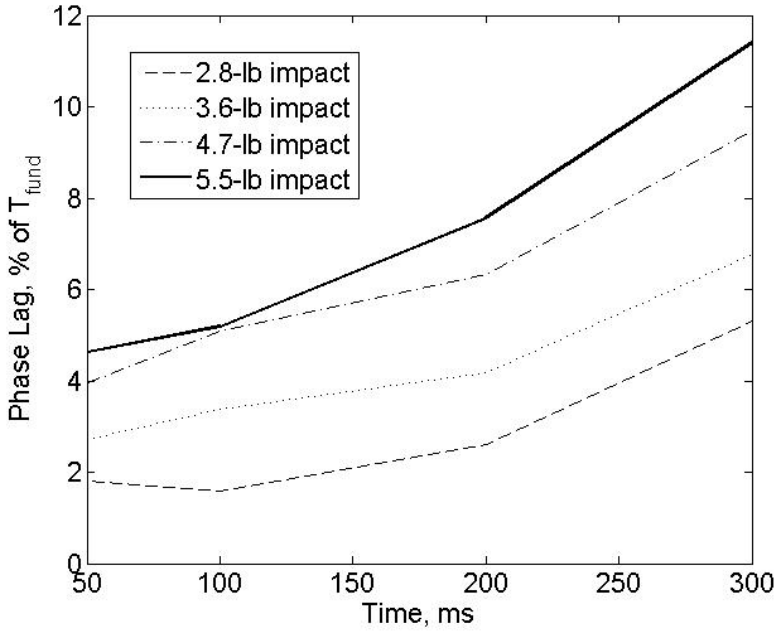

Fig. 5.13 Phase Lag for Various Impulse Magnitudes

Once the presence of the nonlinearity was verified, the beam was excited by three loads applied at points 4, 12, and 16 inches from the root of the beam. The loads applied to the beam were extracted from the load cell output by measuring and subtracting out the

inertial loads as was done for the linear beam. The loads are shown in Fig. 5.14. The tension in the rubber band drew the beam back into contact with the shaker more often, leading to multiple impacts for each load case, sometime for as long as 6 ms after the initial impact.

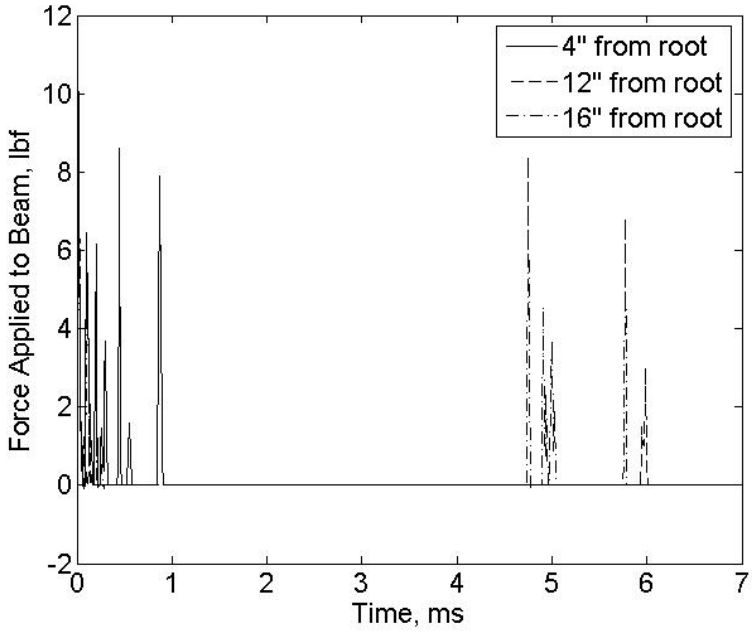

Fig. 5.14 Forced Applied to Locations on Nonlinear Beam

The response of each beam was measured for a fundamental period (10.24 ms) and sampled every 0.01 ms. The POD was calculated from the response to the load applied 12 inches from the root and the SL and ML methods were used to predict the response to the load applied 4" from the root, with the ML method using the response to the load applied 16" from the root as a supplementary data set.

The displacement norms for the SL and ML methods and the actual response are all shown in Fig. 5.15 and the percent errors for the SL and ML methods are shown in Fig.

5.16. The ML method is does not suffer from diagonalization error and is therefore generally more accurate than the SL method, although there is a sharp increase in the percent error for the ML method near 9 milliseconds. This error increase may be caused by errors in the deconvolution procedure or linearization error (the signals are slightly out of phase at 9 ms). The linearization error is smaller than was visible for the nonlinear example in Chapter 4 because the nonlinearity in the experimental beam is not as strong as in the numerical example.

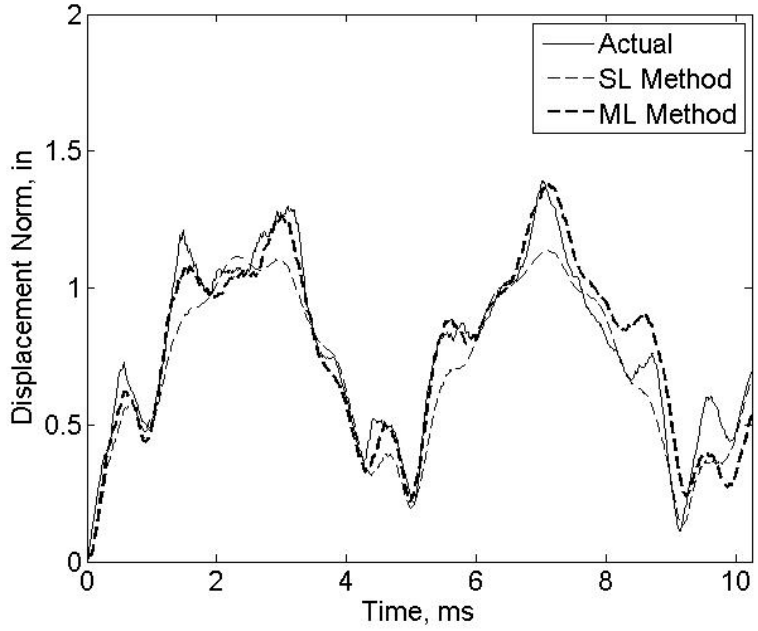

Fig. 5.15 Displacement Norms for NL Experimental Beam Response to Load at 4" Location

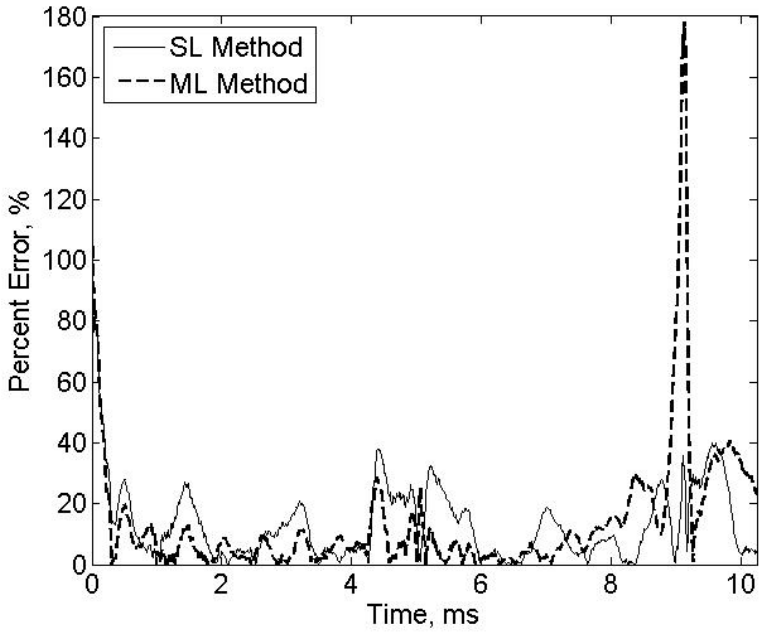

Fig. 5.16 Percent Error of Displacement Norms for NL Experimental Beam Response

5.2 Concluding Remarks

This section applied the SL and ML forced response methods from Section 3.3 to experimental data from a linear beam and a nonlinear beam. The total least squares method was applied to solve the deconvolution problem because the data were corrupted by measurement noise.

Both the SL and ML method produced accurate predictions for both beams without requiring any information about the equations of motion governing the beam, including the geometry, material properties, damping, boundary conditions, form of nonlinearity, etc. The ML method produced more accurate results than the SL method because diagonalization error was not present. The linearization error was much lower for the nonlinear beam presented in this section that for the numerical example in Chapter 4

because the nonlinearity was not as strong as in the example. The results show that the methods may be applied to experimental data to generate accurate predictions

The experimental results show that the SL and ML methods may be successfully applied to actual experimental data, but they also highlight some of the difficulties associated with noisy data. First, a smaller number of POMs were used for the experimental models in order to keep the deconvolution error low. As was explained in Section 3.6, the POD serves as a type of filter and most measurement noise is contained in the POMs and POC histories with low POVs as long as the noise is not the dominant part of the signal. Thus, as more POMs are used for the model, the noise in the POC histories increases and it is more difficult to perform the deconvolution accurately for the less-dominant POC histories. Second, the overall error for the predictions in this section is higher than was visible for the beams in Chapter 4 because the noisy data makes the deconvolution operation less accurate. However, the error increase is relatively small (approximately 5-10%) and we conclude that the total least squares method provided an accurate solution to the deconvolution problems in the SL and ML methods.

6. Conclusions and Recommendations

This chapter summarizes the research presented in the previous chapters and presents conclusions about the strengths and weaknesses of the identification methods that were explained in Chapter 3 and applied to systems in Chapters 4 and 5. The contributions of the research are explained, and several recommendations for future research are also presented.

This dissertation has presented five methods (see Chapter 3) for linear time-varying system identification based on the proper orthogonal decomposition. The methods identify input/output models (i.e. a physical model is not obtained) to predict the dynamic response of a structure to initial conditions and applied loads and do not require any knowledge regarding the equations of motion for the structure such as the form of the time variance, damping, boundary conditions, etc. The method of proper orthogonal value recalculation (POVR) and the multiple data set (MDS) method may be applied when a structure is excited only by initial displacements or velocities, and the single-load (SL) and multiple-load (ML) methods were proposed for systems that start at rest and are subjected to a load. Finally, the mixed response (MR) method is proposed for the case where a structure is excited by a combination of initial conditions and loads.

Chapters 4 and 5 have described the application of the methods to various numerical and experimental systems. The MDS and ML methods were able to provide accurate predictions consistently for linear time-invariant and linear time-varying systems. The POVR, SL, and MR methods provide satisfactory predictions for linear systems in cases

where the proper orthogonal modes are equal (or approximately equal) to the system's eigenmodes, but these methods must be used with caution as their predictions were shown to be inaccurate for systems that do not meet this requirement.

All of the methods were also applied to nonlinear systems to explore the advantages and disadvantages of using time-varying methods for nonlinear system identification. The clear advantage of using the proposed methods is that they may be applied to any nonlinear system, even if the form of the nonlinearity is unknown. The methods, although based on linear system theory, are able to accurately reproduce the original data sets generated by the nonlinear system. However, when they are applied to predict the response of the system to new excitations, errors may be present because the methods rely on linear theory. The methods will not be able to accurately predict responses with new frequency content or other nonlinear phenomena that were not measured in the original response.

The strength of the MDS and ML methods is their ability to construct models without requiring any knowledge of the equations of motion of the structure, unlike most other time-varying identification methods. Although they require measurement of multiple input/output data sets, the number required is minimized by the optimality of the proper orthogonal modes. The advantage of the POVR and SL methods is that they require only a single data set. However, they are only valid for systems with mass, damping, and stiffness matrices that are diagonalized by the proper orthogonal modes and can yield inaccurate results for systems and/or excitations that do not meet these criteria. The MR

method may be applied to systems that are excited by a combination of initial conditions and loads and requires only three data sets to form a model, but it relies on the same assumptions as the POVR and SL methods. All of the methods are also based on familiar ideas of mode summation and linear system theory and are therefore quite intuitive. A weakness of all of the methods is that a method for predicting the error in predicted response is not yet available. In addition, experimental testing of large, complex structures may present difficulties that have not been addressed here.

This work contributes to the existing body of knowledge in several ways. First, the proposed methods extend the capabilities of current linear time-varying identification methods by enabling the identification of multiple-input multiple-output systems without requiring the functional form of the time variance to be known. The research also presents a new application of the proper orthogonal decomposition to system identification and gives insight into the meaning of the proper orthogonal coordinate histories. Finally, the methods have been applied to nonlinear systems and the merits and drawbacks of such an approach have been assessed.

There are several opportunities for continuing research with the proposed methods. Although sources of error present in the various methods have been described in Chapter 3, methods for quantifying and predicting the error were not explored. The ability to generate error bounds for predictions generated by the various methods would enhance the methods considerably.

Another area of potential research lies in adapting the identification methods for substructuring applications. As mentioned previously, the cost and difficulty associated with testing a large and complex structure may be great, and in many cases a finite element model is available before a structure is ever built. In these cases, it may be profitable to define certain components experimentally and incorporate them into the finite element model. An experimental test of a component may be considerably simpler than for a whole structure. If the component is time-varying or nonlinear, it may be simpler to construct an experimental model using these methods than to build a finite element model of the component. Traditionally, substructuring is accomplished by assembling experimentally defined mass, damping, and stiffness matrices for a component into the finite element matrices for a model.

Since the methods proposed in this research do not yield mass, damping, and stiffness matrices explicitly, a nontraditional approach to substructuring may be required. It may be possible to incorporate the effects of a substructure by performing a two-step analysis, i.e. by simulating the response of the finite element portion of the model, translating it into inputs for the experimental component, and using the predicted outputs as inputs for the finite element model at the following time step. The computational costs associated with such an approach may be high and should be included in any study of this concept.

Finally, the methods described in this dissertation have been developed for situations where displacements are measured and forces are applied. However, in many cases, vibration tests are performed by applying base excitations instead of loads. Acceleration,

strain or stress output may be of more interest than displacements. It may be possible to adapt the methods for different types of inputs and outputs that will be useful for other applications.

References

[1] Huebner, K.H., Byrom, T.G., Dewhirst, D.L. and Smith, D.E., *The Finite Element Method for Engineers*, Wiley, New York, 2001, Chap. 1.

[2] Bennighof, J.K., Muller, M.B., and Kaplan, M.F., "Computational Costs for Large Structure Frequency Response Methods," *AIAA Structures, Structural Dynamics, and Materials Conference*, AIAA Paper 1977-1274, AIAA, Kissimmee, FL, April 1997.

[3] Kerschen, G., Worden, K., Vakakis, A.F., and Golinval, J.C., "Past, present and future of nonlinear system identification in structural dynamics," *Mechanical Systems and Signal Processing*, Vol. 20, No. 3, 2006, pp. 505-592.

[4] Ewins, D.J., *Modal Testing: Theory and Practice*, Research Studies Press Ltd., Hertfordshire, 1984.

[5] Friswell, M. and Mottershead, J.E., *Finite Element Model Updating in Structural Dynamics (Solid Mechanics and Its Applications)*. Dordrecht: Kluwer, 1995.

[6] Verhaegen, M. and Yu, X., "A class of subspace model identification algorithms to identify periodically and arbitrarily linear time-varying systems," *Automatica*, Vol. 31, No. 2, 1995, pp. 201-216.

[7] MacNeil, J.B., Kearney, R.E., and Hunter, I.W., "Identification of time-varying biological systems from ensemble data," *IEEE Transactions on Biomedical Engineering*, Vol. 39, No. 12, 1992, pp. 1213-1225.

[8] Berkooz, G., Homes, P., and Lumley, J.L., "The Proper Orthogonal Decomposition in the Analysis of Turbulent Flows," *Annual Review of Fluid Mechanics*, Vol. 25, No. 1, 1993, pp. 539-575.

[9] Juang, J.-N. *Applied System Identification*, Prentice-Hall, Upper Saddle River, NJ, 1994.

[10] Virgin, L.N., *Introduction to Experimental Nonlinear Dynamics: A Case Study in Mechanical Vibration*, Cambridge University Press, New York, 2000.

[11] Worden, K. and Tomlinson, G.R., *Nonlinearity in Structural Dynamics: Detection, Identification, and Modeling*, Institute of Physics Publishing, Pennsylvania, 2001.

[12] Simon, M. and Tomlinson, G.R., "Use of the Hilbert transform in modal analysis of linear and non-linear structures," *Journal of Sound and Vibration*, Vol. 96, No. 4, 1984, pp. 421–436.

[13] Rauch, A., "Coherence: a powerful estimator of nonlinearity, theory and application," *Proceedings of 10th International Modal Analysis Conference*, San Diego, 1992, pp. 784–795.

[14] Al-Hadid, M.A. and Wright, J.R., "Developments in the force-state mapping technique for non-linear systems and the extension to the location of non-linear elements in a lumped-parameter system," *Mechanical Systems and Signal Processing*, Vol. 3, No. 3, 1989, pp. 269–290.

[15] Lin, R. and Ewins, D.J., "Location of localised stiffness non-linearity using measured modal data," *Mechanical Systems and Signal Processing*, Vol. 9, No.3, 1995, pp. 329–339.

[16] Trendafilova, I., Lenaerts, V., Kerschen, G., Golinval, J.C., and Van Brussel, H., "Detection, localization and identification of nonlinearities in structural dynamics," *Proceedings of the International Seminar on Modal Analysis (ISMA)*, Leuven, 2000.

[17] Nayfeh, A.H. and Mook, D.T., *Nonlinear Oscillations*, Wiley-Interscience, New York, 1979.

[18] Adams, D.E. and Allemang, R.J., "Polynomia,l non-polynomial, and orthogonal polynomial generating functions for nonlinear system identification," *Proceedings of the International Seminar on Modal Analysis (ISMA)*, Leuven, 2000.

[19] Schetzen, M., *The Volterra and Wiener Theories of Nonlinear Systems*, Wiley, New York, 1980.

[20] Niedzwiecki, M., "Recursive functional series modeling estimators for identification of time-varying plants-more bad news than good?" *IEEE Transactions on Automatic Control*, Vol. 35, No. 5, 1990, pp. 610-616.

[21] Epureanu, B.I., Hall, K.C., and Dowell, E.H., "Reduced-Order Models of Unsteady Viscous Flows in Turbomachinery Using Viscous-Inviscid Coupling," *Journal of Fluids and Structures*, Vol. 15, No. 2, 2001, pp. 255-273.

[22] Azeez, M.F.A. and Vakakis, A.F., "Numerical and Experimental Analysis of a Continuous Overhang Rotor Undergoing Vibro-Impacts," *International Journal of Non-Linear Mechanics*, Vol. 34, No. 3, 1998, pp. 415-435.

[23] Kappagantu, R., and Feeny, B.F., "An Optimal Modal Reduction of a System with Frictional Excitation," *Journal of Sound and Vibration*, Vol. 224, No. 5, 1999, pp. 863-877.

[24] Liang, Y.C., Lin, W.Z., Lee, H.P., Lim, S.P., Lee, K.H., and Sun, H., "Proper Orthogonal Decomposition and its Applications, Part II: Model Reduction for

MEMS Dynamical Analysis," *Journal of Sound and Vibration*, Vol. 256, No. 3, 2002, pp. 515-532.

[25] Ma, X., Vakakis, A.F., and Bergman, L.A., "Karhunen-Loève Modes of a Truss: Transient Response Reconstruction and Experimental Verification," *AIAA Journal*, Vol. 39, No. 4, 2001, pp. 687-696.

[26] Ma, X., Vakakis, A.F., and Bergman, L.A., "Karhunen-Loève Decomposition of the Transient Dynamics of a Multibay Truss," *AIAA Journal*, Vol. 37, No. 8, 1999, pp. 939-946.

[27] Steindl, A. and Troger, H., "Methods for Dimension Reduction and their Application in Nonlinear Dynamics," *International Journal of Solids and Structures*, Vol. 38, March 2001, pp. 2131-2147.

[28] Kreuzer, E. and Kust, O., "Analysis of Long Torsional Strings by Proper Orthogonal Decomposition," *Archive of Applied Mechanics*, Vol. 67, December 1996, pp. 68-80.

[29] Al-Dmour, A.S. and Mohammed, K.S., "Active Control of Flexible Structures Using Principal Component Analysis in the Time Domain," *Journal of Sound and Vibration*, Vol. 253, No. 3, 2002, pp. 545-569.

[30] De Boe, P. and Golinval, J.C., "Principal Component Analysis of a Piezosensor Array for Damage Localization," *Structural Health Monitoring*, Vol. 2, No. 2, 2003, pp. 137-144.

[31] Feldmann, U., Kreuzer, E., and Pinto, F., "Dynamic Diagnosis of Railway Tracks by means of the Karhunen-Loève Transformation," *Nonlinear Dynamics*, Vol. 22, No. 2, 2000, pp. 183-193.

[32] Tumer, I.Y., Wood, K.L., and Busch-Vishniac, I.J., "Monitoring of Signals from Manufacturing Processes Using K-L Transform," *Mechanical Systems and Signal Processing*, Vol. 14, No. 6, 2000, pp. 1011-1026.

[33] Feeny, B.F., "On Proper Orthogonal Co-ordinates as Indicators of Modal Activity," *Journal of Sound and Vibration*, Vol. 255, No. 5, 2002, pp. 805-817.

[34] Han, S. and Feeny, B.F., "Application of Proper Orthogonal Decomposition to Structural Vibration Analysis," *Mechanical Systems and Signal Processing*, Vol. 17, No. 5, 2003, pp. 989-1001.

[35] Friswell, M. and Inman, D.J., "Sensor Validation for Smart Structures," *Journal of Intelligent Material Systems and Structures*, Vol. 10, No. 12, 1999, pp. 973-982.

[36] Kerschen, G., De Boe, P., Golinval, J.C., and Worden, K., "Sensor Validation Using Principal Component Analysis," *Smart Materials and Structures*, Vol. 14, No. 1, 2005, pp. 36-42.

[37] Trindade, M.A., Wolter, C., and Sampaio, R., "Karhunen-Loève Decomposition of Coupled Axial/Bending Vibrations of Beams Subject to Impacts," *Journal of Sound and Vibration*, Vol. 279, No. 3-5, 2005, pp. 1015-1036.

[38] Bellizzi, S. and Sampaio, R., "POMs Analysis of Randomly Vibrating Systems Obtained from Karhunen-Loève Expansion," *Journal of Sound and Vibration*, Vol. 297, No. 3-5, 2006, pp. 774-793.

[39] Lucia, D.J., Beran, P.S., and Silva, W.A., "Aeroelastic System Development Using Proper Orthogonal Decomposition and Volterra Theory," *AIAA Structures, Structural Dynamics, and Materials Conference*, AIAA Paper 2003-1922, AIAA, Norfolk, VA, April 2003.

[40] Masarati, P., Quaranta, G., Lanz, M., and Mantegazza, P., "Dynamic Characterization and Stability of a Large Size Multibody Tiltrotor Model by POD Analysis," *ASME 19th Biennial Conference on Mechanical Vibration and Noise,* ASME Paper DETC/VIB-48440, ASME, Chicago, IL, September 2003.

[41] Lenaerts, V., Kerschen, G., and Golinval, J.C., "Proper Orthogonal Decomposition for Model Updating of Non-linear Mechanical Systems," *Mechanical Systems and Signal Processing*, Vol. 15, No. 1, 2001, pp. 31-43.

[42] Azeez, M.F.A. and Vakakis, A.F., "Proper Orthogonal Decomposition (POD) of a Class of Vibroimpact Oscillations," *Journal of Sound and Vibration*, Vol. 240, No. 5, 2001, pp. 859–889.

[43] Kerschen, G., Golinval, J.C., Vakakis, A.F., and Bergman, L.A., "The Method of Proper Orthogonal Decomposition for Dynamical Characterization and Order Reduction of Mechanical Systems: An Overview," *Nonlinear Dynamics*, Vol. 41 (1-3), 2005, pp. 147-169.

[44] Feeny, B.F., "On the Proper Orthogonal Modes and Normal Modes of Continuous Vibration Systems," *Journal of Vibration and Acoustics*, Vol. 124, No. 1, 2002, pp. 157-160.

[45] Feeny, B.F., "On the Physical Interpretation of Proper Orthogonal Modes in Vibrations," *Journal of Sound and Vibration*, Vol. 211, No. 4, 1998, pp. 607–616.

[46] Homescu, C., Petzold, L.R., and Serban, R., "Error Estimation for Reduced-Order Models of Dynamical Systems," *Journal of Numerical Analysis*, Vol. 43, No. 4, 2005, pp. 1693-1714.

[47] Meirovitch, L., *Principles and Techniques of Vibrations*, Prentice Hall, New Jersey, 1997, Chaps. 1, 7.

[48] Dacunha, J.J., "Transition Matrix and Generalized Matrix Exponential via the Peano-Baker Series," *Journal of Difference Equations and Applications*, Vol. 11, No. 15, 2005, pp. 1245-1264.

[49] Allison, T.C., Miller, A.K., and Inman, D.J., "Unforced Response Simulation by Proper Orthogonal Value Recalculation," *AIAA Structures, Structural Dynamics, and Materials Conference*, AIAA, Honolulu, HI, April 2007.

[50] Allison, T.C., Miller, A.K., and Inman, D.J., "Free-Response Simulation via the Proper Orthogonal Decomposition," *AIAA Journal*, Vol. 45, No. 10, 2007, pp. 2548-2543.

[51] Pinchover, Y and Rubenstein, J., *Introduction to Partial Differential Equations*, New York Cambridge University Press, 2005.

[52] Woolsey, C., "Linear Differential Systems," *AOE 5224 Lecture 4*, Virginia Polytechnic Institute and University, Unpublished, 2006.

[53] Allison, T.C., Miller, A.K., and Inman, D.J., " A Deconvolution-Based Approach to Structural Dynamics System Identification and Response Prediction," *ASME Journal of Vibration and Acoustics*, in press.

[54] Allison, T.C., Miller, A.K., and Inman, D.J., "Modification of Proper Orthogonal Coordinate Histories for Forced Response Simulation," *Proceedings of the International Conference on Engineering Dynamics,* Paper #1001, Carvoeiro, Portugal, April 2007.

[55] Allison, T.C., Miller, A.K., and Inman, D.J., "System Identification Using the Proper Orthogonal Decomposition with Multiple Loads," *Proceedings of the SEM Annual Conference & Exposition,* SEM, Springfield, MA, June 2007.

[56] Allison, T.C., Miller, A.K., and Inman, D.J., "System Identification Techniques for Mixed Responses Using the Proper Orthogonal Decomposition," *ASME IDETC/CIE 2007,* Paper VIB-35407, ASME, Las Vegas, NV, September 2007.

[57] Allison, T.C., Miller, A.K., and Inman, D.J., " A Time-Varying Identification Method for Mixed Response Measurements," *Journal of Sound and Vibration*, under review.

[58] Rahman, J. and Sarkar, T.K., "Deconvolution and Total Least Squares in Finding the Impulse Response of an Electromagnetic System from Measured Data," *IEEE Transactions on Antennas and Propagation*, Vol. 43, No. 4, April 1995, pp. 416-421.

[59] Riad, S.M., "The Deconvolution Problem: An Overview," *Proceedings of the IEEE*, Vol. 74, No. 1, January 1986, pp.82-85.

[60] Lavrent'ev, M.M. and Savel'ev, L.Y., *Linear Operators and Ill-Posed Problems*, Springer, 1995.

[61] Subbaraj, K. and Dokainish, M.A., "A Survey of Direct Time-Integration Methods in Computational Structural Dynamics – II. Implicit Methods," *Journal of Computers & Structures*, Vol. 32, No. 6, 1989, pp. 1387-1401.

Appendix 1: Matlab Codes

This appendix contains the Matlab codes used for applying the system identification methods described in Chapter 3 and generating the figures in Chapter 4. Separate m-files are provided for (1) initial displacements, (2) initial velocities, (3) forced responses (both single- and multiple-load methods), and (4) mixed responses.

1. Response to initial displacements

```
%Application of POD-based identification method
%Free response to initial displacements
%Tim Allison
%August 2007

clear all
close all
clc

%define the vector of sample times
T = [0:1e-4:499e-4];

%load files that contain responses to various initial displacement
profiles
load disp0
D0 = d;
D00 = d(:,1);

load disp1
D1 = d;
D10 = d(:,1);

load disp2
D2 = d;
D20 = d(:,1);

load disp3
D3 = d;
D30 = d(:,1);

%define a 'true' response, i.e. the response you want to predict
Dtrue = D3;

%use function 'icresp_disp' to predict response using POD method
%the function is defined at the bottom of this m-file
Dnew_povr = icresp_disp(D0,Dtrue(:,1),3);

%use function 'icresp_disp_multi' to predict response using MDS method
%the function is defined at the bottom of this m-file
Dnew_mds = icresp_disp_multi([D0 D1 D2],Dtrue(:,1),T);

%calculate displacement norms and percent errors
for i=1:1:length(T)
    dtnorm(i) = norm(Dtrue(:,i));
```

```
    dnnorm_povr(i) = norm(Dnew_povr(:,i));
    dnnorm_mds(i) = norm(Dnew_mds(:,i));
    perr_povr(i) = 100*abs(dtnorm(i)-dnnorm_povr(i))/dtnorm(i);
    perr_mds(i) = 100*abs(dtnorm(i)-dnnorm_mds(i))/dtnorm(i);

end

%plot displacement norms
plot(100*T,dtnorm,'k')
hold on
plot(100*T,dnnorm_povr,'k--')
plot(100*T,dnnorm_mds,'k--','LineWidth',2)
xlabel('Time, ms')
ylabel('Displacement Norm, in')
legend('FE Model','POVR Method','MDS Method')

%plot percent error
figure(2)
plot(100*T,perr_povr,'k')
hold on
plot(100*T,perr_mds,'k','LineWidth',2)
xlabel('Time, ms')
ylabel('Percent Error, %')
legend('POVR Method','MDS Method')

%----------define function icresp_disp---------------------
function Dnew = icresp_disp(old_disp,new_idisp,nmodes)
%
%definition of inputs and outputs
%
% inputs:  old_disp = old displacement response matrix
%          new_idisp = new initial displacement profile
%          nmodes = number of POMs to use
%
% outputs: Dnew = new displacement prediction matrix
%

%calculate the POD from the old displacement
[U,S,V]=svd(Dold);

%solve for new POVs
Snew = (U(:,1:nmodes)'*D0new)./V(1,1:nmodes)';

%form new response matrix with new POVs
Dnew = U(:,1:nmodes)*diag(Snew)*V(:,1:nmodes)';

end %end of function definition for 'icresp_disp'

%----------define function icresp_disp_multi---------------
function Dnew = icresp_disp_multi(Dold,D0new,T)

%determine number of cases (=nmodes)
ntimes = length(T);
[nrow,ncol] = size(Dold);
nmodes = ncol/ntimes;
```

```
%calculate POD and convert displacements to scaled POC histories
[U,S,V1]=svd(Dold(:,1:ntimes),'econ');

U=U(:,1:nmodes);
Vold = U'*Dold;
V0new = U'*D0new;

%arrange matrix of initial displacements in modal space
for i=1:1:nmodes
    V(:,:,i) = Vold(:,1+ntimes*(i-1):ntimes*i);
    V0(:,i) = Vold(:,1+ntimes*(i-1));
end

%arrange V for all modes at each time step
for j=1:1:ntimes
    for i=1:1:nmodes
        for k=1:1:nmodes %ncases, really
            Vj(k,i) = V(k,j,i);
        end
    end
    phi11j(:,:,j) = Vj*inv(V0);
    Vnew_transp(:,j) = phi11j(:,:,j)*V0new;
end

Dnew = U*Vnew_transp;

end %end of function definition for 'icresp_disp_multi'
```

2. Response to initial velocities

```
%Application of POD-based identification method
%Free response to initial velocities
%Tim Allison
%August 2007

clear all
close all
clc

%define the vector of sample times
T = [0:1e-4:499e-4];

%load files that contain responses to various initial velocity profiles
load vel0
D0 = d;
v00 = v(:,1);

load vel1
D1 = d;
v10 = v(:,1);

load vel2
D2 = d;
```

```
v20 = v(:,1);

load vel3
D3 = d;
v30 = v(:,1);

load vel4
D4 = d;
v40 = v(:,1);

%define a 'true' response, i.e. the response you want to predict
Dtrue = D4;

%use function 'icresp_velo' to predict response using POVR method
%the function is defined at the bottom of this m-file
Dnew_povr = icresp_velo(D0,v00,v40,4);

%use function 'icresp_velo_multi' to predict response using MDS method
%the function is defined at the bottom of this m-file
Dnew_mds = icresp_velo_multi([D0 D1 D2 D3],[v00 v10 v20 v30],v40,T);


%calculate displacement norms and percent errors
for i=1:1:length(T)
    dtnorm(i) = norm(Dtrue(:,i));
    dnnorm_povr(i) = norm(Dnew_povr(:,i));
    dnnorm_mds(i) = norm(Dnew_mds(:,i));
    perr_povr(i) = 100*abs(dtnorm(i)-dnnorm_povr(i))/dtnorm(i);
    perr_mds(i) = 100*abs(dtnorm(i)-dnnorm_mds(i))/dtnorm(i);

end

%plot displacement norms
plot(100*T,dtnorm,'k')
hold on
plot(100*T,dnnorm_povr,'k--')
plot(100*T,dnnorm_mds,'k--','LineWidth',2)
xlabel('Time, ms')
ylabel('Displacement Norm, in')
legend('FE Model','POVR Method','MDS Method')

%plot percent error
figure(2)
plot(100*T,perr_povr,'k')
hold on
plot(100*T,perr_mds,'k','LineWidth',2)
xlabel('Time, ms')
ylabel('Percent Error, %')
legend('POVR Method','MDS Method')

%----------define function icresp_velo---------------------
function Dnew = icresp_velo(old_disp,v0old,v0new,nmodes)
%
%definition of inputs and outputs
%
```

```
% inputs:  old_disp = old displacement response matrix
%          v0old = old initial velocity profile
%          v0new = new initial velocity profile
%          nmodes = number of POMs to use
%
% outputs: Dnew = new displacement prediction matrix
%

%calculate the POD from the old displacement
[U,S,V]=svd(Dold);

%solve for original POC time derivatives
Vdot0(1,1:nmodes) = (U(:,1:nmodes)'*v0old)./diag(S(1:nmodes,1:nmodes));

%solve for new POVs
Snew = (U(:,1:nmodes)'*v0new)./Vdot0(1,1:nmodes)';

%form new response matrix with new POVs
Dnew = U(:,1:nmodes)*diag(Snew)*V(:,1:nmodes)';

end %end of function definition for 'icresp_velo'

%----------define function icresp_velo---------------------
function Dnew = icresp_velo_multi(Dold,V0old,V0new,times)

%determine number of cases (=nmodes)
ntimes = length(times);
[nrow,ncol] = size(Dold);
nmodes = ncol/ntimes;

%calculate POD and scaled POC histories
[U,S,T1]=svd(Dold(:,1:ntimes),'econ');
U=U(:,1:nmodes);
Told = U'*Dold;
Td0new = U'*V0new;
Td0old = U'*V0old;

for i=1:1:nmodes
    T(:,:,i) = Told(:,1+ntimes*(i-1):ntimes*i);
end

%arrange V for all modes at each time step
for j=1:1:ntimes
    for i=1:1:nmodes
        for k=1:1:nmodes %ncases, really
            Tj(k,i) = T(k,j,i);
        end
    end
    phi12j(:,:,j) = Tj*inv(Td0old);
    Vnew_transp(:,j) = phi12j(:,:,j)*Td0new;
end

Dnew = U*Vnew_transp;
```

```
end %end of function definition for 'icresp_velo_multi'
```

3. Response to Applied Forces

```
%Application of POD-based identification method
%Forced response, single- and multiple-load methods
%Tim Allison
%August 2007

clear all
close all
clc

%define the vector of sample times
T = [0:1e-4:499e-4];

%load files that contain responses to various loads
load force1.mat
F1 = F;
D1 = d;

load force2.mat
F2 = F;
D2 = d;

load force3.mat
F3 = F;
D3 = d;

load force4.mat
F4 = F;
D4 = d;

load force5.mat
F5 = F;
D5= d;

%set the exact answer
Dtrue = D5;

%use both multi-load and single-load methods to predict response
%the functions 'podforce' and 'podforce_mloads' are defined at
%the bottom of this m-file

%single load method
Dnew_sl = podforce(D1,F1,F5,T,4);

%multiple load method
Dnew_ml = podforce_mloads([D1 D2 D3 D4],[F1 F2 F3 F4],F5,T);

%calculate displacement norms and percent error
for i=1:1:length(T)
    dtnorm(i) = norm(Dtrue(:,i));
    dnnorm_sl(i) = norm(Dnew_sl(:,i));
```

```
    dnnorm_ml(i) = norm(Dnew_ml(:,i));
    p_err_sl(i) = 100*abs(dtnorm(i)-dnnorm_sl(i))/dtnorm(i);
    p_err_ml(i) = 100*abs(dtnorm(i)-dnnorm_ml(i))/dtnorm(i);
end

%plot displacement norms
plot(100*T,dtnorm,'k')
hold on
plot(100*T,dnnorm_sl,'k--')
plot(100*T,dnnorm_ml,'k--','LineWidth',2)
xlabel('Time, ms')
ylabel('Displacement Norm, in')
legend('FE Model','SL POD Model','ML POD Model')

%plot percent errors
figure(2)
plot(100*T,p_err_sl,'k')
hold on
plot(100*T,p_err_ml,'k--','LineWidth',2)
xlabel('Time, ms')
ylabel('Percent Error, %')
legend('SL POD Model','ML POD Model')

%----------define function podforce----------------------
function Dnew = podforce(Dold,Fold,Fnew,T,nmodes)
%
%definition of inputs and outputs
%
% inputs:  Dold = old displacement response matrix
%          Fold = old force matrix
%          Fnew = new forcing function
%          T = vector of time steps
%          nmodes = number of POMs to use
%
% outputs: Dnew = new displacement prediction matrix
%

%calculate delta t (time step size)
dt = T(length(T))/(length(T)-1);
[ndof,ntimes] = size(Dold);

%calculate the POD using the "old" data set
[U,S,V] = svd(Dold,'econ');

%use only the specified number of POMs
%note that we include POVs in the POC histories
U = U(:,1:nmodes);
S = S(1:nmodes,1:nmodes);
V = (S*V(:,1:nmodes)')';

%Calculate the modal forces (old and new)
Qold = U'*Fold;
Qnew = U'*Fnew;

%for each POC history we form convolution matrices from the old and new
```

```
%modal forces and deconvolve the old one out and convolve the new one
in
%
%If noise is present then the deconvolution step is performed by a
%function called 'tlsdeconv' instead of 'deconvolve'
%
%function definitions for 'form_conv_mat', 'deconvolve', and
'tlsdeconv'
%are given below
for i=1:1:nmodes
    Q_unhat_oldi = form_conv_mat(Qold(i,:)); %form convolution matrix
for the old modal force
    Q_unhat_newi = form_conv_mat(Qnew(i,:)); %form convolution matrix
for the new modal force
    Cii(:,i) = deconvolve(V(:,i),Q_unhat_oldi);
    %Cii(:,i) = tlsdeconv(V(:,i),Q_unhat_oldi); %noisy case
    Vnew(:,i) = Q_unhat_newi*Cii(:,i); %doing the deconvolution and
convolution as matrix multiplications
end

%Finally, calculate Dnew with modified POC histories
Dnew = U*Vnew';

end %end of function definition for 'podforce'

%----------define function podforce_mloads----------------
function Dnew = podforce_mloads(Dold,Fold,Fnew,T)
%
%definition of inputs and outputs
%
% inputs:  Dold = old displacement response matrices
%          Fold = old force matrices
%          Fnew = new forcing function
%          T = vector of time steps
%
%
% outputs: Dnew = new displacement prediction matrix
%

%calculate some dimensions and the time step size
ntimes = length(T);
dt = T(ntimes)/(ntimes-1);
[ndof,ncols] = size(Dold);

%count the number of old load sets. this is equal to the number of POMs
nloads = ncols/ntimes;
nmodes = nloads;

%separate out the old displacement and force data sets from the input
for i=1:1:nmodes
    D(:,:,i) = Dold(:,1+ntimes*(i-1):ntimes*i);
    F(:,:,i) = Fold(:,1+ntimes*(i-1):ntimes*i);
end
clear Dold Fold
```

```
%do the POD of the first load and keep only required number of POMS
[U1,S1,V1] = svd(D(:,:,1),'econ');
U1 = U1(:,1:nmodes);
S1 = S1(1:nmodes,1:nmodes);
V1 = (S1*V1(:,1:nmodes)')'; %scaled POC histories

%form the modal forces for all load cases using the first POMs only
for i=1:1:nmodes
    q(:,:,i) = U1'*F(:,:,i);
end

%form scaled POC histories for other load cases
%
%note that POC histories for supplemental cases are not formed with an
SVD;
%they are formed using the original POMs!
for i=1:1:nmodes
    Vscal(:,:,i) = (U1'*D(:,:,i))';
end
clear D S1 F

%calculate Qbar. this is a giant matrix of convolution matrices with
all
%forces
%
%the function 'form_conv_mat' is defined below
for i=1:1:nmodes
for j=1:1:nmodes
    qi = q(:,:,i);
    Qbar((i-1)*ntimes+1:i*ntimes,(j-1)*ntimes+1:j*ntimes) =
form_conv_mat(qi(j,:));
end
end

%assemble POC histories for load cases into large matrix
V = Vscal(:,:,1);
if nmodes > 1
    for i=2:1:nmodes
        V = [V; Vscal(:,:,i)];
    end
end

%do the coupled deconvolution
%
%if the data are noisy, need to use the 'tlsdeconv' function
%
%function definitions for 'deconvolve' and 'tlsdeconv' are given below
C = deconvolve(V,Qbar);
clear V Qbar

%Calculate new Q_bar matrix. This is not a square matrix...it is just a
row
%of convolution matrices for the new modal forces
Qnew = U(:,1:nmodes)'*Fnew;
for i=1:1:nmodes
    Qbarnew(:,(i-1)*ntimes+1:i*ntimes) = form_conv_mat(Qnew(i,:));
```

```
end

%Now calculate Vnew by convolution
Vnew = Qbarnew*C;

%Finally, calculate Dnew
Dnew = U1*Vnew';

end %end of function definition for 'podforce_mloads'

%----------define function form_conv_mat----------------
function A = form_conv_mat(a)
%
%this function forms a convolution matrix for a vector

ntimes = length(a);

for i=1:1:ntimes
    A(i,1:i) = fliplr(a(1:i));
end

end %end of function definition for 'form_conv_mat'

%----------define function deconvolve-------------------
function h = deconvolve(y,X)
%
%this function deconvolves an input x from an output y for cases when
the
%load measurement has little or no noise
%
%x must be in convolution matrix form

h = pinv(X)*y;

end %end of function definition for 'form_conv_mat'

%----------define function tlsdeconv--------------------
function h = tlsdeconv(y,X)
%
%this function deconvolves an input x from an output y for cases when
the
%load measurement is noisy
%
%x must be in convolution matrix form

%form augmented matrix and calculate its SVD
C = [X y];
[U,S,V] = svd(C);
[nrow,ncol]=size(S);

%choose number of singular vectors to use based on condition number of
%augmented matrix
r=0;
tol = 1000; %based on SNR of data
```

```
for i=1:1:nrow
    cn(i) = S(1,1)/S(i,i);
    if cn(i) <= tol
        r = r+1;
    end
end

%TLS technique using r singular values. calculation of r needs to be
%automated, not specified like it is now
n = length(V) - 1;
num = zeros(n,1);
sum1 = 0;
for i=1:1:r
    num = num + V(n+1,i)*V(1:n,i);
    sum1 = sum1 + V(n+1,i)^2;
end
den = 1 - sum1;
h= num/den;

end %end of function definition for 'tlsdeconv'
```

3. Mixed Response Method

```
%Application of POD-based identification method
%Mixed Response Method
%Tim Allison
%August 2007

clear all
close all
clc

%define the vector of sample times
T = [0:1e-4:499e-4];

%load files that contain responses to various initial displacement
profiles
load comb_a
Da = d;
Velo_a = v;
Fa = F;

load comb_b
Db = d;
Velo_b = v;
Fb = F;

load comb_c
Dc = d;
Velo_c = v;
Fc = F;

%load new_velo %initial velocity
%load new_disp %initial displacement
load new_load
Dtrue = d;
```

```
Vtrue = v;
Fnew = F;

%calculate POD for case a
[Ua,Sa,Va] = svd(Da,'econ');
Ua = Ua(:,1:nmodes);
Sa = Sa(1:nmodes,1:nmodes);
Va = Va(:,1:nmodes);

%calculate scaled POC histories. Note that for cases b and c, POC
histories
%are not calculated from the SVD.
Va_hat = (Sa*Va')';
Vb_hat = (Ua'*Db)';
Vc_hat = (Ua'*Dc)';

%initial displacement profiles, initial velocity profiles, and modal
forces
%for 3 cases
d0a = Da(:,1);
d0b = Db(:,1);
d0c = Dc(:,1);

v0a = Velo_a(:,1);
v0b = Velo_b(:,1);
v0c = Velo_c(:,1);

qa = Ua'*Fti;
qb = Ua'*Fmi;
qc = Ua'*Fbi;

%loop over modes and calculate POC histories for displacements and
%velocities as well as diagonals of the C matrix
for i=1:1:nmodes
    %POV ratios
    rbad =(Ua(:,i)'*d0b)/(Ua(:,i)'*d0a);
    rbav =(Ua(:,i)'*v0b)/(Ua(:,i)'*v0a);
    rcad =(Ua(:,i)'*d0c)/(Ua(:,i)'*d0a);
    rcav =(Ua(:,i)'*v0c)/(Ua(:,i)'*v0a);
    Rcb = (rcav-rcad)/(rbav-rbad);

    %form convolution matrices for modal forces
    %
    %the function 'form_conv_mat' is defined below
    Qa = form_conv_mat(qa(i,:));
    Qb = form_conv_mat(qb(i,:));
    Qc = form_conv_mat(qc(i,:));

    %now start solving the system
    Q = Qc-rcad*Qa-Rcb*(Qb-rbad*Qa);
    dtCbar((i-1)*500+1:i*500,i) = inv(Q)*(Vc_hat(:,i)-rcad*Va_hat(:,i)-
Rcb*(Vb_hat(:,i)-rbad*Va_hat(:,i)));
    V_iv(:,i) = (1/(rbav-rbad))*(Vb_hat(:,i)-rbad*Va_hat(:,i)- (Qb-
rbad*Qa)*dtCbar((i-1)*500+1:i*500,i));
    V_id(:,i) = Va_hat(:,i)-V_iv(:,i)-Qa*dtCbar((i-1)*500+1:i*500,i);
```

```
end
V_id_t = V_id';

%Calculate new free resp to initial displacement
A = (Ua'*Dtrue(:,1))./V_id_t(1:nmodes,1);
D_new_id = Ua*diag(A)*V_id_t;

%Calculate new free resp to initial velocity
delta_t = tspan(2)-tspan(1);

%estimate initial time derivatives of V_iv
for i=1:1:nmodes
    V_iv_dot0(i,1) = (V_iv(2,i) - V_iv(1,i))/delta_t;
end
A = (Ua'*Vts(:,1))./V_iv_dot0;
D_new_iv = Ua*diag(A)*V_iv';

%Calculate new forced resp (assumes 4 POMs are used)
qnew = Ua'*Fnew;
Qnew(:,1:500) = form_conv_mat(qnew(1,:));
Qnew(:,501:1000) = form_conv_mat(qnew(2,:));
Qnew(:,1001:1500) = form_conv_mat(qnew(3,:));
Qnew(:,1501:2000) = form_conv_mat(qnew(4,:));
D_new_f = Ua*(Qnew*dtCbar)';

%add up contributions from initial conditions and loads
Dnew = D_new_id + D_new_iv + D_new_f;

%calculate displacement norms and percent error
for i=1:1:length(T)
    dtnorm(i) = norm(Dtrue(:,i));
    dnnorm(i) = norm(Dnew(:,i));
    p_err(i) = 100*abs(dtnorm(i)-dnnorm(i))/dtnorm(i);
end

%plot displacement norms
plot(100*T,dtnorm,'k')
hold on
plot(100*T,dnnorm,'k--','LineWidth',2)
xlabel('Time, ms')
ylabel('Displacement Norm, in')
legend('FE Model','POD Model')

%plot percent error
figure(2)
plot(100*T,p_err,'k')
xlabel('Time, ms')
ylabel('Percent Error, %')

%----------define function form_conv_mat----------------
function A = form_conv_mat(a)
%
%this function forms a convolution matrix for a vector

ntimes = length(a);
```

```
for i=1:1:ntimes
    A(i,1:i) = fliplr(a(1:i));
end

end %end of function definition for 'form_conv_mat'
```

Vita

Tim Allison was born on April 4, 1980 in San Antonio, Texas. He was home schooled and received a diploma from American High School in Lansing, IL in 1996, after which he studied Aerospace Engineering at San Antonio College and the University of Texas at Austin for several years. Once he completed 3 years of undergraduate study, he moved to Fukuoka, Japan for two years to serve as a volunteer missionary for the Church of Jesus Christ of Latter-Day Saints. After returning, he completed his B.S Aerospace Engineering with High Honors at the University of Texas at Austin in May 2004. He was employed from 2001-2004 at the Applied Research Laboratories for the University of Texas and peformed GPS data quality analyses for the Space and Geophysics Department.

He remained at the University of Texas at Austin for his M.S. Aerospace Engineering, which he earned in December 2005. His M.S. research was supervised by Dr. Jeffrey K. Bennighof and dealt with adapting algorithms for efficiently solving the modal frequency response problem for large structures to multiprocessor computing applications. He also completed an internship at Sandia National Laboratories in the Structural Dynamics Engineering Department in the summer of 2005.

Tim transferred to Virginia Polytechnic Institute & State University in January 2006 in order to pursue his doctoral studies. He was awarded fellowships from the National Physical Science Consortium (sponsored by Sandia National Laboratories) and the Virginia Space Grant Consortium. He has since completed another internship with Sandia National Laboratories and will complete his Ph.D. in December 2007.